Diverse Roles of Nodule-Specific Proteins and Peptides in *Medicago truncatula*: From Symbiotic Function to Antimicrobial Activity

DOCTORAL (Ph.D.) DISSERTATION

Mohamad Anas Al Bouni

Supervisors:

Prof. Éva Kondorosi

Dr. Gabriella Endre

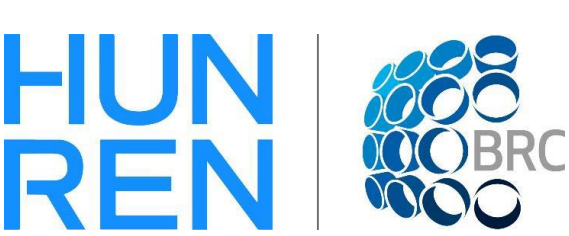

Symbiosis and Plant Genomics group
Institute of Plant Biology
HUN-REN Biological Research Centre, Szeged

Doctoral School of Biology
Faculty of Science and Informatics
University of Szeged

Szeged, 2026

Table of Contents

List of Abbreviations

3-SGC	3-sulfogalactosylceramide
Ab	*Acinetobacter baumannii*
AMPs	Antimicrobial peptides
ARA	Acetylene reduction assay
BacA	Bacterial ABC transporter, Symbiotic role is the uptake of NCRs into the cell
BiFC	Bimolecular fluorescence complementation
BP	Biological process
bp	Basepair
BSA	Bovine serum albumin
CaCl2	Calcium chloride
CaMV	Cauliflower Mosaic Virus
CC	Cellular component
cDNA	Complementary DNA
CH	Cholesterol
CL	Cardiolipin
CR	Cysteine-rich domain
CRISPR	clustered regularly interspaced short palindromic repeats
CSD	Cold-shock domain
CV	Crystal Violet
DAG	Diacylglycerol
DEGs	Differentially expressed genes
DMPC	Dimyristoyl- phosphatidylcholine
DNA	Deoxyribonucleic acid
Dpi	Days post-inoculation
dsRNA	Double stranded ribonucleic acid
E buffer	Elution buffer
Ec	*Escherichia coli*
EDTA	Ethylene diamine tetraacetic acid
Ef	*Enterococcus faecalis*
ER	Endoplasmic reticulum
ESI-MS	Electrospray Ionization Mass Spectrometry
FBC	Fractional bactericidal concentration
FDA	U.S. Food and Drug Administration

FITC	Fluorescein isothiocyanate
GC	Gas chromatography
GFP	Green fluorescent protein
GGX, GGXXXGG, GXGX, GGX/GXGX	Glycine-rich repeats (G-Gly, X-any amino acid)
GR	Glycine-rich domain
GRPs	Glycine-rich proteins
GUS	Beta-glucuronidase protein
H_2SO_4	Sulphuric acid
HRP	Horseradish Peroxidase
IPTG	Isopropyl β-D-1-thiogalactopyranoside
IRLC	Inverted repeat-lacking clade
Irr	Iron response regulator
IT	Infection thread
IZ	Zone II-III, interzone
KEGG	Kyoto Encyclopedia of Genes and Genomes
Kp	*Klebsiella pneumoniae*
LB	Luria-Bertani medium
LjUBQ10	*Lotus japonicus* ubiquitin 10
Lm	*Listeria monocytogenes*
LTPs	Lipid transfer proteins
MBC	Minimal bactericidal concentration
MES	2-(N-morpholino) ethanesulfonic acid
MF	Molecular function
MHB	Mueller Hinton Broth
mRNA	messenger RNA
Ms	*Medicago sativa*
MST	Microscale thermophoresis
Mt	*Medicago truncatula*
N2	dinitrogen gas
NC	Net charge
NCR	Nodule-specific cysteine-rich
NFs	Nodulation factors
NH_3	Ammonia
NH_4^+	ammonium ion

NO_3^-	nitrate ion
Nod	Nodulation
NodD	Nodulation protein D
nodGRPs	Nodule-specific glycine-rich proteins
OD	Optical density
OE	Overexpression
ON	Overnight
p	Pellet
p35S	Cauliflower mosaic virus (CaMV) 35S promoter
Pa	*Pseudomonas aeruginosa*
PA	Phosphatidic acid
PBM	Peribacteroid membrane
PBS	Phosphate-buffered saline
PC	Phosphatidylcholine
PCA	Polymerase chain reaction
PCR	Polymerase chain reaction
PE	Phosphatidylethanolamine
PG	Phosphatidylglycerol
pI	Isoelectric point
PI	Propidium iodide
PI(3,4,5)P3	Phosphatidylinositol-3,4,5-trisphosphate
PI(4,5)P2	Phosphatidylinositol-4,5-bisphosphate
PI4P	Phosphatidylinositol-4-phosphate
PMB	Polymyxin B
PMSF	Phenylmethylsulfonyl fluoride
PPB	Phosphate potassium buffer
PS	Phosphatidylserine
RFU	Relative Fluorescence Units
rirA	Rhizobial iron regulator A
RISC	RNA-induced silencing complex
Rm41	*Sinorhizobium meliloti* Rm41
RNA	Ribonucleic acid
RNAi	RNA interference
RP-HPLC	Reversed-phase high-performance liquid chromatography

RRM	RNA-recognition motif
RT	Room temperature
RT-qPCR	Reverse Transcription quantitative Polymerase Chain Reaction
Sa	*Staphylococcus aureus*
SD	Synthetic dropout
SD-AHLT	Synthetic dropout medium lacking adenine, histidine, leucine and tryptophan
SD-HLT	Synthetic dropout medium lacking histidine, leucine, and tryptophan
SD-LT	Synthetic dropout medium lacking leucine and tryptophan
SDS	Sodium dodecyl sulphate
Se	*Salmonella enterica*
SEM	Scanning electron microscope
SM	Sphingomyelin
Sn	Supernatant
SN	Spontaneous Nodules
SP	Signal peptide
SPC	signal peptidase complex
SPPS	solid-phase peptide synthesis
STM	Streptomycin
SYTO 9	SYTO 9 fluorescent dye
TA	Tetrazolium and arabinose medium
TBST	Tris-Buffered Saline with Tween-20
TEM	Transmission Electron Microscope
TG	Triglyceride
W buffer	Wash buffer
Wpi	Weeks post inoculation
Wt/WT	Wild-type
Y2H	Yeast two-hybrid
YFP	Yellow fluorescent protein
ZI	Nodule Zone I, meristematic zone
ZII	Nodule Zone II, infection zone
ZIII	Nodule Zone III, nitrogen fixation zone
ZIV	Nodule Zone III, senescence zone

1. Introduction

1.1. Nitrogen is a key element in the ecosystem

Nitrogen is the most abundant element in Earth's atmosphere making up, approximately 78% of it. It is also an essential element for life, as it is required for the synthesis of amino acids, nucleic acids and other vital biomolecules. However, atmospheric nitrogen exists primarily as dinitrogen gas (N_2), a form largely inaccessible to most organisms. Only certain bacteria and archaea possess the ability to fix atmospheric nitrogen into biologically usable forms, making nitrogen a relatively scarce resource that often limits primary productivity in many ecosystems. Only after nitrogen is converted from dinitrogen gas into ammonia (NH_3) it becomes available to primary producers, such as plants. Animals and humans obtain nitrogen indirectly by consuming plants or other organisms in the food chain. Nitrogen continuously undergoes various transformations in the environment as part of the nitrogen cycle, shifting between different chemical forms as organisms utilize it for growth and metabolism. The major transformations of nitrogen are nitrogen fixation, nitrification, denitrification, anammox, and ammonification (Gruber & Galloway, 2008; Canfield et al., 2010; Schlesinger & Bernhardt, 2013; Kuypers et al., 2018).

1.2. The nitrogen cycle converts nitrogen into various usable forms

Plants primarily obtain nitrogen from the soil in the form of inorganic compounds, mainly nitrate ions (NO_3^-) and ammonium ions (NH_4^+). Nitrate is the most accessible form, as it is highly soluble in water and readily absorbed by plant roots, whereas ammonium tends to bind to soil particles and is less mobile (Taiz et al., 2015). The nitrogen available in soil originates from multiple sources (Fig. 1.). One major source is the decomposition of nitrogen-containing compounds in organic matter, where microorganisms like *Azospirillum*, *Klebsiella*, *Enterobacter*, *Bacillus*, *Clostridium* break down dead plants and animals (de Bertoldi et al.,1983). This process releases ammonia (NH_3), which is subsequently converted to ammonium ions (NH_4^+) through ammonification, or nitrate (NO_3^-) via microbial processes such as nitrification (Sylvia et al., 2005). Ammonification and nitrification are essential natural processes within the nitrogen cycle, but on their own, they are not sufficient to supply nitrogen to crops on a large scale. These processes are relatively slow and inconsistent, as several environmental factors such as soil temperature, moisture, pH, and organic matter availability. Small amounts of nitrogen are also naturally fixed by lightning and volcanic activity, but these

sources are negligible compared to agricultural demands. A major contributor to the natural nitrogen cycle is biological nitrogen fixation, carried out by specific bacteria and archaea collectively referred to as diazotrophs. In recent times, human activities have also had a major impact on the nitrogen cycle (indicated by red arrows in Fig. 1.), through industrial nitrogen fixation, the products of which are used for agricultural purposes.

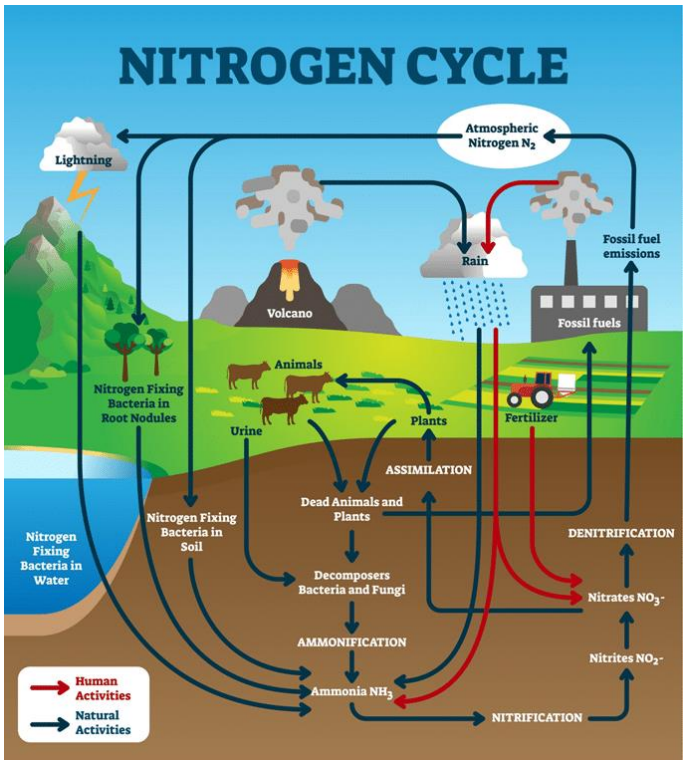

Figure 1. The nitrogen cycle (Shalom Education Ltd., n.d.)

1.2.1. The importance of industrial nitrogen fixation and its consequences

Synthetic fertilizers play a crucial role in enhancing soil nitrogen levels, primarily through the Haber-Bosch process, developed in the early 20th century by Fritz Haber and Carl Bosch. This industrial process synthesizes ammonia by combining atmospheric nitrogen with hydrogen (usually derived from natural gas) under high pressure (150–350 atm) and temperatures ranging from 400 to 500 °C, using an iron-based catalyst. The ammonia produced can be further processed into nitrate and ammonium fertilizers, providing plants with a direct and readily available nitrogen source. This innovation revolutionized global agriculture by dramatically increasing crop yields and supporting food security (Smil, 2001).

However, the Haber-Bosch process has significant environmental drawbacks. It is highly energy-intensive, relying heavily on fossil fuels, which contributes to carbon dioxide (CO_2) emissions and exacerbates climate change (Erisman et al., 2008). Moreover, the excessive use of synthetic fertilizers and low efficiency of their utilization by plants often leads to nitrogen runoff into surface- and groundwater, causing nutrient imbalances. This can trigger

eutrophication, the rapid growth of algae, which, as the algae decompose, depletes oxygen levels and disrupts aquatic ecosystems. The long-term accumulation of excess nitrogen not only threatens biodiversity but also impacts water quality and public health (Vitousek et al., 1997, Galloway et al., 2004).

1.2.2. Biological nitrogen fixation

1.2.2.1. Nitrogen fixation in diazotrophs

Diazotrophs are microorganisms capable of converting atmospheric nitrogen into bioavailable forms of nitrogen such as ammonia. This process is catalyzed by the nitrogenase enzyme complex (Hardy et al. 1968; Fay et al., 1992) that is able to fix nitrogen at normal temperature and under ambient temperature atmospheric pressure in contrast to the extreme conditions needed for the industrial process. The first isolation of the enzyme in its active form was done by Bulen and LeComte (1966). Subsequent structural and mechanistic studies in the 1970s and 1980s revealed that nitrogenase consists of two components and is highly oxygen-sensitive. Only microorganisms possessing the nitrogenase enzyme complex are capable of fixing nitrogen, and they have evolved diverse strategies to create suitable conditions for this process and to benefit from the utilization of the fixed nitrogen produced even through different associative lifestyles.

1.2.2.2. Diversity of nitrogen-fixing plant-microbe associations

Diazotrophs can be classified into four different types based on their lifestyles and associations with other organisms. Free-living diazotrophs can fix nitrogen independently, and are often found in soil, water, or sediments (*Azotobacter*, *Clostridium*, *Klebsiella* and *Cyanobacteria* like *Anabaena* and *Nostoc* (Burris & Roberts, 1993)). Associative diazotrophs live in the rhizosphere (the root zone) of plants but do not form any structural relationship with the plant (*Azospirillum and Herbaspirillum).* The endophytic diazotrophs that live inside plant tissues without causing harm, these bacteria fix nitrogen directly within their plant hosts like *Gluconacetobacter diazotrophicus* found in sugarcane and other tropical plants (Reinhold-Hurek & Hurek, 2011). Finally, symbiotic diazotrophs that form mutualistic relationships with plants, providing fixed nitrogen in exchange for carbon (*Rhizobium* and *Bradyrhizobium, Frankia and* Cyanobacteria like *Nostoc* in lichens (Dixon & Kahn, 2004; Mus et al., 2016).

1.3. Symbiotic nitrogen fixation in legumes

The symbiotic relationship between legumes and rhizobia bacteria can add anywhere from 20 to 200 kg of nitrogen per hectare annually, representing a crucial input for sustainable agriculture (Pearson & Stewart, 1993). This process is considered the most efficient form of biological nitrogen fixation. In these interactions, specific soil bacteria known as rhizobia infect the roots of leguminous plants and induce the formation of specialized organs called root nodules, where nitrogen fixation takes place. Within nodules, rhizobia differentiate into bacteroids, which are metabolically active forms capable of expressing nitrogenase and reducing atmospheric nitrogen to ammonia. The plant, in turn, provides the bacteroids with a protective, low-oxygen environment and carbon sources derived from photosynthesis, ensuring optimal nitrogenase activity (Sprent, 2009; Oldroyd et al., 2011). Inside the nodule, the plant also tightly regulates oxygen levels through the production of leghemoglobin, a heme-containing protein, that gives the nodules its pink color, and buffers oxygen to protect nitrogenase while allowing sufficient respiration for energy production. The resulting symbiotic system allows legumes to thrive in nitrogen-poor soils and contributes substantially to global nitrogen input, highlighting the ecological and agricultural importance of these associations (Bergersen, 1997; Mus et al., 2016).

As it was mentioned above, the most efficient biological nitrogen fixation occurs within legume–rhizobium symbioses. Consequently, the formation and development of nitrogen-fixing symbiotic root nodules, along with the genes regulating these processes, have been intensively studied (Roy et al., 2020). *Medicago truncatula*, a Mediterranean relative of alfalfa, has emerged as a principal model species for such studies.

1.3.1. *Medicago truncatula* as a model plant for molecular biology studies

Medicago truncatula is widely recognized as an excellent model for investigating legume–rhizobium symbiosis (Fig. 2.). The species possesses diverse ecotypes that respond differently to various rhizobial strains, making it well-suited for studying host specificity in symbiotic associations. In addition, it combines short generation time with high seed yield, which, together with efficient genetic manipulation techniques, enables systematic analysis of gene function. Its compact genome (~500 Mbp, 2n = 16) and the availability of rich genomic resources, including a high-quality reference sequence (Young et al., 2011), offer strong support for genome sequencing projects of further legume relatives and for diverse functional genomics research. These features establish *M. truncatula* as a versatile model organism for investigating the molecular and genetic mechanisms governing symbiosis in legumes.

Figure 2. The model plant *M. truncatula*. Symbiotic root nodules are on the upper left picture.

1.3.2. Initiation of symbiotic root nodule formation in leguminous plants

The establishment of a legume–rhizobium symbiosis is a highly orchestrated process involving molecular signaling between the host and microbe (Fig. 3.). Plant roots secrete flavonoids, which are recognized by rhizobial NodD proteins, that act as transcription factors to induce the expression of bacterial nodulation (*nod*) genes (Kondorosi et al., 1984). These genes encode enzymes responsible for the synthesis of lipochitooligosaccharide signaling molecules called Nod factors (NF) (Lerouge et al., 1990). The recognition of NFs by host roots triggers calcium spiking in root hair cells, which induces cytoskeletal rearrangements and curling of the hairs. This curling traps rhizobia in an infection pocket, while NFs simultaneously stimulate cortical cell divisions that give rise to the nodule primordium (Ehrhardt et al., 1996; Catoira et al., 2000; Oldroyd & Downie, 2008).

The host root hair cell invaginates its plasma membrane at the site of bacterial accumulation. Instead of breaking through the wall, the plant cell generates a new inward-growing tube called the infection thread (IT), which guides rhizobia across cell layers toward the primordium (Fournier et al. 2008). As the primordium develops a meristem, the IT branches within it and delivers bacteria into newly divided host cells, ensuring effective colonization (Mylona et al., 1995; Gage, 2004; Limpens & Bisseling, 2003). Once inside host cells, rhizobia are released from the IT and surrounded by a plant derived membrane known as peribacteroid membrane, which both prevents pathogenic interactions and mediates nutrient exchange (Udvardi & Day,

1997; Kereszt et al., 2011). This compartmentalization creates the symbiosomes, where bacteria divide and differentiate into nitrogen-fixing bacteroids (Vasse et al., 1990; Roth & Stacey, 1989; Oke & Long, 1999). The coordinated infection and differentiation processes ultimately create the root-derived new organ called the nodules specialized for symbiotic nitrogen fixation (Brewin, 2004; Murray, 2011).

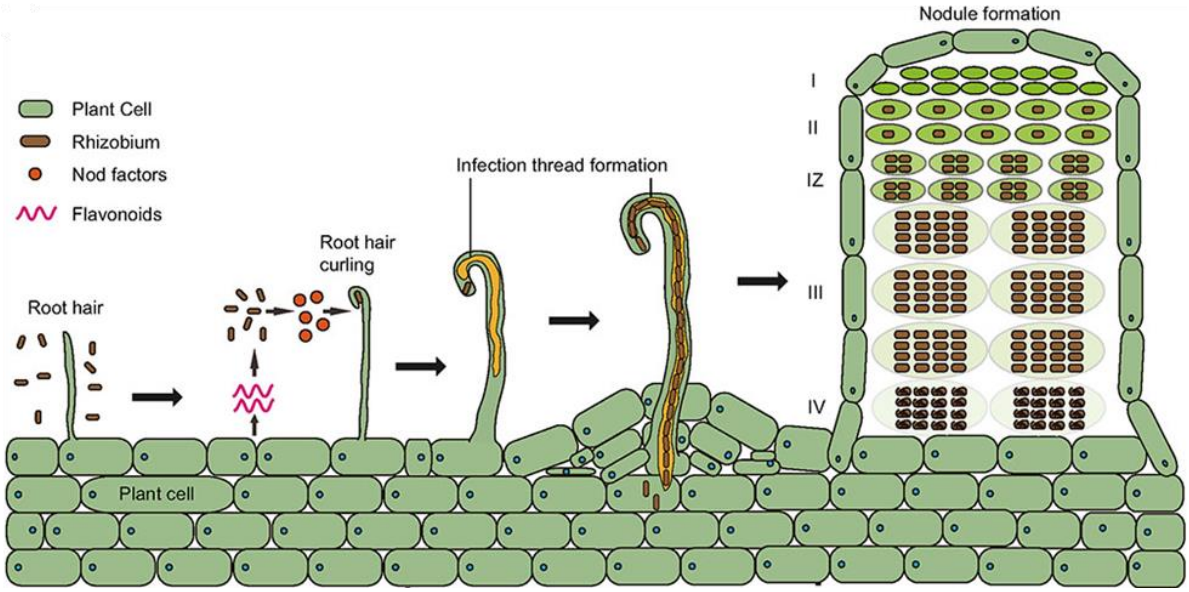

Figure 3. Consecutive steps of the cellular processes leading to the formation of symbiotic root nodule (Wang et al., 2018**).**

1.3.3. Nodule organogenesis and structures

Mature legume nodules can be divided into two main morphological categories: determinate and indeterminate ones (Fig. 4.). Determinate nodules, typical of tropical legumes such as *Glycine max* and *Lotus japonicus*, are generally spherical and lack a persistent meristem (Fig. 4.a). After the initial cortical divisions that establish the primordium, meristematic activity stops, and further growth occurs through cell enlargement (Franssen et al., 1992; Downie, 2014). As a result, these nodules contain a relatively uniform population of nitrogen-fixing bacteroids that maintain a morphology similar to free-living rhizobia (undifferentiated U-type) and can revert to this state when released from the tissue (Oke & Long, 1999). In contrast, indeterminate nodules (Fig. 4.b), found in temperate legumes such as *Medicago sativa* (alfalfa), *Pisum leguminosarum* (pea), *Vicia sativa* (vetch) and other members of the so-called Inverted Repeat Lacking Clade (IRLC), are elongated or cylindrical in form and sustain a permanent apical meristem. Continuous cell proliferation produces distinct developmental zones: the meristematic zone (ZI), infection zone (ZII), interzone (IZ), nitrogen fixation zone (ZIII), and senescence zone (ZIV) (Xiao et al., 2014; Łotocka et al., 2012).

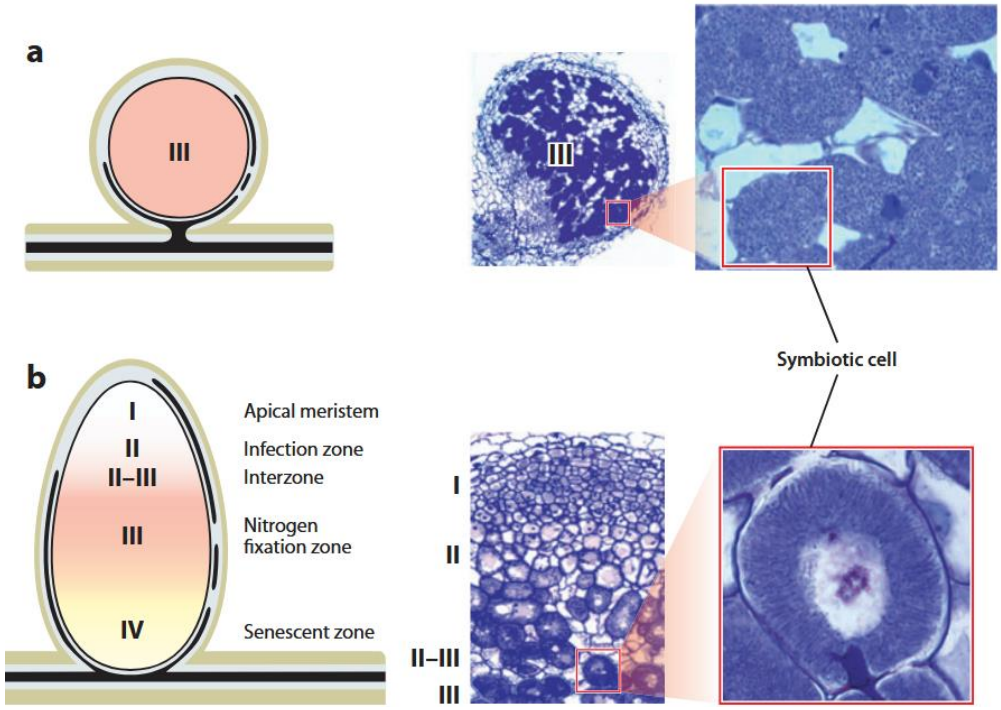

Figure 4. Structure of determinate and indeterminate root nodules. (a) Determinate nodules are spherical, with a central region (ZIII) that harbor nitrogen-fixing bacteria. A magnified view of the symbiotic cells reveals the endosymbionts residing within the host cell cytoplasm. (b) Indeterminate nodules possess an active apical meristem (ZI), followed by an infection zone (ZII), an interzone (IZ), a nitrogen fixation zone (ZIII), and, in old nodules, a senescence zone (ZIV). Symbiotic cells differentiate along ZII and IZ, reaching their mature form in ZIII. The nucleus and cell volume of the infected plant cells increase through successive endoreduplication cycles, and the fully developed nitrogen-fixing cells become densely filled with the endosymbionts (Kondorosi et al., 2013).

Our model legume *M. truncatula* forms indeterminate nodules, in which rhizobia are released from infection threads into the plant cells in ZII. The host cells in this infection zone become larger, their cell division is stopped, and inside they enclose rhizobia in a so-called peribacteroid membrane, generating symbiosomes (Fig. 5a.) (Kereszt et al., 2011). As cells transition through the interzone, bacteroids undergo endoreduplication, elongation, and terminal differentiation (Fig. 5b.). Infected host cells also undergo substantial enlargement that drives the nodule growth. These cells exhibit high levels of endopolyploidy, with DNA contents reaching 64C to 128C (Cebolla et al., 1999; Kondorosi et al., 2005). This increase arises from a modified cell cycle known as endoreduplication, in which repeated rounds of DNA replication occur without mitosis or cytokinesis. The extent of endoreduplication is closely correlated with bacteroid elongation (Mergaert et al., 2006). Symbiotic cells in zone III (ZIII) are also rich in leghemoglobin, which regulates oxygen levels to maintain optimal conditions for nitrogenase activity (Ott et al., 2005; Mergaert et al., 2006; Van de Velde et al., 2010; Montiel et al., 2017.).

By contrast, the senescence zone (ZIV) at the proximal part of the nodule harbors degraded cells and non-functional bacteroids, often visible as yellow-green tissue due to heme breakdown (Puppo et al., 2005).

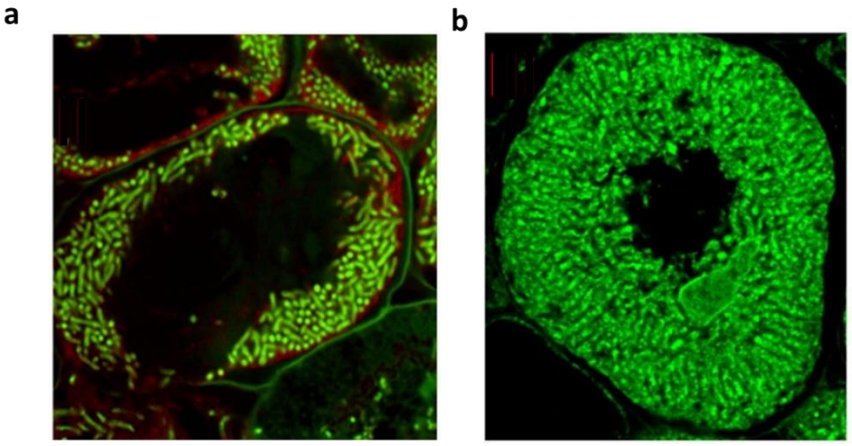

Figure 5. **Symbiotic cells in a *M. truncatula* nodule.** Cells in ZII (a) contain the differentiating endosymbionts while cells in ZIII (b) are fully packed with the long fully differentiated nitrogen-fixing bacteroids. Active endosymbionts stained with Syto9 green fluorescent dye (Maróti & Kondorosi, 2014)

1.4. Plant factors that induce bacteroid differentiation in indeterminate nodules

Bacteroid differentiation is not an autonomous process of the bacteria but is tightly regulated by the host plant (Mergaert et al., 2006). In legumes belonging to the Inverted Repeat-Lacking Clade (IRLC), such as *M. truncatula*, the host controls rhizobial development through the production of nodule-specific peptides or small proteins. Two main families were discovered to have a direct role in symbiosis: the NCR (nodule-specific cysteine-rich) peptides (Mergaert et al., 2003) and the nodGRP (nodule-specific glycine-rich) proteins (Kevei et al., 2002; Alunni et al., 2007). These peptides are produced in the symbiotic cells (Guefrachi et al., 2014) and reach the symbiosomes via the secretory pathway after the signal peptide (SP) is cleaved from the peptides by the signal peptidase complex (SPC) in the endoplasmic reticulum (ER), and the mature peptides arrive in trans-Golgi vesicles via the Golgi apparatus to the symbiosome (Fig. 6.) (Wang et al., 2010; Van de Velde et al., 2010). Mature NCR peptides typically range from 20 to 50 amino acids in length and contain either four or six conserved cysteine residues arranged in characteristic motifs. These cysteines form two or three disulfide bridges that influence peptide folding, thereby stabilizing the structure and likely playing a crucial role in their biological activity. Interestingly, this structural organization closely resembles that of small cysteine-rich antimicrobial defensins, which share a similar overall fold. However, defensins generally possess longer mature peptides containing eight cysteines that form four

disulfide bonds (Kereszt et al., 2011; Kondorosi et al., 2013; Maróti et al., 2015; Farkas et al., 2018).

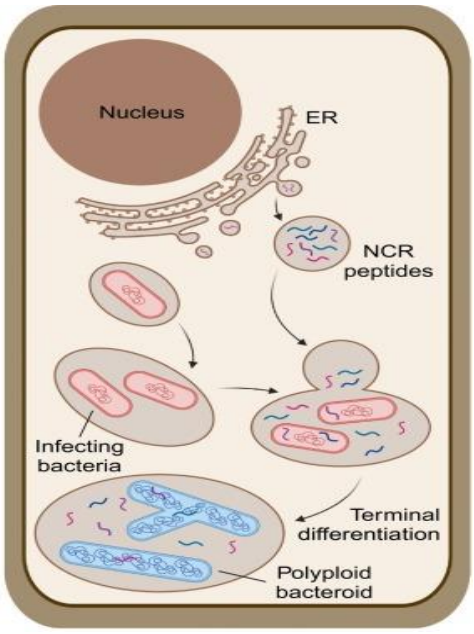

Figure 6. Production of NCRs in nodule cells and their effect on bacteroid transformation of rhizobia. NCR peptides play a crucial role in the differentiation of the bacteria into elongated, polyploid bacteroids specialized for nitrogen fixation.

In the *M. truncatula* genome there are over 700 NCR genes that are widely distributed, often occurring in clusters that likely arose from recent duplication events (Alunni et al., 2007; Pecrix et al., 2018, Downie & Kondorosi, 2021). Their gene structure typically consists of two coding exons (one for SP, the other for the mature peptide), and some NCR genes may also contain a third exon. NCR genes are expressed after the invasion of bacteria into nodule cells (around 4 days post inoculation) and usually reach the highest levels of expression at differentiation and elongation stage of bacteroids at 10 dpi or 14 dpi in *M. truncatula*. The expression of these *NCR*s in other plant organs are not inducible with any biotic or abiotic stress indicating the strict nodule specific expression of *NCR* genes (Guefrachi et al. 2014).

RNA-seq data of two weeks old *M. truncatula* laser-dissected nodules confirmed that NCR transcripts are not detected in the meristem, but was restricted to infected nodule cells (Roux et al., 2014). Furthermore, a staged expression pattern was observed, with about 15% of the genes expressed early, mainly in the distal and proximal infection zones (ZII), whereas the majority (around 56%) were predominantly expressed in the interzone (IZ) and nitrogen fixation zones (ZIII). This close association between the spatial and temporal expression of NCR genes during nodule development has led to their classification into early and late NCRs, based on the timing and location of their activation within the nodule (Van de Velde et al., 2010; Nallu et al., 2013).

1.4.1. Symbiotic functions of NCR peptides.

Despite the extensive research on NCR peptides, their precise roles and mechanisms of action during symbiosis for that many members remain poorly understood. Given their structural similarity to defensins (key effector molecules in innate immunity), their potential antimicrobial function has been explored and several cationic NCRs were found to display broad-spectrum antimicrobial activity (see below in more details). Some even kill the free-living *S. meliloti* cells, however, these rhizobia are able to survive in the nodules. This may be explained by differences in NCR peptide concentrations between nodules and *in vitro* conditions (Maróti et al., 2015; Kereszt et al., 2018), or by the concurrent presence of multiple NCR peptides within nodule cells. It remains unclear how the antibacterial properties of some cationic NCRs contribute to bacteroid differentiation.

Nonetheless, the bacterial peptide transporter BacA has been identified as a crucial factor for bacteroid formation in NCR-producing legumes (Karunakaran et al., 2010). The BacA protein plays an essential role in supporting bacterial survival and differentiation during symbiosis. Mutant *bacA* strains are unable to survive upon exposure to NCRs following their release from the infection thread into the host cytosol, thereby halting nodule development (Haag et al., 2011). These findings suggest that there is delicate balance in nodule environment between death and terminal differentiation imposed by the host. Experimental evidence strongly supports the crucial role of NCR peptides in driving bacteroid differentiation. Ectopic expression of *NCR035* gene in *L. japonicas* and *NCR169* in soybean, legumes that does not naturally produce NCR peptides, resulted in creating enlarged bacteroids (Van de Velde et al., 2010; Zhang et al., 2023). Similarly, *in vitro* treatment of *S. meliloti* with NCR035 peptide promoted endoreduplication, leading to an increased DNA content (4C), a hallmark of bacteroid differentiation (Van de Velde et al., 2010). Increased bacteroid DNA content was also detected in soybean nodules expressing NCR169 (Zhang et al., 2023). Consequently, NCR peptides are not limited to acting on the bacteroid surface; they can also penetrate the bacterial cytosol, where they exert regulatory functions from within. Several NCRs, including NCR001, NCR035, NCR169, and NCR247, have been shown to localize within bacteroids inside the symbiosome, confirming their intracellular localization and activity (Van de Velde et al., 2010; Farkas et al., 2014; Horváth et al., 2015; Kim et al., 2015).

NCR247, one of the best-characterized and smallest NCR peptides secreted by *M. truncatula*, exhibits zone-specific expression in the late infection zone (ZII) and interzone (IZ), as shown by a GUS promoter-reporter fusion (Fig. 7A). FITC-labeled NCR247 penetrates bacterial membranes and accumulate in the cytosol of free-living rhizobia (Fig. 7B, C) and bacteroids

(Fig. 7D, E), where it triggers endoreduplication and extensive transcriptional reprogramming in *S. meliloti*, including downregulation of basic cellular function genes and upregulation of stress response genes (Farkas et al., 2014; Tiricz et al., 2013; Lima et al., 2020). NCR247 binds multiple rhizobial proteins, including FtsZ, a conserved cell division protein, disrupting Z-ring formation and suppressing cell division, thereby promoting endoreduplication and bacteroid differentiation (Farkas et al., 2014; Penterman et al., 2014). GroEL has also been identified as an interacting partner, though its functional significance remains unclear; it may assist in the proper folding of NCR peptides or, conversely, NCR247 might influence GroEL-dependent processes critical for infection and terminal differentiation (Farkas et al., 2014).

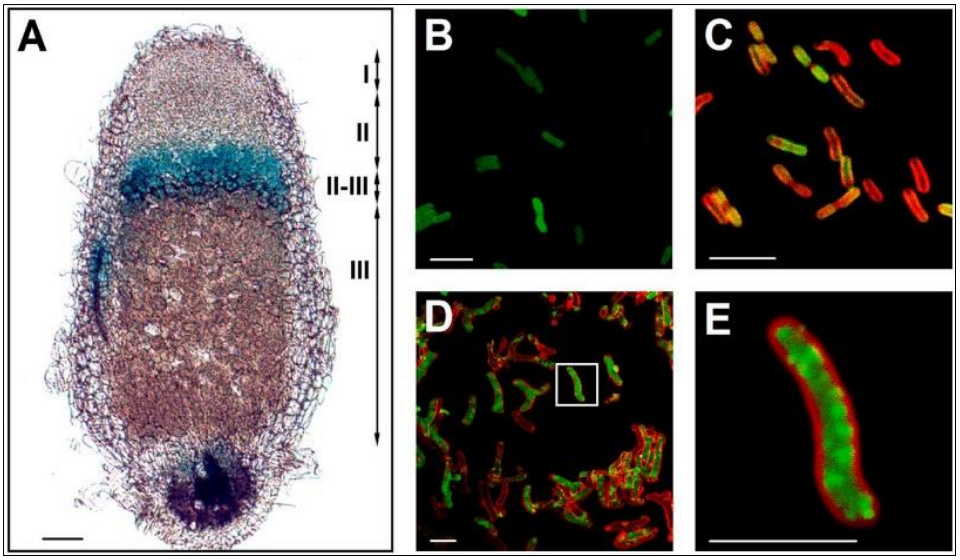

Figure 7. NCR247 expression and localization *in planta* and proposed function in symbiosis. (A) Blue staining in the cells of late infection zone II and in the interzone (II-III) corresponds to pNCR247 promoter activity visualized by GUS reporter gene in transgenic *M. truncatula* nodules. (B) *S. meliloti* culture stained with FITC-labeled NCR247 and PI. (C) *S. meliloti* culture stained with FITC-labeled NCR247 and membrane-dye FM 4-64. (D and E) *S. meliloti* bacteroids stained with FITC-labeled NCR247 and FM 4-64. (E) Enlarged image of the boxed bacteroid from D. Scale bars: 5 μm. (Farkas et al., 2014).

Another role for NCR247 was uncovered in controlling iron homeostasis during the *M. truncatula* and *S. meliloti* symbiosis. NCR247 plays a unique role in sequestering heme and keep bacterial iron homeostasis fine-tuned to ensure iron availability for nitrogenase enzyme (Sankari et al., 2022).

1.4.2. Mutations in single NCR genes cause impaired symbiotic phenotype

Recent research has shown that despite the >700 members of the *NCR* family, the loss of certain individual *NCR* genes can lead to an inefficient nitrogen-fixing symbiosis (Fig. 8.). In *dnf7-2* mutant and in a CRISPR mutant lacking of *NCR169* function, the plant–rhizobia symbiosis fails

to fix nitrogen properly. These mutants show early nodule senescence and defective differentiation of bacteroids (Horváth et al., 2015, Güngör et al. 2023). Similarly, the loss of NCR211 is responsible for the nitrogen-starvation phenotype observed in the *dnf4-1* mutant (Kim et al., 2015). Mutants Mtsym19, Mtsym20, and NF-FN9363 exhibit similar symbiotic defects and further genetic characterization disclosed that Mtsym19 and Mtsym20 share defects in the same NCR peptide, NCR-new35, while the ineffective symbiosis observed in NF-FN9363 results from the loss of NCR343 (Horváth et al., 2023). Therefore, NCR169, NCR211, NCR343 and NCR-new35, respectively, play critical roles as positive regulators in bacteroid differentiation and maintenance within mature nodules.

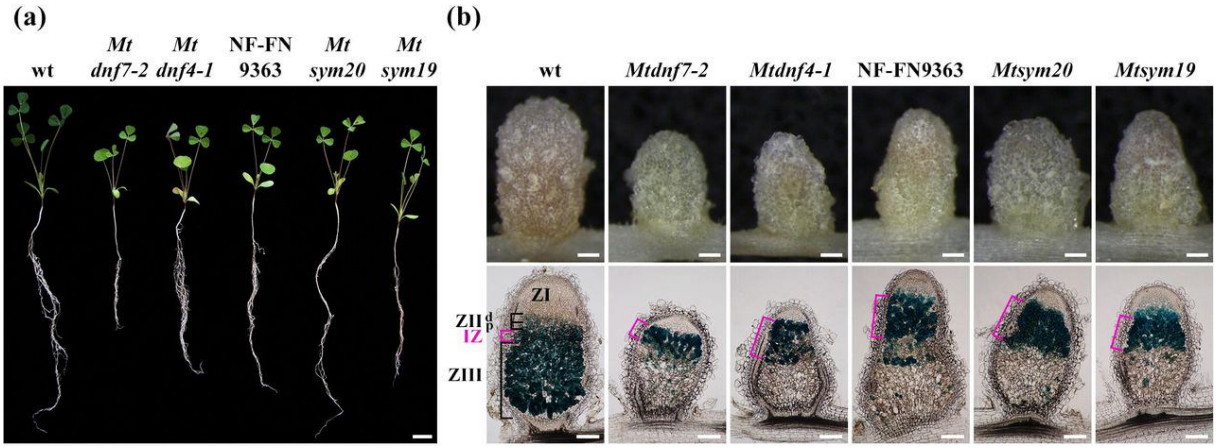

Figure 8. The phenotype of *M. truncatula* symbiotic mutants with ineffective nodulation, *Mtdnf7-2* (deletion of NCR169), ***Mtdnf4-1*** (deletion of NCR211)**, NF-FN9363 (**deletion of *NCR343*) ***Mtsym20*** **and** ***Mtsym19*** (both defective in the same gene, NCR-new35) (a) Ineffective nitrogen-fixing (Fix-) symbiotic mutants showed the symptoms of the nitrogen starvation compared with wild-type (wt) plant (2 wpi) with *S. medicae* WSM419 carrying the *lacZ* reporter gene. (b) Slightly elongated white/pinkish nodules were formed on the roots of the Fix^- plants compared to pink pink elongated nodules on wt roots. Nodule sections stained with β-galactosidase show the ZIII of Fix^- nodules are devoid of rhizobia infected cells. Magenta brackets label the IZ. Scale bars, (a) 2 cm; (b) 200 μm (Horváth et al., 2023).

1.4.3. Glycine-rich proteins in plants

Plant glycine-rich proteins (GRPs) belong to heterogeneous families that are characterized by a high glycine content (up to 70%) and the presence of repetitive glycine-rich motifs, which provide structural flexibility and the potential to interact with various macromolecules (Sachetto-Martins et al., 2000; Czolpinska & Rurek, 2018). Based on domain organization, GRPs are broadly divided into two main groups and different classes (Fig. 9.): structural GRPs (Classes I, II, and III), which are typically secreted to the cell wall and contribute to its assembly, strengthening, and remodeling; and RNA-binding GRPs (Class IV with different sub-classes), which localize to the cytoplasm or nucleus and regulate post-transcriptional processes such as mRNA splicing, stability, and transport (Czolpinska & Rurek, 2018; Zhu et

al., 2021). The eucalyptus GRPs are characterized by high glycine content and irregular repeat patterns and proposed a novel GRP class, Class V. (Mangeon et al., 2010). Czolpinska & Rurek (2018) advised a classification of GRPs based on the arrangement of glycine repeats and the presence of conserved motifs (Fig. 9.).

a

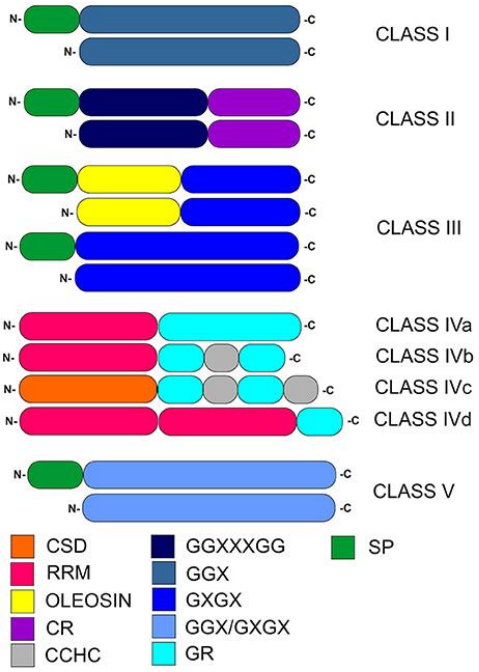

b

GRP classes	Characteristic features
Class I	Signal peptide followed by high glycine-content region with $(GGX)_n$ repeats
Class II	Signal peptide and presence of a characteristic cysteine-rich C-terminal domain
Class III	Signal peptide and contain lower glycine content (in comparison to other GRPs classes), the oleosin domain is the signature motif for their sub-group
Class IV	RNA-binding GRPs, glycine-rich domain with RNA-recognition motif (RRM) or a cold shock domain (CSD), CCHC zinc-fingers might be also present in their structure, four sub-groups: (**IVa**) RRM motif besides the glycine-rich domain, (**IVb**) single RRM and CCHC zinc-finger motif, (**IVc**) cold shock domain and two or even more zinc-fingers, (**IVd**) two RRM motifs
Class V	Signal peptide followed by GGX/GXGX motif or only GGX/GXGX motif without signal peptide

Figure 9. **Classification of plant glycine-rich proteins**. (a) Domain organization of GRPs belonging to the different classes and sub-classes. CSD, cold-shock domain; RRM, RNA-recognition motif; oleosin, oleosin-conserved domain; CR, cysteine-rich domain; CCHC, zinc-finger; GR, glycine-rich domain; GGX, GGXXXGG, GXGX, GGX/GXGX, glycine-rich repeats (G-Gly, X-any amino acid); SP, signal peptide. (b) Description of the characteristic features of the GRP classes (Czolpinska & Rurek, 2018).

Plant GRPs were proposed to play structural roles in cell walls, by acting as scaffolds for wall component deposition (Keller et al. 1988), and this was later proven by experimental results. For example, a bean GRP (PvGRP1.8) localizes to primary cell walls and contributes to protoxylem development, likely strengthening the walls by linking lignin rings (Ringli et al. 2001; Rayser et al. 2004). In *Arabidopsis taliana*, reverse genetics identified a GRP involved in protoxylem maintenance (Yokoyama et al. 2006). Another GRP called AtGRP9 found to be interacting with AtCAD5 in *A. taliana* (an enzyme from the lignin biosynthesis pathway), suggesting a role in lignin biosynthesis (Chen et al. 2007). A GRP from *Nicotiana tabacum*, NtCIG1, enhances callose deposition in vascular tissue, with its activity promoted by the interacting protein GrIP (Ueki & Citovsky, 2002).

Functional studies have further linked GRPs to roles in signaling pathways, such as the WAK1 receptor kinase cascade regulated by Arabidopsis AtGRP3 (Park et al., 2001). GRPs in

Arabidopsis also play important roles in plant defense. The bacterial effector HopU1 from *Pseudomonas syringae* specifically mono-ADP-ribosylates AtGRP7 (also called AtRBG7 at arginine residues within its RRM domain (Fu et al., 2007). This modification inhibits its RNA-binding ability, compromising immune-related RNA regulation. AtRBG7 mutants show enhanced susceptibility to *P. syringae*, demonstrating that it contributes to innate immunity by maintaining proper defense gene expression.

Therefore, GRPs are not just structural proteins with lots of glycine, many of them have regulatory and signaling functions. Their expression is developmentally regulated and strongly influenced by environmental cues, being induced by abiotic stresses such as cold, dehydration, salinity, and wounding, as well as by biotic challenges including pathogen and nematode infection (Mangeon et al., 2010; Carpenter et al., 1994).

1.4.4. Nodule-specific glycine-rich proteins (nodGRPs) in legumes

Like other plant species, legumes also contain canonical GRPs that are broadly expressed in various tissues. They play diverse roles in cell wall organization and remodeling, responses to abiotic stresses (such as drought, salinity, and cold), as well as RNA-binding and post-transcriptional regulation. What is particularly remarkable, that IRLC legumes have evolved a distinct, GRP gene family specific to symbiotic cells in nitrogen fixing root nodules. These genes were first identified through screening of nodule-specific cDNA libraries constructed from mRNA isolated from developing root nodules. In *Vicia faba*, for instance, five GRP-encoding genes were described that are exclusively expressed in nodules (Perlick et al., 1996; Küster et al., 1995) (Fig. 10.a), suggesting a specialized role in legume–rhizobium symbiosis and nodule development, potentially through structural remodeling or regulation of symbiosis-specific gene expression (Küster et al., 1995; Schröder et al., 1997).

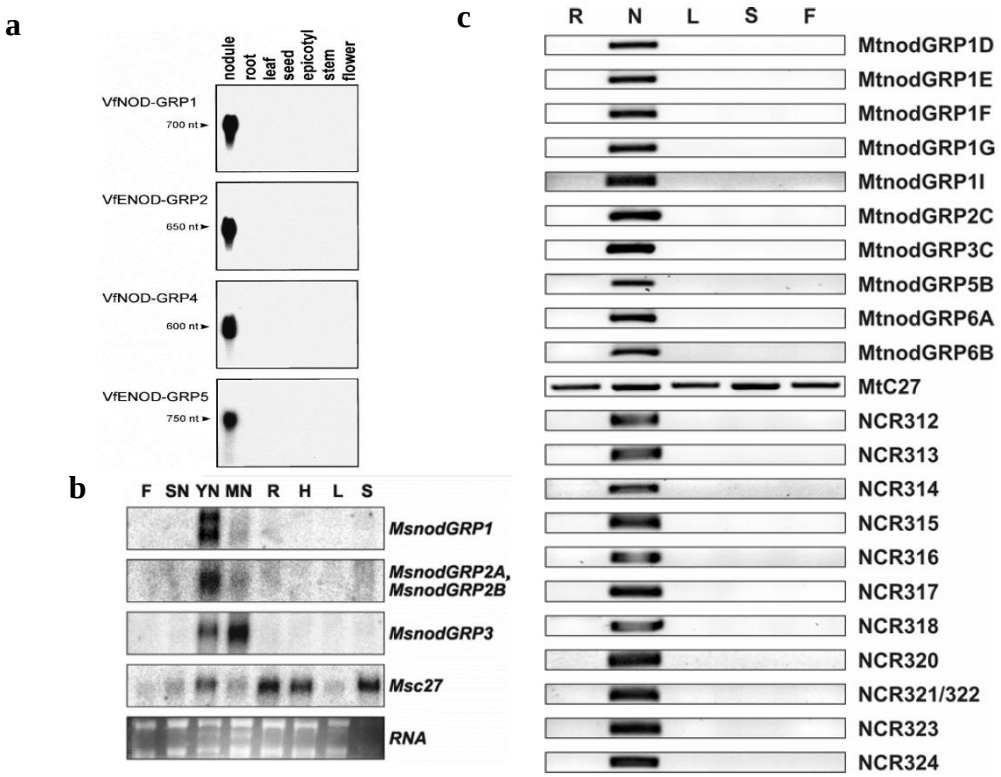

Figure 10. Nodule-specific GRPs identified in several IRLC legume plants. (a) Organ-specific expression of *Vicia faba* (broad bean) *VfNOD-GRP1*, *2*, *4*, and *5* genes in different organs (mature nodules, uninfected roots, leaves, seeds, epicotyls, stems, flowers) exhibited by Northern blot analysis. **(b)** Expression of *MsnodGRP1, 2a, 2b* and *3* genes is nodule specific and depends on *Sinorhizobium meliloti* infection shown by Northern analysis. Loaded alfalfa RNA samples: flowers (F), spontaneous nodules (SN), young nodules at 7 dpi (YN), mature nodules at 21 dpi (MN), roots (R), hypocotyls (H), leaves (L), and stems (S). *Msc27* was used as an internal control, and the corresponding RNA samples were visualized on an ethidium bromide–stained gel to visualize RNA loading. **(c)** Expression profiles of selected *nodGRP* and *NCR* genes (listed on the right) in *M. truncatula* tissues determined by RT-PCR. Reactions were carried out on cDNA from roots (R), nodules (N), leaves (L), stems (S), and flowers (F). The amplification of the constitutive marker *MtC27* served as a positive control (Alunni et al., 2007).

Similar nodule-specific GRPs have also been described in *Medicago spp*., including homologues of VfENOD-GRP5 (Jiménez-Zurdo et al., 2000; Györgyey et al., 2000). The *nodGRP* gene family in *M. sativa* was first characterized through nodule-specific cDNA library screenings, which revealed four genes (nodGRP1-4) encoding small GRPs characterized by an N-terminal hydrophobic signal peptide and a glycine-rich C-terminal region (Jiménez-Zurdo et al., 2000) (Fig. 10.b). While glycine-rich repeats represented the major structural feature, not all proteins contained distinct repetitive blocks, and many lacked the canonical glycine-rich motifs typical of non-nodule-specific GRPs (Kevei et al. 2002). Expression analyses revealed that all these genes were strictly nodule-specific, being activated only upon infection by

rhizobia, though the onset and intensity of expression varied across different stages of nodule development (Kevei et al., 2002).

The discovery of *nodGRP* genes in the model legume *M. truncatula* was achieved through BLAST searches to identify homologous genes, by mainly focusing on the highly conserved signal peptide regions of the *nodGRP*s. They uncovered multiple related genes distributed across six regions of the *M. truncatula* genome. This comprehensive analysis led to the identification of several new members of the *nodGRP* gene family, including *nodGRP1D–L*, *nodGRP2C–D*, and *nodGRP3A–C*, thereby expanding the known diversity and genomic organization of this nodule-specific gene family (Fig. 10.c and Fig. 11.). Interestingly, the nodGRPs share a key feature with NCRs - the presence of a signal peptide – indicating that they are secreted proteins. On the other hand, they resemble less to canonical GRPs, containing only 20–30 % glycine residues and lacking recognizable glycine-rich motifs. Moreover, their signal peptide sequences display unique characteristics not shared with those of GRPs from other plant species, further supporting their functional specialization within IRLC legumes (Kereszt et al. 2018).

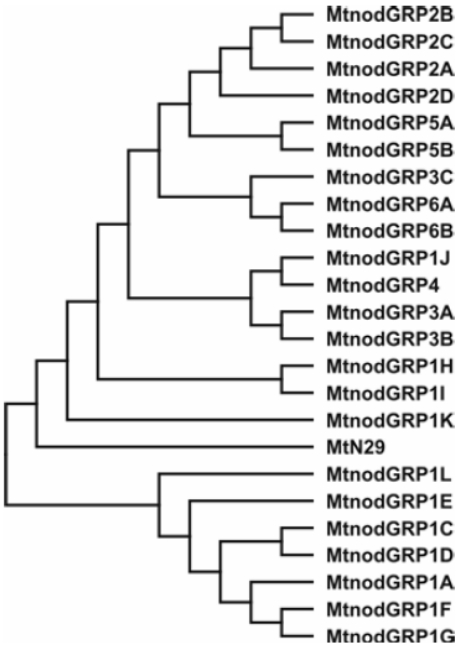

Figure 11. Phylogenetic relationship between nodGRPs in *M. truncatula* based on the amino acid sequence of the proteins (Alunni et al., 2007)

1.4.5. The nodGRP1 family in *M. truncatula*

Alunni et al. (2007) mapped 23 nodGRPs belonging to six subgroups in *M. truncatula* at that time. The phylogenetic comparison of the 23 MtnodGRP proteins divided them into two major groups separating most nodGRP1 proteins (nodGRP1A, nodGRP1C, nodGRP1D, nodGRP1E,

nodGRP1F, nodGRP1G, nodGRP1L) from the others (Figure 6). The *nodGRP1* genes are found in one contig that contains 11 genes scattered in a 270-kb region of the chromosome 5, but eight of them are within a 70-kb distance (Alunni et al., 2007) (Figure 7a). They are composed of 2-3 exons, where most of the first exon (approximately 80 bp) codes for the signal peptide and the second exon (between 200 and 700 bp) for the glycine rich domain (Figure 7b).

The *nodGRP1A*, *nodGRP1D*, *nodGRP1E*, *nodGRP1F*, and *nodGRP1G* genes are closely clustered, while the six other genes in the *nodGRP1* contig, namely *nodGRP1C*, *nodGRP1H*, *nodGRP1I*, *nodGRP1J*, *nodGRP1K*, and *nodGRP1L*, are distributed more widely along the contig. While the gene products of the latter genes share similar signal peptide sequences, their glycine-rich domains exhibit considerable divergence. This pattern suggests that the duplication events giving rise to nodGRP1C, H, I, J, K and L occurred earlier than those leading to the formation of the more recently duplicated subgroup comprising nodGRP1A, D, E, F and G. This evolutionary scenario is further supported by the presence of numerous intervening genes and the greater genomic distances separating the presumably older nodGRP1 members. Among these nodule-specific GRPs we conducted functional studies of several members that have specific expression patterns in the nodule development zones. My PhD thesis work focused on nodGRP1L.

Contig name[a]	Genes	Orientations in contig	ORF coding exons
MtnodGRP1A/C/D/E/F/G/H/I/J/K/L	11	+/+/+/+/+/+/-/+/+/-/+	2/3/2/2/2/2/2/2/2/2/2

Figure 12. (a) Genomic organization of the *nodGRP1* contig in *M. truncatula*. The Mtnod *GRP1* contig contains 11 GRP1 genes (called GRP1A to GRP1L). The location and orientation of genes are indicated by arrows. Genes and intergenic regions are not drawn on a scale. Black arrows represent the GRP genes. (b) Genomic organization of GRP clusters. (Modified from Alunni et al., 2007)

1.4.6. Selection of nodule-specific GRP1L

The *nodGRP1L* gene encodes a short protein of 113 amino acids, consisting of a 21-amino-acid N-terminal signal peptide and a 92-amino-acid mature domain. The signal peptide targets the nascent protein to the secretory pathway, facilitating its translocation. The mature region is notably glycine-rich, containing 17 glycine residues, which make up approximately 18% of its total amino acid composition. The nodGRP1L peptide exhibits an anionic nature, with an isoelectric point (pI) of (5.032), and a negative net charge of (-3.874) at physiological pH (7.4).

This charge property may play a key role in mediating its interactions with other proteins or cell wall components within the nodule environment. Expression analyses reveal that *nodGRP1L* is induced in the proximal infection zone, reaches its maximum expression in the interzone, and remains weakly expressed in the nitrogen fixation zone. Moreover, nodGRP1L exhibits a markedly higher expression level than other *nodGRP* genes (Roux et al., 2014), suggesting its potential significance in nodule development and function.

1.5. Antimicrobial peptides

Both NCRs and nodGRPs are related to antimicrobial peptides (AMPs), which are small naturally occurring molecules that act as natural antibiotics and form a fundamental component of the innate immune defense in nearly all living organisms. Typically, AMPs are short, about 10 to 50 amino acids in length, amphipathic peptides and mostly positively charged (cationic); and these properties allow them to bind electrostatically to negatively charged microbial membranes (Maroti et al., 2011). This interaction is often followed by membrane permeabilisation or disruption, and/or may also involve targeting essential intracellular components. AMPs can be produced through both ribosomal and non-ribosomal biosynthetic pathways, or by enzymatic cleavage of larger precursor proteins (Wang, 2022). To date, over 5600 naturally occurring AMPs have been identified across diverse species (Antimicrobial Peptide Database; https://aps.unmc.edu), yet only 270 of them are of plant origin, despite plants representing an exceptionally rich and diverse source of such molecules (Tang et al., 2018). From an evolutionary perspective, AMPs represent one of the most ancient and conserved defense mechanisms, providing critical protection that contributed to the successful evolution of complex multicellular life forms (Ageitos et al., 2017). They act as host defense peptides, capable not only of direct antimicrobial action but also of modulating immune responses, making them promising candidates for developing new drugs and therapies. A defining feature of AMPs that distinguishes them from classical antibiotics is their ability to act on multiple targets, such as microbial membranes, thereby reducing the likelihood of resistance development (Spohn et al., 2019). Furthermore, their relatively simple structure and responsiveness to mutagenesis or peptide engineering have enabled the design of numerous synthetic derivatives with enhanced antimicrobial activity and reduced cytotoxicity (Mazu et al., 2016).

1.5.1. Antimicrobial peptides classification

Based on their biological source, AMPs are broadly categorized into five main groups: viral, bacterial, fungal, plant, and animal-derived peptides.

- **Bacterial AMPs:** often termed bacteriocins and vary widely in length 10–100 amino acids long, produced by both Gram-positive and Gram-negative bacteria. In Gram-positive bacteria, they can be ribosomally synthesized or produced via enzymatic pathways (non-ribosomal) (Tajbakhsh et al., 2017).
- **Fungal AMPs:** mainly consist of two families: fungal defensins and peptaibols. Fungal defensins are cysteine-rich peptides with disulfide-bridge that stabilize β-sheet structures (Qi et al., 2022), granting resistance to proteolysis and thermal denaturation. Peptaibols, typically 5–21 amino acids long, are distinguished by their inclusion of non-proteinogenic residues (Leitgeb et al., 2007).
- **Plant-derived AMPs:** constitute a structurally and functionally diverse family forming a crucial line of defense against microbial pathogens. Most plant AMPs are cysteine-rich and form multiple disulfide bridges, providing high structural stability and resistance to proteolysis, heat, and pH changes. These include thionins, which are short, cationic peptides with antibacterial and antifungal activities (Stec, 2006); hevein-like peptides, characterized by chitin-binding domains that target fungal cell walls (Slavokhotova et al., 2017); and defensins, which contain cysteine-stabilized αβ motifs conferring potent antimicrobial resistance to various environmental conditions (Lima et al., 2022). Other important families include knottin-type peptides (or cystine-knot peptides), which exhibit enzyme inhibition and antiviral activities (Pallaghy et al., 1994); lipid transfer proteins (LTPs) that mediate lipid exchange between membranes and possess antifungal properties (Carvalho & Gomes, 2007); snakins, which contain 12 conserved cysteines and exhibit antimicrobial and antinematode effects (Su et al., 2020); and cyclotides that are macrocyclic peptides stabilized by a cystine knot motif, and known for antibacterial, antiviral, and anticancer properties (Dini et al., 2022).
- **Animal-derived AMPs:** represent the most studied group, encompassing thousands of peptides identified across invertebrates and vertebrates. The major AMPs are defensins which are small cysteine-rich peptides that target microbial membranes. Animals like fishes, amphibians, reptiles and birds produce potent AMPs with strong antibacterial activity. Mammalian AMPs are primarily represented by defensins (α-, β-, and θ-defensins) and cathelicidin. These peptides not only disrupt bacterial membranes but also modulate immune responses (Zhang et al., 2025).

1.5.2. Structural classification of antimicrobial peptides

AMPs display remarkable structural and functional diversity, and their classification can be approached from multiple perspectives. Based on conformational characteristics, AMPs are grouped into five major classes: α-helical peptides, β-sheet peptides, structured linear peptides and mixed structure or can be disordered (Büyükkiraz et al., 2022).

The α-helical peptides represent the most extensively studied group. Typically composed of 12–40 amino acids and rich in helix-promoting residues such as alanine, leucine, and lysine, these peptides adopt amphipathic α-helical structures upon membrane binding. Their helical nature facilitates deep insertion into lipid bilayers, leading to membrane permeabilization and cell death. In contrast, β-sheet peptides are stabilized by two or more disulfide bridges linking β-strands, forming rigid, conformationaly stable structures. Members of this group include defensins**.** Mixed structure AMPs**,** combining α-helices and β-sheets, are found across diverse taxa and retain stability through multiple disulfide bonds. Structured linear AMPs lack well-defined secondary structures and are often rich in glycine, proline, histidine, or tryptophan residues, conferring flexibility and enabling varied target interactions. They can also be disordered with a flexible structure which can help interaction of peptides with microbial membrane and formation of a stable conformation.

In addition to structure, AMPs may also be categorized by amino acid composition (Huan et al., 2020). Glycine-rich AMPs are flexible and capable of targeting multiple cellular components, whereas cysteine-rich AMPs stabilize β-sheet motifs via disulfide bonds, facilitating pore formation. Arginine-, lysine-, or leucine-rich AMPs commonly form amphipathic α-helices with strong membrane affinity. Hydrophobicity and amphipathicity are critical determinants of antimicrobial potency: highly hydrophobic peptides insert deeply into lipid bilayers, while moderately hydrophobic AMPs rely on cooperative aggregation for effective permeabilization.

1.5.3. Mechanisms of actions of antimicrobial peptides

Based on their mechanisms of action, AMPs can be classified into two main categories: membrane-disrupting peptides and non-membrane-targeting peptides, although many AMPs can display a combination of both behaviors simultaneously (Brogden et al., 2005)

1.5.3.1. Membrane-disrupting peptides

The majority of AMPs execute their antimicrobial effects by directly compromising membrane integrity. Electrostatic attraction between the cationic peptides and negatively charged

microbial surfaces facilitates selective binding, followed by insertion and destabilization of the lipid bilayer. Several mechanistic models are described (Singh et al., 2023) (Fig. 13.):

- **Barrel-stave model:** Peptides initially align parallel to the membrane, then insert perpendicularly to form transmembrane pores resembling barrels with the peptides acting as "staves." This leads to leakage of cytoplasmic contents.
- **Toroidal pore model:** Peptides induce continuous bending of lipid monolayers, integrating both peptides and lipids within the pore structure. These pores are transient and less stable than barrel-stave pores.
- **Carpet model:** Peptides accumulate parallel to the membrane, covering it like a carpet. Once a threshold concentration is reached, they disrupt the bilayer in a detergent-like manner, leading to micellization and rupture.
- **Molecular electroporation model:** Peptides bound to the membrane generate electric potential differences; once the potential difference exceeds ~0.2 V, transient pores form, causing ion imbalance and cell lysis.
- **Sinking raft model:** Amphipathic AMPs preferentially bind specific lipid domains, induce local curvature and mass imbalance that generate transient pores upon peptide aggregation.
- **Aggregate (channel-forming) model:** Peptides form unstructured aggregates upon membrane insertion, often associating with water molecules to produce transient channels that allow leakage of ions and metabolites.
- **Peptide-induced lipid segregation model:** Some AMPs trigger phase separation of anionic peptide from zwitterionic lipids, forming lipid–peptide domains that alter membrane curvature and permeability. Arouri et al. (2009) demonstrated this effect in PG/PE membranes, suggesting that lipid segregation underlies the specificity of AMPs toward bacterial membranes.
- **Leaky slit model:** The insertion of lipid-protein aggregates increases the positive curvature in the membrane which causes transient leakage in the cell membrane (leaky slit) and thus enhances membrane permeabilization.

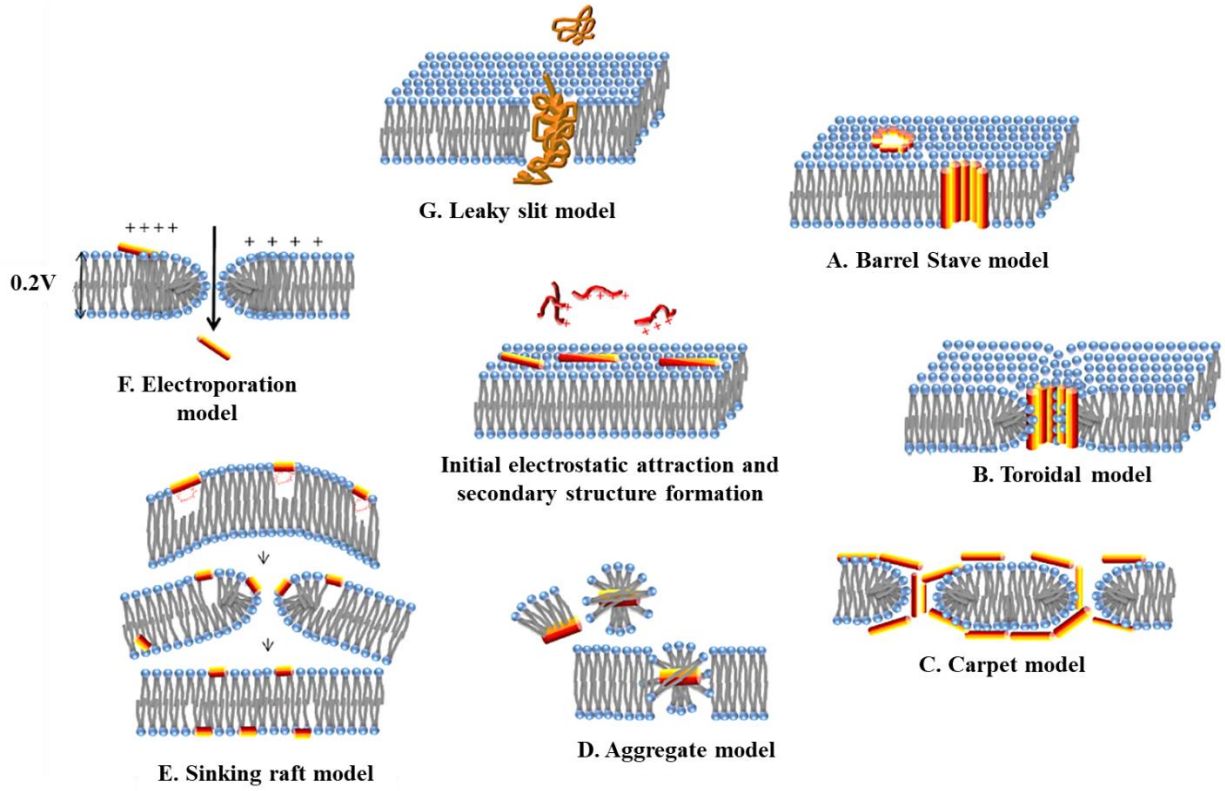

Figure 13. Mechanisms of action of the membrane-disrupting. (A) barrel stave model, (B) toroidal model, (C) carpet model, (D) aggregate model, (E) sinking raft model, (F) electroporation, and (G) leaky slit model (Singh et al., 2023).

These models illustrate that membrane disruption is not restricted to a single universal process but rather encompasses multiple dynamic and context-dependent pathways.

1.5.3.2. Non-Membrane Targeting peptides

Beyond membrane disruption, several AMPs traverse the bilayer to interfere with vital intracellular processes (Lin et al., 2021). Some inhibit protein synthesis or folding and impede enzyme activity, while others bind to nucleic acids interfering with replication and transcription or bind ribosomes halting translation. This demonstrates that AMPs can exert potent intracellular toxicity independent of lytic membrane disruption. AMPs can even modulate the immune or stress-related systems of pathogenic microbes. For example, Shang et al. (2021) reported that tryptophan-rich AMPs suppress quorum sensing and virulence genes in the pathogenic bacterium *Pseudomonas aeruginosa*, and Hayes et al. (2013) showed that the plant defensin NaD1 activates the HOG stress-response pathway in the fungus *Candida albicans*. AMPs can modulate host immune responses, allowing beneficial bacteria to survive inside the plant such as nodule-specific NCR peptides that act on their symbiotic partner, *Sinorhizobium meliloti*, where they reprogram bacterial gene expression and suppress stress responses (Van de

Velde et al., 2010). This demonstrates that while some AMPs act on pathogens, others like NCRs modulate the physiology of valuable microbes within the host.

1.5.4. Antimicrobial peptides are less prone to resistance development and possess broad application potential.

AMPs are considered as next-generation therapeutic agents against multidrug-resistant microbial infections (Bechinger et al., 2017). Unlike conventional antibiotics that typically act on specific molecular targets, AMPs exert their antimicrobial action through multiple modes, including membrane disruption and intracellular interference. This multifaceted activity greatly reduces the likelihood of bacteria developing stable resistance (Browne et al., 2020). Nevertheless, some adaptive strategies have been reported that enable bacteria to partially tolerate AMP exposure. One of the most common resistance mechanisms involves modification of the bacterial cell surface, since the cell envelope is the primary site of AMP interaction. Alterations in membrane charge, hydrophobicity, and fluidity can diminish electrostatic attraction between cationic peptides and the negatively charged bacterial surface, thereby reducing AMP binding and insertion (Joo et al., 2016). Another widespread strategy is proteolytic degradation, where bacteria secrete extracellular proteases that cleave the peptides before they reach their targets. The efficiency of this mechanism depends strongly on the structure of the peptide, but many bacterial proteases have limited substrate specificity (Pfalzgraff et al., 2018). Additional resistance mechanisms include efflux pumps, which actively expel substances from the cytoplasmic membrane, and the presence of capsular polysaccharides or other surface polymers that act as physical barriers limiting AMP access to the membrane (Abdi et al., 2019). Moreover, biofilm formation is known to significantly enhance bacterial tolerance to AMPs. Within biofilms, the extracellular polymeric matrix impedes AMP penetration and facilitates the survival of the cells (Singh et al., 2025). Conventional antibiotic resistance often develops through a specific mutation in a single gene or through the acquisition of a resistance gene via horizontal gene transfer. In contrast, microbes cannot counter the multifaceted actions of AMPs by altering a single gene; doing so would require the simultaneous acquisition of multiple resistance strategies, making them promising candidates as alternatives or complementary agents to traditional antibiotics (Hancock et al., 2006; Silva & Gomes, 2017).

AMPs have emerged as promising candidates to address the escalating problem of multidrug-resistant infections due to their broad-spectrum activity and unique mechanisms of action. AMPs can be employed either individually or in combination with conventional antibiotics,

antivirals, or other antimicrobial agents to produce synergistic therapeutic effects (Gordon et al., 2005). Their versatile biological functions have led to potential applications across multiple fields, including food preservation, agriculture, environmental protection, animal husbandry, and pharmaceutical development (Tscherner et al., 2011). Currently, over 100 peptide-based drugs have received approval from the U.S. Food and Drug Administration (FDA), while more than 400 peptide candidates are in various stages of clinical evaluation (Xiao et al., 2025). In the food industry, AMPs can function as natural preservatives or be integrated into antimicrobial packaging materials to extend product shelf life. The bacteriocin nisin is an example for AMPs that is effective against foodborne pathogens. Another example is the lactoferrin that has been approved to be used as an antimicrobial additive in meat products (Villalobos-Delgado et al., 2019). Beyond food applications, AMPs show significant potential in animal husbandry, where they may serve as alternatives to antibiotic feed additives, promoting both growth performance and disease resistance. Furthermore, numerous AMPs exhibit antiviral properties, demonstrating efficacy against pathogens such as severe acute respiratory syndrome coronavirus (Elnagdy et al., 2020), porcine epidemic diarrhea virus (Guo et al., 2015), transmissible gastroenteritis virus (Liang et al., 2020), infectious bronchitis virus (Sun et al., 2010), and influenza A virus (Hsieh & Hartshorn, 2016). In agriculture, AMPs offer an environmentally friendly alternative to synthetic pesticides, which are heavily used to prevent crop loss but contribute to pollution and adverse health effects (Rekha et al., 2006). AMPs can protect plants from phytopathogens without posing risks to humans, animals, or ecosystems (Zasloff et al., 1987).

1.5.5. Rational design and production strategies for antimicrobial peptides

Recent advances in peptide engineering have enabled the rational design of synthetic AMPs derived from natural sequences to improve their potentials. This approach focuses on retaining functional antimicrobial motifs while removing toxic or protease-sensitive regions, thereby improving safety and stability (Ciumac et al., 2019). Several sequence modification strategies have been employed, including truncation, amino acid substitution, hybridization, and cyclization. Minor alterations in amino acid composition can significantly influence conformation, charge distribution, and hydrophobicity, ultimately modifying biological activity. For instance, truncated peptides derived from natural AMPs are more cost-effective to produce, while cyclic peptides exhibit enhanced stability and membrane permeability compared to linear analogs. Moreover, hybrid peptide design, which merges fragments from different AMPs, allows the combination of high activity with low cytotoxicity, yielding novel chimeric

AMPs optimized for therapeutic use (Buyukkiraz et al., 2022). Chemical synthesis of AMPs is typically performed via solid-phase peptide synthesis (SPPS), which is well-suited for short peptides. However, the production of longer sequences (>35 amino acids) or peptides requiring post-translational modifications increases complexity and cost (Cao et al., 2018). Additionally, SPPS often involves the use of high concentrations of hazardous chemicals, generating environmentally detrimental waste products (Chan et al., 1999). To overcome these limitations, recombinant expression systems provide a cost-effective and scalable alternative. Several microbial hosts have been successfully employed to produce heterologous proteins and endogenous AMPs, offering a promising approach for large-scale peptide production.

1.5.6. Physicochemical properties of NCRs play a role in the antimicrobial activity

As mentioned above, *M. truncatula* produces several hundreds of nodule-specific cysteine-rich peptides (NCRs). These peptides have a great diversity in their physicochemical properties, as reflected by the wide range of the isoelectric point (pI) of the peptides (Lima et al., 2022). Computational prediction tools were applied to estimate the antimicrobial potential of more than a hundred NCR peptides; however, their predictions did not always align with experimental outcomes. Fifty peptides exhibited antimicrobial activity in the tests against at least one of the ESKAPE bacterial pathogens *(Enterococcus faecalis*, *Staphylococcus aureus*, *Klebsiella pneumoniae*, *Acinetobacter baumannii*, *Pseudomonas aeruginosa*, *Escherichia coli*) as well as *Listeria monocytogenes* and *Salmonella enterica*, differing in both spectrum and potency. The most active NCRs eradicated bacteria at concentrations ranging from 0.8 to 3.1 μM. While a high positive net charge contributed significantly to activity, this was not the sole determinant. Whereas many of the cationic NCR peptides exhibited antibacterial activities *in vitro*, several NCRs with high isoelectric points (pI) and positive net charges, predicted to be antimicrobial, showed no activity in laboratory assays (Fig. 14.).

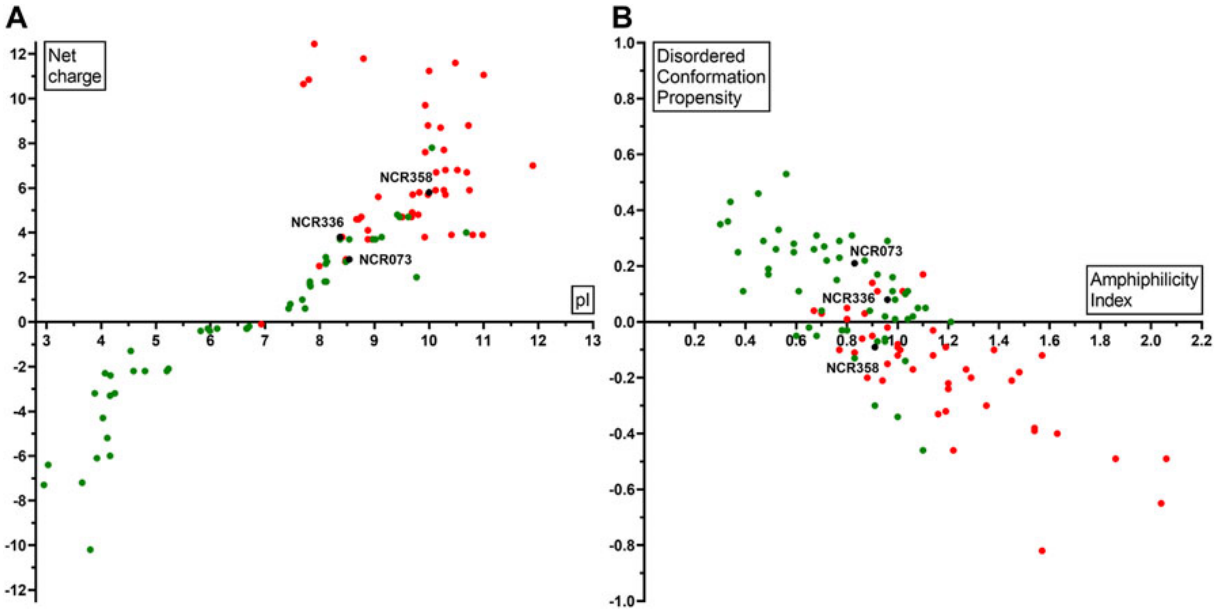

Figure 14. Physicochemical properties of NCRs in correlation with their antimicrobial activity (A) pI (X axis) and net charge (Y axis) values; (B) Amphiphilicity Index (X axis) and Disordered conformation propensity (Y axis) values in correlation with the antimicrobial activity. Black dots show NCR073, NCR336, NCR358 which are active against all the eight tested pathogens. Red dots represent NCRs which are active against at least one pathogen. Green dots indicate the inactive NCRs (Lima et al., 2022).

Accordingly, active and inactive peptides were compared based on their net charge, isoelectric point (pI), structural disorder propensity, and amphiphilicity index. The analysis confirmed that while a high pI and positive net charge are key contributors to antimicrobial activity, they are not sufficient on their own (Fig. 14.A). NCR peptides with a net charge above +2 can display activity, but nearly all peptides with a charge greater than +5 were antimicrobial. Additionally, most of the active NCRs exhibited higher structural disorder and amphiphilicity index (Fig. 14.B), suggesting that their antimicrobial potential likely arises from an increased capacity to adopt secondary structures at membrane–water interfaces (Lima et al., 2022).

Among the cationic NCR peptides, NCR073, NCR336, NCR358 (Lima et al. 2022), NCR247, NCR335 (Tiricz et al., 2013), NCR044 (Velivelli et al., 2020) and NCR169 (Isozumi et al., 2021) exhibit broad-spectrum antimicrobial activity, whereas others with a similar positive net charge do not, indicating that the amino acid sequence also plays a key role in determining antimicrobial potency (Lima et al., 2022).

1.5.7. Several members of NCR peptides were characterized for their antimicrobial activity

The bactericidal effect of NCR247 and NCR335 was evaluated against a selection of Gram-negative and Gram-positive pathogenic bacteria using a high peptide concentration (50 μg/mL) in phosphate–potassium buffer (PPB). The natural symbiont *S. meliloti* was tested first, and both peptides reduced the viable cell number by three to four orders of magnitude. When further tested against a range of human/animal pathogens (*Escherichia coli, Salmonella typhimurium, Pseudomonas aeruginosa, Staphylococcus aureus, Listeria monocytogenes, Bacillus cereus, Bacillus megaterium*) and plant pathogens (*Xanthomonas campestris, Clavibacter michiganensis, Agrobacterium tumefaciens*), both NCR peptides - despite displaying different activity spectra - significantly reduced the number of viable cells across all tested species, ranging from at least a tenfold decrease to complete elimination (Tiricz et al., 2013; Mikuláss et al., 2016). NCR247 exhibited strong antimicrobial activity in PPB buffer against *E. coli* and *Bacillus subtilis*, and moderate activity against *Saccharomyces cerevisiae*. In contrast, NCR335 showed potent, broad-spectrum activity against all these organisms, matching or exceeding the effectiveness of the control antibiotics streptomycin (STM) and polymyxin B (PMB). The greatest sensitivity was observed in *B. subtilis*, which was more susceptible to both NCR peptides than to STM or PMB. However, when tested in Mueller–Hinton medium, the antimicrobial activity of the NCR peptides decreased for all microorganisms, likely due to the presence of divalent cations, which compete with binding of cationic AMPs with bacterial membranes, indicating a potential limitation in their application under such conditions that needs to be overcome for their practical applications (Hancock & Sahl, 2006). As a next step in their analyses, various derivatives of NCR247, including shorter fragments and various chimeric derivatives were tested for their antimicrobial activity (Jenei et al., 2020). While the positive charge of the AMPs is essential for killing, in the case of the C-terminal fragment of NCR247 (NCR247C) the increased positive charge did not result in the improvement of the antimicrobial activity. Adding the neutral StrepII tag or extending the N- or the C- terminus with extra amino acids to create chimeric peptides improved either slightly or significantly the antibacterial properties (Jenei et al., 2020).

In another study the potential antifungal ability of 19 cationic NCRs was tested against the yeast and the filamentous forms of *Candida albicans, C. glabrata, C. krusei*, and *C. parapsilosis*. These *Candida* species are the cause of fungal infections in humans and often show resistance to antifungal drugs. NCR247 and NCR335, together with other cationic NCRs such as NCR192, NCR137, NCR147, NCR280, NCR183, NCR247, NCR044 and NCR030 exhibited

anticandidal activity at a concentration range from 1.42 to 10.5 μM, which was comparable to the conventional drug amphotericin B (Ördögh et al. 2014). In this study, the weakly cationic NCR169 peptide did not show antifungal characteristics. On the other hand, in subsequent studies, its strongly cationic C-terminal fragment (NCR169C_{17-38}) exhibited potent antifungal activity against human-pathogenic *Candida* and *Cryptococcus* species (Szerencsés et al., 2021 and 2025). The antimicrobial potential and the structure of NCR169, its oxidized form, and its shorter derivatives were recently evaluated by Isozumi et al. (2021), revealing that the two oxidized forms of NCR169 displayed antimicrobial activity against both *E. coli* and *S. meliloti*. Given its strong anticandidal activity, NCR169$C_{17–38}$ was further evaluated against the clinically significant ESKAPE pathogens, where it demonstrated remarkable efficacy. Several amino acid substitutions were designed in NCR169$C_{17–38}$, and the new peptide derivatives were tested for their antibacterial activity (Howan et al., 2023). To assess the role of the disulfide bridge, the two cysteine residues were substituted with serines. This modification unexpectedly enhanced antimicrobial activity against most tested bacteria, revealing that disulfide bond formation is not essential for function. The role of tryptophan residues which can facilitate interactions with bacterial membranes membranes was investigated by substitution of tryptophan with alanine or 5-fluoro-typtophan and the latter modification improved the antimicrobial potency.

1.5.8. NCR peptides exhibit no detectable cytotoxic or hemolytic effects

A major limitation of potent AMPs particularly from animal sources is their cytotoxicity toward mammalian cells. NCRs from edible legume plants behave differently. Cationic antimicrobial NCRs were tested by by Lima et al. (2022) for hemolysis of human red blood cells (HRBC) (Fig. 15.). Compared to the detergent-lysed controls (Triton X-100), none of the peptides provoked hemolysis of HRBC above the background level even at 100 μM concentration except one peptide (MsNCR465), which provoked limited hemolysis at 50 and 100 μM (Fig. 15).

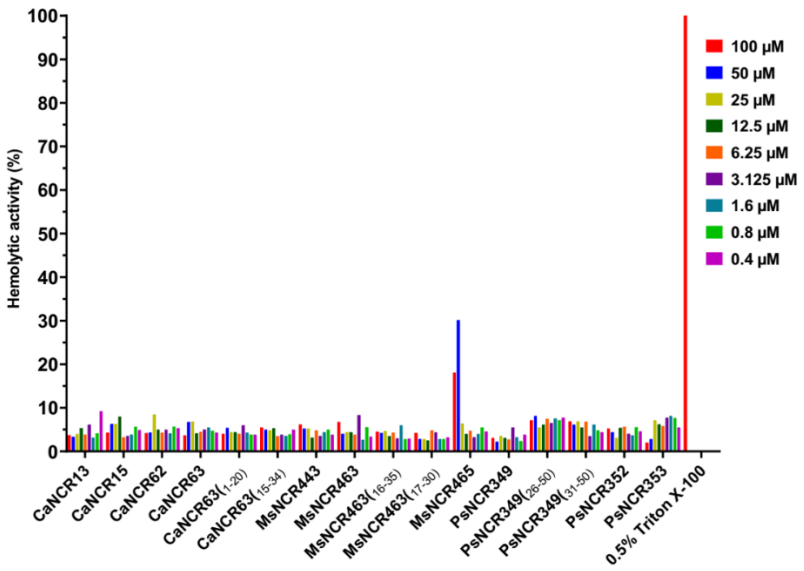

Figure 15. Hemolytic activity of NCRs. Human red blood cells were treated with different NCRs with different concentrations (0.4 -100 µM). Hemolysis of red blood cells with 0.5% Triton X=100 represents 100% hemolytic activity on the right of the x axis (Lima et al., 2022).

The same result was reported for NCR169C$_{17–38}$ and four of its most active derivatives as none of the peptides caused lysis of human red blood cells (Howan et al., 2023). Cytotoxicity assays were also performed on mouse macrophages that confirmed minimal or no toxicity at therapeutically relevant concentrations of the most active NCR peptides studied by Szerencsés et al. (2025), reinforcing their favorable safety profile for antifungal applications. Similarly, NCR peptides exhibiting anti-*Candida* activity showed no or only moderate cytotoxicity toward human keratinocytes (Szerencsés et al. 2021), in contrast to conventional antifungal agents such as amphotericin B, whose cytotoxicity can restrict therapeutic use. The non-hemolytic nature of NCR peptides and their derivatives is further supported by the NCR247C peptide and its chimeric variants. Despite exhibiting high antibacterial activities, these peptides did not show hemolytic activity toward human red blood cells (Jenei et al., 2020).

Collectively, these favorable properties highlight plant-derived peptides as a promising and underexploited source of antimicrobial peptides, providing a strong foundation for their development as safe, effective, and versatile antimicrobial agents across medical, agricultural, and biotechnological applications.

2. Aims

This study aims to deepen our understanding of the symbiotic peptides of *M. truncatula*. My PhD work is composed of two parts, one related to nodule development (I) and the other to potential applications (II)

I.

The nodule-specific glycine-rich peptides (nodGRPs) represent a poorly characterized family but their developmental stage-specific expression during symbiotic cell maturation suggests a crucial role in the symbiotic process. I focused on the elucidation of the function of *nodGRP1L* in development of nitrogen fixing root nodules with answering the following questions:

1. Is nodGRP1L essential for nodule development?
2. How does nodGRP1L affect the physiology of symbiotic cells?
3. Does nodGRP1L interact with the bacterial membranes?
4. Does nodGRP1L bind to bacterial or other symbiotic plant proteins?
5. How is nodGRP1L regulated?

II.

Building on previous findings concerning the antibacterial activity of NCR169 peptide and its derivatives, this work focused on NCR169$C_{17–38}$ aiming to characterize its antibacterial action using a combination of microbiological, biochemical, biophysical, and molecular approaches.

1. Assess the antimicrobial activity of short NCR169 fragments, including the C-terminal region (NCR169C_{17-38}).
2. Examine potential synergistic effects between NCR169C_{17-38} and conventional antibiotics, as well as other NCR-derived peptide fragments.
3. Determine the impact of NCR169C_{17-38} on the bacterial biofilm formation and the viability of the bacterial cells within.
4. Investigate the membrane-permeabilizing effects of NCR169C_{17-38} on bacterial cells.
5. Characterize the ability of NCR169C_{17-38} to interact with different bacterial targets.
6. Analyze differential gene expression in *E. coli* exposed to NCR169C_{17-38}.

3. Materials and Methods

3.1. Plant material and growth conditions

We used different plant ecotypes. The Jemalong A17, and R108 ecotypes of *M. truncatula* were used as wild-type controls in our experiments. Seeds extracted from pods were incubated in 96% sulfuric acid (H_2SO_4) for 8 minutes, which opens pores in the seed coat, and then rinsed at least three times in ice-cold distilled water to avoid burning the seeds due to the exothermic reaction. The seeds were then sterilized by hypochlorite (3%) and washed five times in distilled water. The sterilized seeds were incubated on a 0.8% inverted water agar plates at 4 °C for 1 night at least, then kept at room temperature overnight for germination.

The plants were grown under long-day light conditions (16 h light/8 h dark) at 25 ºC in a greenhouse. All of the experiments were performed in sterilized zeolite. The medium was low-nitrogen Fahreus (*Medicago truncatula* Handbook, https://www.noble.org/medicago-handbook) and was watered every two days to maintain adequate moisture for plant development.

3.2. Bacterial strains and growth conditions

3.2.1. Competent *Escherichia coli* Top10 cells, preparation and transformation.

A single colony of *E. coli* Top10 was inoculated into LB medium and incubated at 37 °C with shaking overnight. The overnight culture was diluted at a 1:200 ratio and grown at 37 °C with shaking until (OD_{600}) reached 0.3 to 0.4. The culture was then chilled on ice for 1 hour and centrifuged at 7,000 K for 6 minutes at 4 °C. The pellet was resuspended in an ice-cold 0.1 M $CaCl_2$ solution at a 1:4 ratio of the original culture volume. The resuspended cells were incubated on ice for 4 hours to increase cell wall permeability to DNA, followed by another centrifugation at 7,000 K for 6 minutes at 4 °C. The pellet was then resuspended in 0.1 M $CaCl_2$. Glycerol was added to a final concentration of 10%, and the competent cells were aliquoted into pre-chilled sterile tubes, frozen in liquid nitrogen, and stored at -80 °C.

Constructs were introduced into *E. coli* strain Top10 competent cells using the heat shock method. Competent cells were thawed by incubating on ice for 15 minutes. Four µl of reaction mix containing 150 ng/ul DNA was combined with the thawed *E. coli* Top10 competent cells and incubated on ice for 30 minutes to facilitate DNA uptake. To enhance membrane permeability, samples were placed into a 42 °C thermo block for 1 minute and subsequently cooled down by leaving on ice for 5 minute. After that it was transferred to a 37 °C shaking incubator for one hour to allow for recovery and expression of antibiotic resistance markers.

The suspension was centrifuged at 4,000 K for 5 minutes to pellet the cells, then the pellet was resuspended in 100 µl of the supernatant. This suspension was spread onto solid LB agar plates containing the corresponding antibiotics for selection of the transferred vectors. Bacteria were cultured overnight at 37 °C.

3.2.2. Competent *Agrobacterium rhizogenes* Arqua1 cells, preparation and transformation

A single colony of *A. rhizogenes* Arqua1 was inoculated into LB liquid medium and cultivated with shaking overnight. The overnight culture was diluted at a 1:100 ratio in fresh LB medium and grown at 37 °C with shaking until (OD_{600}) reached 0.4 to 0.5. The culture was subsequently cooled on ice for 15 minutes and centrifuged at 7,000 K for 5 minutes at 4 °C. The pellet was gently resuspended in 10 ml chilled 10% glycerol solution, then the bacterial culture was centrifuged for 5 minutes at 7,000. The supernatant was poured off, and this washing step was repeated for at least four cycles in 10% glycerol. Eventually the competent cells were resuspended in 10% glycerol to make a 100x concentration of the initial culture, and then were aliquoted into pre-chilled sterile tubes, frozen in liquid nitrogen, and stored at -80 °C.

A. rhizogenes Arqua1 competent cells were thawed on ice, mixed with 1–3 µl of plasmid DNA (<100 ng),) and incubated on ice for 10 min. The mixture was then introduced into a pre-chilled 1-2 mm cuvette. The cuvette was placed in BIO-RAD GenePulser XcellTM, and a high voltage shock (2.5 kV, 4-9 ms) was applied. After electroporation, 750 µl of LB was added to recover the cells. The samples were subsequently transferred to a microcentrifuge tube and incubated at 30 °C for 1 hour. Following incubation, samples were centrifuged at 4,000 K for 1 minute. The 100 µl of the cell culture was plated onto solid LB media supplemented with the corresponding selective antibiotics for the transformed plasmids and incubated at 30 °C for 48 hours.

3.2.3. Bacteria used for plant inoculation

Sinorhizobium medicae WSM419 and *Sinorhizobium meliloti* Rm41 cultures were grown in TA medium at 30 °C for 48 hours. Plants were then inoculated with a bacterial suspension adjusted to an optical density of OD_{600} = 0.6 - 0.8. The inoculum was resuspended in low-nitrogen Fahreus medium and applied to the surface of sterile zeolite surrounding the seeds. Following inoculation, plants were maintained in a growth chamber under a 16-hour light / 8-hour dark photoperiod at 22 °C. Most experiments were conducted using sterilized zeolite, in accordance with the guidelines provided in the *Medicago truncatula* Handbook. Plants were supplied with low-nitrogen Fahreus medium twice weekly to maintain adequate moisture for proper growth and nodule development.

3.2.4. Bacteria used for hairy root transformation

To prepare a culture for hairy root transformation, *A. rhizogenes* Arqua1 bacteria carrying the proper vector were grown on LB agar containing the selective antibiotics and incubated at 30 °C or 2 days prior to transformation, which resulted in a dense bacterial lawn on the agar surface for subsequent experiments.

3.2.5. Bacteria used for infiltrating *Nicotiana benthamiana* leaves

For transient gene expression in *N. benthamiana* leaves, *A. tumefaciens* C58C1 strain was used. This strain carries virulence genes on the pCh32 plasmid, thereby efficiently transforms plant cells. For the preparation of *A. tumefaciens* C58C1 competent cells and plasmid introduction, the same method was used as described for *A. rhizogenes* Arqua1. *A. tumefaciens* C58C1 carrying the different plasmid constructs were grown on LB medium supplemented with the appropriate antibiotics at 30 °C for two days, cells were collected, and resuspended in MMA buffer (10 mM MES, pH 5.6; 10 mM $MgCl_2$; 20 μM acetosyringone, Sigma-Aldrich). The optical density at 600 nm (OD_{600}) was adjusted to 0.2.

3.2.6. Bacterial strains used in antimicrobial assays

The Gram-positive *Enterococcus faecalis* (ATCC 29212), *Staphylococcus aureus* (HNCMO112011), and *Listeria monocytogenes* (ATCC 19111), and the Gram-negative *Pseudomonas aeruginosa* (ATCC 27853), *Escherichia coli* (ATCC 8739), *Salmonella enterica* (ATCC 13076), *Klebsiella pneumoniae* (NCTC 13440), and *Acinetobacter baumannii* (ATCC 17978) were obtained from ATCC (United States) and NCTC (National Collection of Type Cultures – England).

3.3. Generation of transgenic constructs

3.3.1. RNA interference construct

RNAi is a eukaryotic, cellular regulatory and defense mechanism that recognizes double-stranded RNA molecules. One of the RNA strands is incorporated into the RISC complex (RNA-induced silencing complex), which cleaves complementary RNAs. Therefore, constructs containing the *nodGRP1L* gene region in the transformed plants will be transcribed into double-stranded RNA, which will be recognized and cleaved by the RNAi mechanism, hence silencing the gene. Stable transformant plants were generated to have more reliable results, as the entire plant develops from a single transformant cell therefore, all the cells are genetically identical,

and in the case of a homozygous plant through self-pollination, all the offspring are identical to their parent with respect to the transgene.

Of the coding sequence of *nodGRP1L* gene, 186 bp was amplified from A17 cDNA using a primer pair containing the adaptor regions (attB1 and attB2) for BP recombination (Gateway BP Clonase II Enzyme Mix, Thermo Scientific) into the pDONR207 donor vector (Invitrogen). Subsequent LR recombination was performed into the pUB-GWS-GFP destination vector (Maekawa et al., 2008) containing the RNA interference cassette. The RNA interference box contains two copies of the gene segment to be silenced, the second of which was inserted in the opposite orientation to the first, so that the vector expresses the specific segment in double-stranded form driven by *L. japonicus* ubiquitin 10 (Ljubq10) promoter.

3.3.2. Overexpression construct

A 348 bp fragment of the *nodGRP1L* coding sequence was amplified from *M. truncatula* A17 cDNA and cloned into the pCR8/GW/TOPO vector (Invitrogen, Cat. No. K2500-20) according to the manufacturer's instructions, producing entry clones. The fragment was subsequently transferred via LR recombination into the pUB-GWS-GFP destination vector, enabling overexpression of *nodGRP1L* under the control of the *L. japonicus* ubiquitin10 (Ljubq10) promoter. This vector also carries GFP, expressed independently from the *nodGRP1L* under the control of the Cauliflower Mosaic Virus (CaMV) 35S promoter, allowing the selection of transgenic roots.

3.3.3. Yeast two hybrid construct

A 296 bp fragment of the *nodGRP1L* coding sequence and a 502 bp fragment of the *SecB* coding sequence were amplified from *M. truncatula* A17 using Thermo Scientific *Nde*I and *Bam*HI restriction sites. The destination vectors pDest-GBKT7 and pDest-GADT7 were digested with the same enzymes, and the resulting large fragments of each vector were purified and subsequently ligated with either the *nodGRP1L* or *SecB* fragments using Thermo Scientific T4 DNA ligase.

3.3.4. BIFC construct

A 279 bp fragment of the *nodGRP1L* coding sequence was amplified from *M. truncatula* A17 cDNA and cloned into the pCR8/GW/TOPO vector to get the entry clone and subsequently transferred via LR recombination into the pUBC-nYFP-GRP1L destination vector.

A 504 bp fragment of the *SecB* coding sequence was amplified from *M. truncatula* A17 cDNA and cloned into the pCR8/GW/TOPO vector to get the entry clone and subsequently transferred via LR recombination into the pUBC-cYFP-SecB destination vector.

3.3.5. Promoter activity constructs

Fragments of the *nodGRP1L* promoter region (1079 bp, 703 bp, and 419 bp) were amplified from *M. truncatula* A17 genomic DNA and cloned into the pCR8/GW/TOPO vector (Invitrogen Cat. No. K2500-20) following the manufacturer's protocol, to generate entry clones. These promoter fragments were then transferred from the entry clones via LR recombination into the pMDC164-RR destination vector, placing them upstream of the GUS reporter gene to drive its expression. The destination vector also contained the DsRED fluorescent protein, expressed independently under the control of the *A. thaliana* ubiquitin10 promoter (pAtUb10), enabling the visual selection of transgenic roots.

3.3.6. Strep-tagged *nodGRP1L* expression construct

3.3.6.1. T7 promoter–driven expression construct suitable for use in *E. coli*

The recombinant construct pTXB1-GRP1L-StrepII was generated by restriction digestion and ligation. The pTXB1 plasmid was first digested with the restriction enzymes *Nde*I and *Bam*HI to remove the native intein fragment, and the linearized vector was purified from agarose gel. The *nodGRP1L* coding sequence lacking the signal peptide was amplified from *M. truncatula* A17 cDNA and fused to a C-terminal StrepII tag through an additional PCR reaction. The resulting product was digested with the same enzymes and subsequently ligated into the prepared pTXB1 backbone using T4 DNA ligase. This strategy effectively replaced the intein fragment with the *nodGRP1L* insert, thereby generating a construct designed to express nodGRP1L fused to a Strep-tag for affinity purification.

3.3.6.2. Native promoter-driven expression construct suitable for use *in planta*

The recombinant construct pMDC164-RR_*nodGRP1L*pro::*nodGRP1L*-StrepII was generated by amplifying the 1079 bp 5′ promoter region of the *nodGRP1L* gene from *M. truncatula* A17 genomic DNA by PCR, followed by fusion to a C-terminal StrepII tag through an additional PCR reaction. The resulting fragment was cloned into the pCR8/GW/TOPO vector (Invitrogen, Cat. No. K2500-20) according to the manufacturer’s instructions, producing entry clones that were subsequently transferred via LR recombination into the pMDC164-RR destination vector.

This vector carries a DsRED fluorescent marker expressed under the control of the *A. thaliana* ubiquitin10 promoter (pAtUb10), enabling selection of transgenic roots.

3.4. *Agrobacterium rhizogenes*-mediated hairy root transformation

The transformation of the roots of *M. truncatula* was performed using the *A. rhizogenes* Arqua1 strain, based on a modified protocol of the method described by Boisson-Dernier et al., 2001. The root tip of the seedlings with 0.8-1 cm radicle length was first cut using a sterile scalpel, then carefully pulled along the bacterial culture so that an appropriate amount of bacteria was placed on the cut surface. The cut seedlings were placed on a 0.8% agar plate and left to rest, covered, for 2 hours. Then these seedlings were planted in zeolite supplemented with Fahraeus medium, and the resulting transformant roots were checked for fluorescent marker genes (GFP or DsRED) using a Nikon C-DSS230 stereomicroscope.

3.5. Sectioning of *M. truncatula* nodule samples for symbiotic phenotypic characterization

For the characterization of the symbiotic phenotype, nodules were collected from rhizobia-inoculated wild type and/or transgenic plants and prepared for microscopic analysis following the fixation, sectioning, and staining procedures. Nodules were collected into 1x phosphate buffered saline (PBS) solution (8 g NaCl, 0.2 g KCl, 1.44 g Na_2HPO_4, 0.24 g KH_2HPO_4, in 1000 ml deionized H_2O, pH 7.4) and then were embedded into 5% (wt/vol) agarose gel and 75 μm thick longitudinal sections were prepared with the help of microtome (MICROM HM 650 V). For samples prepared to be checked with transmission electron microscope (JEOL; Tokyo, Japan) PBS solution was replaced with 2,5% glutaraldehyde.

3.5.1. Live/dead staining

To investigate the morphology of bacteria and the cellular structure of host cells in different nodule zones, 75 μm nodule sections were stained with 5 μM SYTO9 and 1 μM propidium iodide dissolved in 1xPBS pH 7.4 buffer. Staining solution was removed, and sections were rinsed twice with 1xPBS before the preparation of microscope slides. SYTO9 is a green fluorescent dye that can penetrate and stain the nucleic acids of both live and dead cells. PI, on the other hand, is a red fluorescent dye that can only penetrate cells with damaged membranes and displace SYTO9 from DNA due to PI's stronger binding affinity, making it a marker for dead or dying cells. Stained nodule sections were observed under the Leica SP5 confocal laser scanning microscope. The microscope was configured with the following settings: objective lenses: HC PL APO 20x (NA:0.7) and HCX PL APO 63x OIL (N.A: 1.40); line sampling speed: 400 Hz; 2x line averaging; pinhole: 1 airy unit; scanning mode: sequential unidirectional;

excitation: 488 nm laser (SYTO9, green) and 543 nm laser (PI, red); spectral emission detectors: 510-540 nm (SYTO9) and 555–655 nm (PI).

3.5.2. GUS staining

Histological staining based on β-glucuronidase (GUS) activity was performed using X-Gluc containing staining solution. The nodules were collected from roots transformed with *S. medicae* WSM419 at 14 dpi. Nodules were fixed and 75 μm thick sections were prepared as detailed in section 5.2.1. Nodule sections were then treated with X-Gluc staining solution (2 mM 5-bromo-4-chloro-3-indolyl-β-D-glucuronic acid substrate, 50 mM sodium phosphate buffer (pH 7.4), 1 mM potassium ferrocyanide, 1 mM potassium ferricyanide, 1mM EDTA, 0.1% Sarcosyl, 0.05 % SDS and 0.1 % Triton X-100) (Horváth et al., 2023). Nodule sections added to GUS staining solution were vacuum infiltrated for 30 minutes, followed by incubation at 37 °C in the dark for 1-3 hours to detect GUS activity. The images of GUS-stained nodule sections were evaluated and documented under a light microscope. The 10x and 20x objectives of the Leica DM LB2 light microscope, and the images were captured with the QImaging MicroPublisher 3.3 RTV machine using the software recommended by the manufacturer.

3.6. Acetylene reduction assay (ARA)

The acetylene reduction assay was employed to measure nitrogenase activity of the rhizobia as an indicator of nodule nitrogen fixation. The assay relies on the ability of nitrogenase to reduce acetylene to ethylene, which can then be quantified by gas chromatography (GC). Transformed nodules were collected and placed in 2-ml airtight containers, after which 200 μl of acetylene was injected. Following incubation at room temperature for 2–3 hours, 100 μl of gas was sampled and directly injected into an Agilent 6890 gas chromatograph. Ethylene production was quantified using standards of known concentration, and the values were normalized to both nodule fresh weight and incubation time.

3.7. Expression of *nodGRP1L*-StrepII in *E. coli* for protein production

The recombinant construct pTXB1_GRP1L-StrepII was transformed into *E. coli* BL21(DE3) cells. A 200 ml culture was grown in a 1000 ml Erlenmeyer flask at 37 °C with shaking until the optical density at 600 nm reached 0.4–0.6. Gene expression was induced with 1 mM IPTG and cultures were incubated for an additional 3 h at 37 °C. Cells were harvested by centrifugation (4500 rpm, 10 min, 4 °C) and resuspended in 4 ml of 1× W buffer (100 mM Tris-HCl, 150 mM NaCl, 1 mM EDTA, pH 8.0). Cell disruption was performed by sonication, with the configuration of 2 minutes' pulse and 3 minutes' rest with 25% amplitude for 10 minutes on ice and repeated twice. The lysate was centrifuged (15,000 rpm, 15 min, 4 °C) to separate

soluble and insoluble fractions. The resulting pellet was resuspended in 1 ml of W buffer containing 1% SDS, vortexed, and incubated for 20 min at room temperature. A final centrifugation (13,000 rpm, 5 min, RT) was performed, and the supernatant containing the solubilized protein fraction was retained for further analysis.

3.8. Affinity purification of nodGRP1L-StrepII protein

Gravity-flow columns were employed for the purification of recombinant nodGRP1L-Strep. Columns were first equilibrated with 10 ml of W buffer, after which 4 ml of Strep-Tactin Sepharose resin (IBA Lifesciences) was packed. The soluble fraction of the bacterial lysate was then applied to the column, and unbound proteins were removed by eight washes of 5–6 ml W buffer (~40 ml in total). Bound GRP1L-Strep was subsequently eluted with 10 ml of E buffer (100 mM Tris-HCl, 150 mM NaCl, 1 mM EDTA, 2.5 mM desthiobiotin, pH 8.0), which was collected as five fractions of 2 ml each in separate microcentrifuge tubes.

3.9. Bacteroids isolation and Western blot analysis

Transformed nodules were collected in microcentrifuge tubes and homogenized in PBS buffer using small plastic pestles. Cell debris was removed by gentle centrifugation at 800 g for 5 minutes at 4 °C, and the resulting supernatant was sequentially filtered through 50 µm and 10 µm filters. The filtrate was centrifuged at 3000 g for 5 minutes at 4 °C to pellet the bacteroids. The supernatant was collected and the pellet washed three times with PBS. For microscopic analysis, SYTO 9 and FM 4-64 dyes were used, and imaging was performed with an Olympus Fluoview FV1000 confocal laser microscope at 60× magnification. SYTO 9 was excited at 488 nm, and emission was collected between 500 - 530 nm, while FM 4-64 was excited at 514 nm , emission was detected between 640 - 725 nm. For protein preparation, 2 µl of 1× Laemmli buffer (Bio-Rad #1610737) was added to 20 µl of both the supernatant and bacteroid fractions, followed by boiling for 10 minutes and separation on a 12% Tris-glycine SDS-PAGE gel. The resolved proteins were electrotransferred onto a nitrocellulose membrane at 18 V for 16 hours at 4 °C. The membrane was then processed under slow rocking, beginning with blocking in 3% BSA in TBST (1× PBS + 0.1% Tween-20) for 1 hour. It was subsequently incubated with the primary anti-StrepII antibody (Invitrogen, Cat. #26183) at a 1:5000 dilution in 3% BSA/TBST for 3 hours, washed three times for 10 minutes each in TBST, and then incubated with the secondary anti-mouse antibody at a 1:10,000 dilution in 3% BSA/TBST for 1 hour. Following three additional 10-minute washes in TBST and three washes in PBS, the chemiluminescent signal was detected with the Invitrogen iBright FL1500 Imaging System.

3.10. Microscale thermophoresis assay

Binding interactions were analyzed using a Monolith NT.115 microscale thermophoresis (MST) instrument (NanoTemper Technologies, Munich, Germany). The instrument was equipped with a capillary tray, enabling successive measurements within each run using coated capillaries. For the binding check assays, measurements were performed with four samples, while for the affinity determination assays, sixteen samples were analyzed. Data acquisition and processing were conducted with the NT Analysis software (NanoTemper Technologies). All experiments were carried out under optimized MST settings, with the LED excitation power set to 30% and the MST laser power maintained at the low-power setting. Synthetic peptides were used throughout, prepared in Tris buffer supplemented with 500 mM NaCl and 0.05% Tween-20.

3.11. Yeast Two-Hybrid (Y2H) assay

Yeast two-hybrid experiments were carried out to identify potential interaction partners of nodGRP1L. A *S. meliloti* gene library had previously been cloned into the GADT7 vector, while *nodGRP1L* was inserted into the GBKT7 vector. The constructs were co-transformed into the *Saccharomyces cerevisiae* AH109 strain following the manufacturer's protocol (Clontech Laboratories, Inc., Protocol No. PT1172-1). Double transformants were selected on synthetic dropout (SD) medium lacking leucine and tryptophan (SD-LT), which permits growth only of yeast cells carrying both GADT7 and GBKT7 constructs. To test for protein–protein interactions, yeast cells were grown on selective media lacking histidine (SD-HLT) or lacking both histidine and adenine (SD-AHLT). Growth on these media indicates a positive interaction between the tested proteins. Because selection on histidine-free medium alone may yield false positives, the adenine-deficient medium was used as a more stringent condition. To further validate interactions, candidate partners were re-cloned into both GADT7 and GBKT7 vectors, and drop assays were performed by spotting 5 µl of yeast suspensions onto SD-LT, SD-HLT, and SD-AHLT plates.

3.12. Infiltration of *Nicotiana benthamiana* leaves for transient gene expression

Alongside the *A. tumefaciens* C58C1 carrying the constructs of interest, a strain harboring a construct encoding the p19 RNA-silencing suppressor (Silhavy et al., 2002; Voinnet et al., 2003) was also infiltrated to inhibit RNA silencing in the plant and thereby enhance protein production. *Agrobacterium* suspensions were mixed in equal proportions and incubated in the dark at room temperature for 3 h before infiltration. The mixtures were then infiltrated into the abaxial side of *N. benthamiana* leaves. Leaves were harvested 3 - 4 days post-infiltration for

analysis. Intracellular localization and BiFC assays were performed using a Leica Stellaris 8 confocal laser scanning microscope, with excitation at 514 nm and emission collected between 525–600 nm for yellow fluorescent protein (YFP).

3.13. Preparation of RNA samples

3.13.1. RNA isolation from *M. truncatula* nodules

Nodules from *nodGRP1L* RNAi plants and wild-type R108 were grown in zeolite and inoculated with *S. meliloti* Rm41. After 8 days of infection, nodules were harvested and immediately frozen in liquid nitrogen. Total RNA was extracted using the Quick-RNA Plant Miniprep Kit (Zymo Research). A total of eight RNA-seq samples were prepared, comprising three controls and five nodGRP1L RNAi samples. Each sample was generated from pooled nodule RNA of several plants.

3.13.2 RNA isolation from *E. coli* culture

E. coli starter cultures in the exponential growth phase were diluted to OD_{600} = 0.05 and grown to early logarithmic phase (OD_{600} = 0.2) in six separate flasks in 10 - 10 ml LSM (MBC = 6.2 μM) liquid medium (Farkas et al., 2018). Three biological replicates were treated at OD_{600} = 0.2 with a final concentration of 1.6 μM $NCR169C_{17-38}$ peptide for 20 minutes, while the control samples were treated with the same amount of water for 20 minutes. Total bacterial RNA was purified from samples using the RNeasy Mini Kit/QIAGEN (cat. no. 74104) following the instructions in the protocol, prior the purification with treatment of RNAprotect Bacterial Reagent/QIAGEN (cat. no. 76506). Residual DNA was eliminated using Ambion DNase I (RNase-free). The samples were precipitated with ethanol and resuspended in RNase free water.

3.13.3. cDNA synthesis

The quantity of RNA was checked with a NanoDrop spectrophotometer and RNA quality and integrity were assessed with an Agilent 2200 TapeStation (Agilent Technologies). cDNA was synthesized from 100 ng of total RNA in a 20 μl reaction using the High-Capacity cDNA Reverse Transcription Kit (Applied Biosystems) following the instructions stated in their protocol.

3.14. RT-qPCR

The relative expression of genes from the cDNA samples was measured with a StepOne Plus (Thermo Fisher) real-time PCR device using PowerUp SYBR Green Master Mix (Applied

Biosystems). Three technical replicates were performed on all biological replicates. The sequences of the primers used for RT-qPCR can be found in Appendix.

3.14.1. RT-qPCR on RNA from *M. truncatula* nodules

Quantitative real time PCR (qRT-PCR) was performed on selected genes (nod GRP1L, *nodGRP3A*, *nodGRP3C,* and *nodGRP4*). The 40S ribosomal S19-like gene (Medtr3g013640) was used as an internal control for normalization of the results (Nagymihály, 2017).

3.14.2. RT-qPCR on RNA from *E. coli* cells

Quantitative real time PCR (qRT-PCR) was performed on selected genes (*cysG*, *hcaT*, *osmB*, *rplK*, *ompF*, *rpsJ*, *tufAB*, *ihfB*, *rpoA*, *metK*, *lpp*). Data were normalized to *cysG* gene that proved to be a reliable reference gene during stress conditions (Zhou et al., 2011, Peng et al., 2014), and the results were compared to the sequencing data.

3.15. Peptides synthesis

NCR169, NCR169C$_{17-38}$ and derivatives were synthesized by standard Fmoc solid-phase peptide synthesis (SPPS) on a TentaGel S RAM resin using an automated peptide synthesizer (CEM Liberty Blue) followed by RP-HPLC purification and ESI-MS confirmation of identity (Jenei et al., 2020, Howan et al., 2023).

3.16. Antimicrobial assays

Minimal bactericidal concentrations (MBC) of peptides and reference antibiotics were determined in 20 mM potassium phosphate buffer (PPB, pH 7.4) and Mueller–Hinton broth (MHB) as described by Jenei et al. (2020). Briefly, bacterial cultures were grown to mid-log phase, washed, adjusted to OD_{600} = 0.1 (~10^7 CFU/ml), 10 µl of it was added into 100 µl mixture and incubated in 96-well plates with 2-fold serial dilutions of peptides starting from 25 µM. After incubation at 37 °C with shaking, bacterial viability was assessed by plating 5 µl aliquots on LB agar. MBC was defined as the lowest concentration yielding no colony growth.

3.17. Combined treatment of *E. coli* with NCR169C$_{17-38}$ and antibiotics or NCR335 fragments

The effects of the different combinations of NCR169C$_{17-38}$ with streptomycin, meropenem, polymyxin B and fragments of NCR335 (NCR335N$_{1-19}$: RLNTTFRPLNFKMLRFWGQ; NCR335C$_{13-33}$: KDCPKLRRANVRCRKSYCVPI) were determined by standard checkerboard titration method. Streptomycin was tested at concentrations ranging from 25 µM to 0.4 µM, meropenem from 200 µM to 3.1 µM, and polymyxin B from 6.3 µM to 0.1 µM. NCR335N$_{1-19}$

was tested in a concentration range from 3.1 μM to 0.05 μM, while NCR335C_{13-33} from 12.5μM to 0.2 μM. NCR169C_{17-38} concentrations ranged from 25 μM to 0.4 μM when tested with antibiotics, whereas in combinations with peptide fragments, lower concentrations of NCR169C_{17-38} (3.1 μM to 0.05 μM) were applied. The initial *E. coli* density in each well were adjusted to OD_{600} = 0.01 corresponding to ~10^6 CFU/ml. From the antibiotic 45 μl dissolved in MHB medium were combined with 45 μl of NCR169C_{17-38} or NCR335 fragments dissolved in PPB. Into the 90 μl mixture, 10 μl of bacterial suspension were added and incubated for 3 h at 37 °C with 250 rpm shaking, 5 μl from each sample was placed on LB agar and MBC was detected after overnight incubation at 37 °C. The effectiveness of combination treatments was measured using the fractional bactericidal concentration (FBC) index, which is a metric used to assess the interaction between antimicrobial agents, determining whether their combined effect is synergistic, additive, or antagonistic. First, the MBC values of polymyxin B, meropenem, streptomycin, NCR335N_{1-19}, and NCR335C_{13-33} were determined in *E. coli*. Subsequently, their combinations with NCR169C_{17-38} were examined using the FBC index. FBC = FBCA + FBCB. FBCA = (MBCA in combination) / (MBCA alone); FBCB = (MBCB in combination) / (MBCB alone).

3.18. Biofilm inhibition and biofilm eradication assays on *Acinetobacter baumannii*

For the biofilm inhibition assay the antimicrobial activity test was done in 1/10 MHB using *A. baumannii* treated with the respective dilutions of NCR169C_{17-38}, meropenem or polymyxin B for 24 h. After taking the 5 ul samples at the end of the treatment (to determine MBC values), the rest of the bacterial suspensions were removed from the wells and the remaining biofilm at the bottom and walls of the wells was then washed three times with sterile water and stained using 1% Crystal Violet (CV) for 15 minutes to visualize the produced biofilm. The non-adherent CV dye was then removed by washing with water three times. The plate was left for complete drying, then the biofilm-bound CV dye was dissolved in 200 μl of 30 % acetic-acid with shaking over 15 minutes. The absorbance was measured at OD_{550} using a HIDEX Plate Reader (Hidex Sense Microplate Reader with Plate Reader Software version 5064, Hidex, Finland). All measurements were repeated three times.

For the biofilm eradication assay the bacteria were pre-cultured for 24 h in MHB with a starting OD_{600} = 0.01. Then the supernatants were removed from the wells and the biofilm was washed three times with 200 μl of 1/2 MHB. Subsequently fresh 1/10 MHB containing the respective dilutions of NCR169C_{17-38}, meropenem or polymixin B was added to the wells, the treatment lasted either 3 h or 24 h.

3.19. Cell membrane damage assessed by different methods

Microbial cell membrane integrity or damage was assayed with Live/Dead staining. *E. coli* were grown as for the antimicrobial activity assay and washed with PPB. Cells were resuspended in PPB, and diluted to OD_{600} = 0.1 and then treated with 3.125 or 1.6 μM of $NCR169C_{17-38}$ at room temperature. Untreated cells served as negative control. Cells were subsequently stained with 5 μM SYTO 9 and 5 μM propidium iodide (PI). After a 10-minute incubation in the dark, 5 μL of each cell suspension was placed on a microscope slide, covered with thin 2% (w/v) agar slices, and examined using an Olympus Fluoview FV1000 confocal laser microscope at 60× magnification. For SYTO 9, excitation was at 488 nm and emission was collected between 500–530 nm; for PI, excitation was at 543 nm with emission detected between 555–655 nm. Sequential scanning was used to avoid crosstalk of the fluorescent dyes.

To visualize morphological changes on the bacterial surface *E. coli* culture in the log phase (OD_{600} = 0.1) were treated with $NCR169C_{17-38}$ peptide at concentrations of 1.6 μM and 3.1 μM in PPB. After treatment, 5 μl of the above bacterial suspensions were spotted on a 0.1 μm PC membrane (Merck Isopore). The samples were then fixed with 2.5% (v/v) glutaraldehyde in phosphate buffered saline (PBS, pH 7.4). The membranes were washed twice with PBS and gradually dehydrated with ethanol series (30, 50, 70, 80%, and three times 100% ethanol, each for minimum 30 min). The samples were dried with a critical point dryer (K850: Quorum Technologies Ltd.), followed by 12 nm gold coating using a Quorum Q150T ES (Quorum Technologies, Lewes, UK) sputter coater and observed with a JEOL JSM-7100F/LV scanning electron microscope.

To monitor PI uptake in real time, 10 μL of *E. coli* suspension (OD_{600} = 0.1, prepared as described above) was mixed with 90 μL of PPB containing a two-fold serial dilution of $NCR169C_{17-38}$ (12.5 μM to 0.8 μM) or polymyxin B (0.8 μM), along with 200 ng/mL PI. Fluorescence was recorded using a Hidex Sense Microplate Reader (software version 5064) with excitation and emission wavelengths set at 535 nm and 617 nm, respectively. Experiments were repeated three times.

3.20. Heat stability assay using dot-blot

For heat stability test, serial dilutions of the $NCR169C_{17-38}$-StrepII peptide were prepared in PPB at concentrations of 25, 12.5, 6.3, 3.1 μM, following the same protocol used in the antimicrobial assay. One set of samples was incubated overnight at 37 °C with shaking, another set was subjected to heat stress at 80 °C for 20 minutes, while one set was freshly prepared. Dot-blot analysis was performed by spotting 5 μL of each peptide solution onto a 0.22 μm

nitrocellulose membrane (Bio-Rad). Detection of the StrepII-tagged peptide was carried out using the Precision Protein StrepTactin-HRP conjugate (Bio-Rad), following the manufacturer's recommended protocol. Signal development was achieved using the Clarity Western ECL Substrate (Bio-Rad), with the membrane incubated for 5 minutes at room temperature, followed by exposure to Fuji Medical X-ray film for visualization.

3.21. Lipid overlay assay

Membrane lipid strips (Echelon Biosciences, P-6002) were incubated for 1 h in blocking solution (3 % BSA in TBS-Tween 0.1%) with gentle agitation followed by four 8-min washes in TBS-Tween. Then, strips were incubated with 2 μM of NCR169C_{17-38} in blocking solution for 1 h. Unbound peptide was washed off by four 8-min washes in TBS-Tween. The bound StrepII-tagged peptide was then detected on the strips using the same procedure described for the dot blot, except that chemiluminescence was visualized with an iBright™ FL1500 Imaging System (Invitrogen).

3.22. Liposome sedimentation assay

To prepare the liposomes, phospholipids DMPC and Cardiolipin purchased from Avanti Polar Lipids (Alabaster, AL, USA) were dissolved in Chloroform:Methanol:Water in the ratio of (65:25:4) and (73:23:3) respectively, and dried under vacuum for 1 h. The lipid film was suspended in the assay buffer (20 mM HEPES, 150 mM NaCl, pH 7.0), vortexed, and sonicated for 15 min to form the liposomes. The assay was carried out by incubating 2 mM of the liposomes with 20 μM of NCR169C_{17-38} peptide and incubated for 30 min at room temperature, followed by ultracentrifugation at 200,000×g for 15 min at 20 °C. After centrifugation, the supernatant (sn) and pellet (p) fractions were collected separately and were subjected to glycine-SDS-PAGE. The peptides were detected by Coomassie Brilliant Blue staining.

3.23. Nucleic acid binding assays

The DNA- and RNA-binding abilities of NCR169C_{17-38}, its parental peptide NCR169, and two shorter derivatives (NCR169$_{16-27}$ and NCR169$_{17-27}$) were initially evaluated using a gel retardation assay. In this setup, 100 ng of either *E. coli* genomic DNA or total RNA was incubated with 10 μM or 100 μM of each peptide for 30 min at 37 °C. Reaction mixtures, along with untreated controls, were then subjected to agarose gel electrophoresis, and the resulting nucleic acid migration patterns were examined for changes indicative of peptide binding. The interaction of NCR169C_{17-38} with circular plasmid DNA (pDEST-GBKT7) was also

characterized using peptide concentrations ranging from 50 μM to 0.8 μM, prepared by 2-fold serial dilution.

In addition, DNA-binding kinetics were monitored in real time using a Hidex Sense plate reader at room temperature in three independent experiments. Reaction mixtures contained 100 ng of *Hind*III-digested lambda phage DNA in 1× SYBR Gold (Thermo Scientific), either without peptide or with 10 μM of NCR169C_{17-38} (2.74041 μg), NCR169 (4.56545 μg), NCR169$_{16-27}$ (1.56597 μg), or NCR169$_{17-27}$ (1.40279 μg). Peptides were added either at the start (0 min) or at 14 min. Fluorescence from DNA-bound SYBR Gold was measured every 3 min (excitation 490 nm, emission 535 nm). At 27 min, proteinase K (1 mg/ml; 100 μg final) was added to peptide-treated samples to assess the effect on peptide–DNA binding.

4. Results

4.1. Identification and functional analysis of plant-derived nodule-specific glycine rich protein GRP1L

Based on differential spatial and temporal expression pattern of *NCR* and *nodGRP* genes in successive stages of symbiotic cell development it was hypothesized that these genes play specific roles in nodule formation. To investigate their roles, RNAi gene silencing constructs were produced for several selected genes. To ensure reliable results, stable transgenic *M. truncatula* plants were generated earlier in the lab, as each plant develops from a single transformed cell, producing genetically uniform tissues throughout the organism. Seeds were collected from each transgenic plant so that the symbiotic phenotype could be later determined in the offspring.

4.1.1. Screening of RNAi transgenic *M. truncatula* plants identified *nodGRP1L* as essential for symbiotic nodule development

As it was described above, a set of stable transgenic *M. truncatula* lines were generated earlier targeting various *NCR* and *nodGRP* genes to check the effect of their silencing on the nitrogen-fixing symbiosis. For this purpose, wild-type (WT) *M. truncatula* R108 plants and the progeny of the different transgenic RNAi lines (Table 1.) were inoculated with their symbiotic partner, *Sinorhizobium meliloti* Rm41. Since the presence of the transgene could segregate in the progeny of the lines, at least 15 individuals per line were tested.

The plants were grown under nitrogen-free condition to allow a clear assessment of nodule development following inoculation with its compatible symbiont. Symbiotic phenotypes were evaluated at 14 days post-inoculation (14 dpi). By this time there were already clear signs of nitrogen starvation of several individuals of two distinct transgenic *nodGRP1L* RNAi-silenced lines (no. 1 and 3; Fig. 16.) that suggested impaired symbiotic nodule development. Among the tested genes, the *nodGRP1L* was particularly interesting, as it is one of the highly expressed nodGRPs and its expression can be detected in the nodule interzone (Roux et al., 2014), suggesting that this gene plays a role in the process of transforming the bacteria into fully differentiated bacteroids.

Table 1. List of the *Medicago truncatula* stable transgenic RNAi lines targeting various *NCR* or *nodGRP* genes. The number of distinct transgenic lines available for a targeted gene is indicated in the first column. The progeny of these lines (grown from available seeds per lines) were evaluated for their symbiotic phenotypes in plant assays. Among the X independent transgenic lines targeting *nodGRP1L*, there were two lines in which several individuals exhibited Fix$^-$ mutant symbiotic nodules.

Number of lines	Targeted gene	Plant ecotype/ rhizobial strain
9	*nodGRP1L*	R108/Rm41
1	*nodGRP3A*	R108/Rm41
3	*nodGRP3A, 3B*	R108/Rm41
1	*nodGRP3C*	R108/Rm41
1	*nodGRP2A*	R108/Rm41
7	*15 nodGRPs (1H, 1I, 1K, 2A,2B, 2C, 2D, 3A, 3B, 3C, 4, 5A, 5B, 6A, 6B)*	R108/Rm41
5	*NCR335*	R108/Rm41
6	*NCR001*	R108/Rm41
4	*NCR164*	R108/Rm41
2	*NCR247*	R108/Rm41
1	*NCR209*	R108/Rm41
2	*NCR084*	R108/Rm41
1	*NCR235*	R108/Rm41
2	*NCR209*	R108/Rm41
4	*NCR025*	R108/Rm41
2	*NCR 025*	2HA/WSM419
1	*NCR209*	2HA/WSM419

Morphological characterization of *nodGRP1L* RNAi-silenced plants inoculated with *S. meliloti* Rm41, compared to the WT R108, revealed pronounced differences in shoot growth, root architecture, and nodule development. WT plants exhibited normal growth, with a well-branched shoot system bearing numerous nitrogen fixing nodules (Fig. 16. A). In contrast, silencing of *nodGRP1L* provoked reduced growth, a less developed root system, and visibly fewer nodules (Fig. 16. B). WT nodules were elongated and pink, indicating the accumulation of functional leghemoglobin, which is essential for maintaining reduced oxygen levels to ensure the activity of nitrogenase enzyme required for symbiotic nitrogen fixation. This reflects proper bacteroid differentiation and efficient nitrogen-fixing activity. In contrast, nodules from the silenced plants were smaller, mostly round shaped and white that collectively indicated the absence of nitrogen fixation (Fix$^-$).

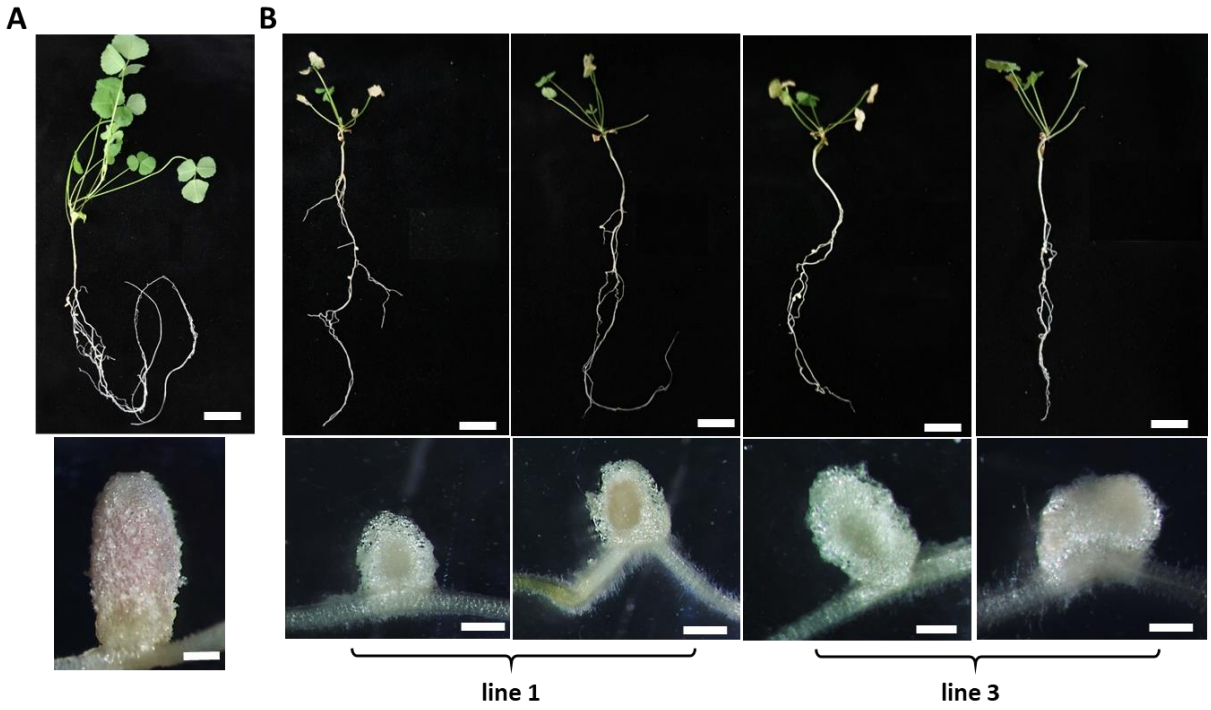

Figure 16. Symbiotic phenotype of WT and *nodGRP1L* RNAi transgenic *M. truncatula* plants. (a) R108 plant with a WT nodule below. (b) Four T_2 individuals originating from two distinct T_1 transgenic *nodGRP1L* RNAi-silenced lines. These plants are smaller in size than the WT and their nodules below show the symptoms of nitrogen starvation: white, small and Fix^-. Nodules are from plants after 2 weeks of inoculation with strain *S. meliloti* Rm41. Scale bar of plants, 2 cm. Scale bar, of nodules, 10 mm

4.1.2 Verification of *nodGRP1L* gene silencing using real-time PCR

In order to prove the efficiency of gene silencing we examined the expression level of the *nodGRP1L* gene in the WT and in the Fix^- nodules of the *nodGRP1L* RNAi-silenced lines (line 1 and 3) using quantitative real-time PCR (qRT-PCR). In the nodules of the two independent RNAi lines, *nodGRP1L* transcript levels were reduced to 0.11 and 0.25 relative to the WT (Fig. 17), indicating a strong and significant downregulation that confirms effective gene silencing. To assess the specificity of this silencing, we also analyzed the expression of three additional members of the *nodGRP* gene family: *nodGRP3A, nodGRP3C,* and *nodGRP4*. The results showed that none of these genes were down-regulated, with relative expression values of 1.86 and 1.33 for *nodGRP3A*, 1.71 and 1.20 for *nodGRP3C*, and 2.13 and 1.41 for *nodGRP4* in the nodules of the two RNAi lines (Fig. 17.). These data indicate that the silencing was specific to *nodGRP1L* gene and did not extend to other *nodGRP* family members.

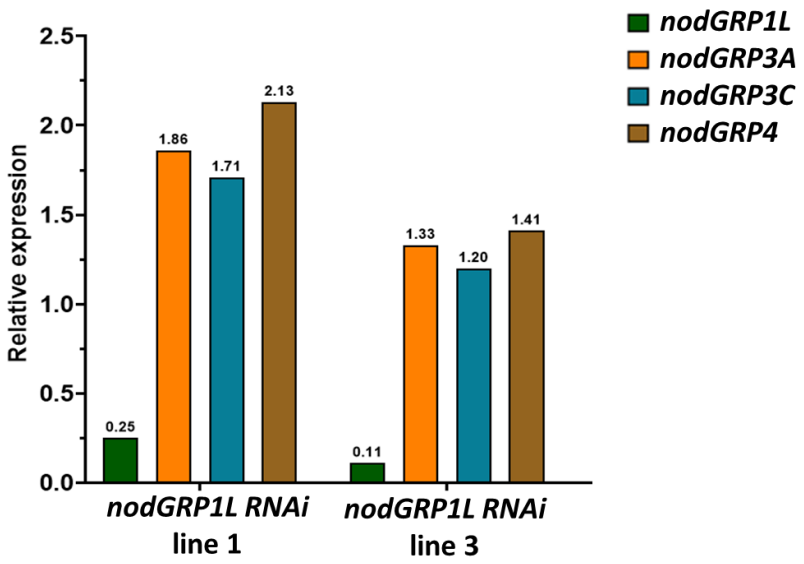

Figure 17. Silencing of the *nodGRP1L* gene confirmed by qRT-PCR reaction. The expression of the *nodGRP1L* gene decreased with 75% in line 1 and 89% in line 3 compared to the control. The expression levels of the other tested *nodGRP* genes (*nodGRP3A*, *nodGRP3C* and *nodGRP4*) did not decrease compared to the control R108.

4.1.3. Structural analysis of the symbiotic nodules of the *nodGRP1L* RNAi-silenced *M. truncatula* plants

To examine nodule development, colonization and the fate of the microsymbiont, we compared the morphology of the symbiotic cells in the nodule sections of the *nodGRP1L* RNAi-silenced and WT nodules using laser scanning confocal microscopy (Fig. 18.). Live - dead staining was performed to assess the viability of *S. meliloti* Rm41 cells, with SYTO9 labeling viable cells and Propidium iodide (PI) entering and marking non-viable (dead) bacterial cells and staining the plant nuclei. Longitudinal sections of WT nodules displayed the characteristic zonation of indeterminate nodules from meristem (ZI) containing red nuclei to nitrogen fixation zone (ZIII). Bacterial colonization of host cells in the infection zone (ZII) and interzone (IZ), as well as the presence of bacteroids in the nitrogen fixation zone (ZIII), proceeded normally (Fig. 18. A, B). This distribution across the zones reflect the typical progression of symbiotic colonization. In contrast, *nodGRP1L* RNAi-silenced nodules exhibited an altered zonation pattern. Nodule cells were colonized by rhizobia in the infection zone (ZII) and interzone (IZ), but the region corresponding to the nitrogen fixation zone (ZIII) was devoid of live rhizobia (Fig. 18. E, F), indicating abnormal bacteroid and symbiotic cell differentiation. Higher magnification of nodule cells revealed that, in WT nodules, rhizobia became elongated in both the interzone (IZ) and the nitrogen fixation zone (ZIII) (Fig. 18. C, D), indicating their complete differentiation into bacteroids. In *nodGRP1L* RNAi-silenced nodules, colonized cells displayed similar elongated rhizobia in the interzone, comparable to WT nodules (Fig. 18. D, G). The major steps

of terminal differentiation of bacteroids occur in the WT interzone (IZ), and marked by elongation of bacteroids (Fig. 18. D). This is also visible in the IZ of silenced nodules, but these bacteroids after their elongation almost immediately lose their viability at this stage, indicated by their red staining (Fig. 18. G, H). In the nitrogen fixation zone (ZIII) of WT nodules, large plant cells containing fully elongated bacteroids were evident (Fig. 18. C). By comparison, no elongated bacteroids were observed in the ZIII of *nodGRP1L* RNAi-silenced nodules (Fig. 18. F).

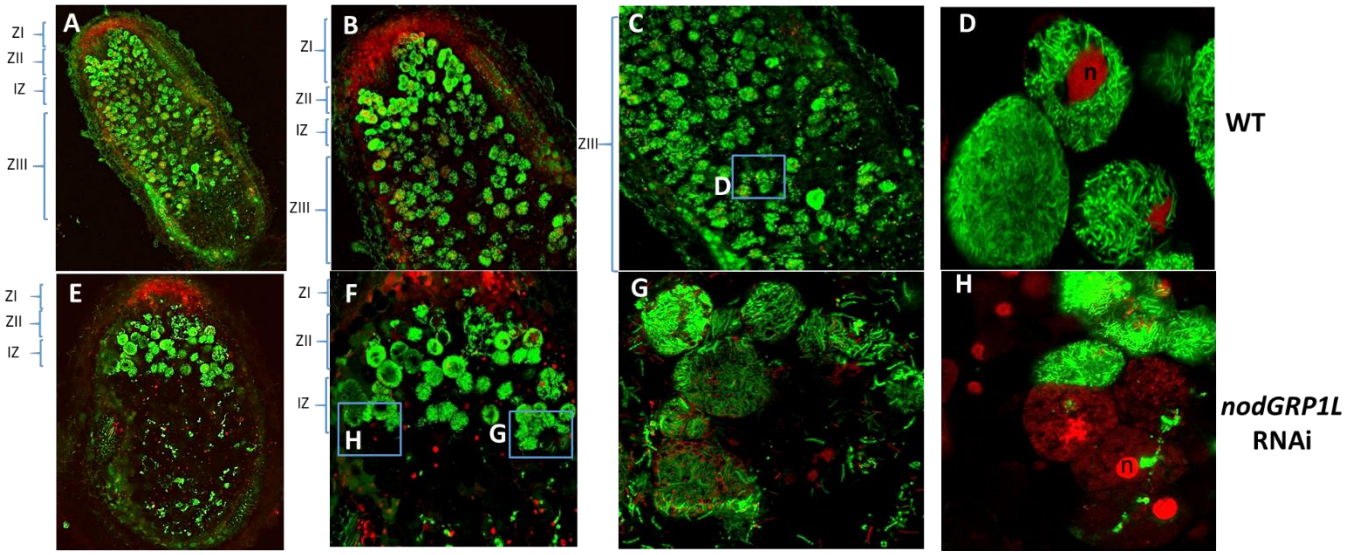

Figure 18. Morphological comparison of 14 dpi symbiotic nodules in *nodGRP1L* RNAi transgenic plant and WT nodules using confocal laser scanning microscopy. 14 dpi nodule sections of (A-D) WT plant and (E-H) *nodGRP1L* RNAi transgenic plant stained with SYTO9 (green) and PI (red). In the transgenic nodule, the elongated rhizobia in the interzone (IZ) lose their viability (G, H) compared to the WT nodule (D). The nitrogen fixing zone (ZIII) is missing in the transgenic nodule (F), while the WT nodule has a functional (ZIII) (D, D). (n) plant cells nuclei. Scale bar, 200 µm (A, B, C, F, G) 4 µm (D, H, F)

To determine whether the observed phenotype in transgenic nodules reflected a developmental delay or a distinct fate, nodules were collected at later time points as well: 28 dpi (Fig. 19. A-C) and 42 dpi (Fig. 19. D-F) and analyzed as described previously. In WT plants, nodules appeared healthy and contained abundant, fully functional, living bacteroids. (Fig 19. A, D), while no nitrogen fixation zone (ZIII) appeared in the *nodGRP1L* RNAi-silenced nodules (Fig. 19. B, E). Moreover, some of the elongated rhizobia present in the interzone (IZ) started to stain red at 28 dpi (Fig. 19. C) and became all red at 42 dpi indicating complete loss of viability of the rhizobia. Interestingly, many viable bacteria continued to be released from infection threads in zone II apparently as an attempt by the symbiotic system to maintain function; however, these bacteria failed to differentiate into nitrogen-fixing bacteroids in the interzone (IZ).

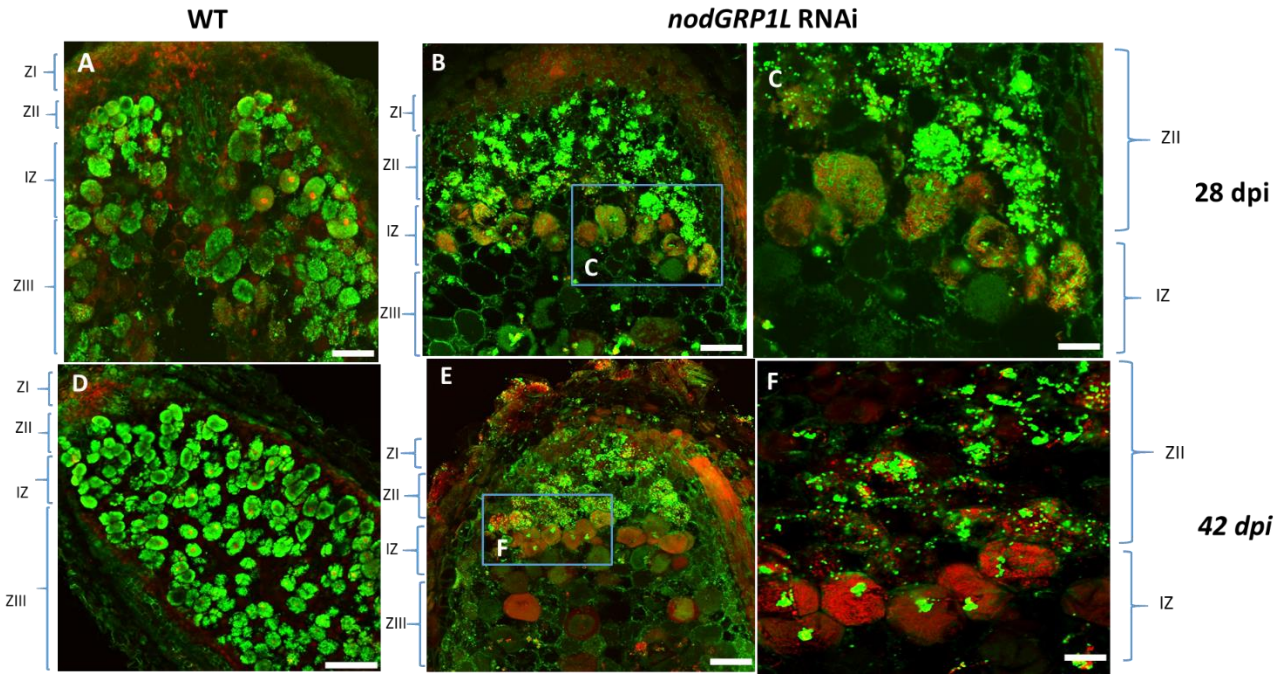

Figure 19. Morphological comparison of symbiotic nodules in *nodGRP1L* RNAi transgenic plant and WT nodules at 28 and 42 dpi by confocal laser scanning microscopy. Nodule sections of (A-C) 28 dpi and (E-F) 42 dpi plants stained with SYTO9 (green) and PI (red). The *nodGRP1L* RNAi transgenic plants (B, C, E, F) show extensive release of viable bacteria from infection threads in zone II (ZII); however, these bacteria fail to differentiate into nitrogen-fixing cells in the interzone (IZ), which is filled with dead rhizobia. In contrast, WT plants (A, D) contain nodules rich in viable bacteroids. Scale bars, 200 µm (A, B, D, E) 10 µm (C, F).

4.1.4. Ultrastructural characterization and starch deposition in *nodGRP1L* RNAi-silenced nodules

To investigate the abnormal morphology of the symbiotic organ, nodules of *nodGRP1L* RNAi-silenced plants were sectioned to 50 nm and examined by transmission electron microscopy (TEM). The focus was on the nodule (IZ) where *nodGRP1L* is predominantly expressed and confocal microscopy pictures indicated the complete arrest of the symbiotic cell development process. TEM analysis revealed significant ultrastructural differences in this region compared to that of the WT nodules (Fig. 20.). In WT nodules (Fig. 20.A-D), cells contained regular bacteroids tightly enclosed in peribacteroid membranes characteristic for nitrogen fixing bacteroids (Fig. 20. A). Mitochondria displayed normal morphology, suggesting a stable energy supply that adequately supported both the bacteroid and the host cell function (Fig. 20. D). Amyloplasts containing accumulated starch granules were present in the interzone in large and irregularly shaped form near the cell membrane (Fig. 20. A), which later became smaller and elongated in the nitrogen fixation zone, while the uninfected cells kept the irregular shape of the amyloplasts (Fig. 20. B, D). In contrast, *nodGRP1L* RNAi-silenced nodules exhibited

pronounced ultrastructural abnormalities (Fig. 20. E-H). Although bacteroids initially appeared normal, the peribacteroid membrane around them was looser, creating wider peribacteroid space than in WT cells (Fig. 20. E). In the proximal interzone, bacteroids showed signs of degeneration, visible as less-dense areas within the bacteroids (Fig. 20. F). Eventually, fully degraded bacteroids left behind only empty peribacteroid membranes (Fig 20. F, G). Mitochondria generally exhibited a normal morphology even when bacteroids began to degenerate toward the end of the interzone. However, their size was reduced compared to mitochondria in the WT, (Fig. 20. H). Furthermore, high number of small vesicles were frequently observed within the empty peribacteroid membranes compared to the WT nodules, reflecting cellular responses associated with bacteroid degeneration (Whitehead & Day, 1997) (Fig. 20. G). Remarkably and in contrast to the WT nodules, *nodGRP1L* RNAi-silenced nodules were completely devoid of amyloplasts in all developmental zones.

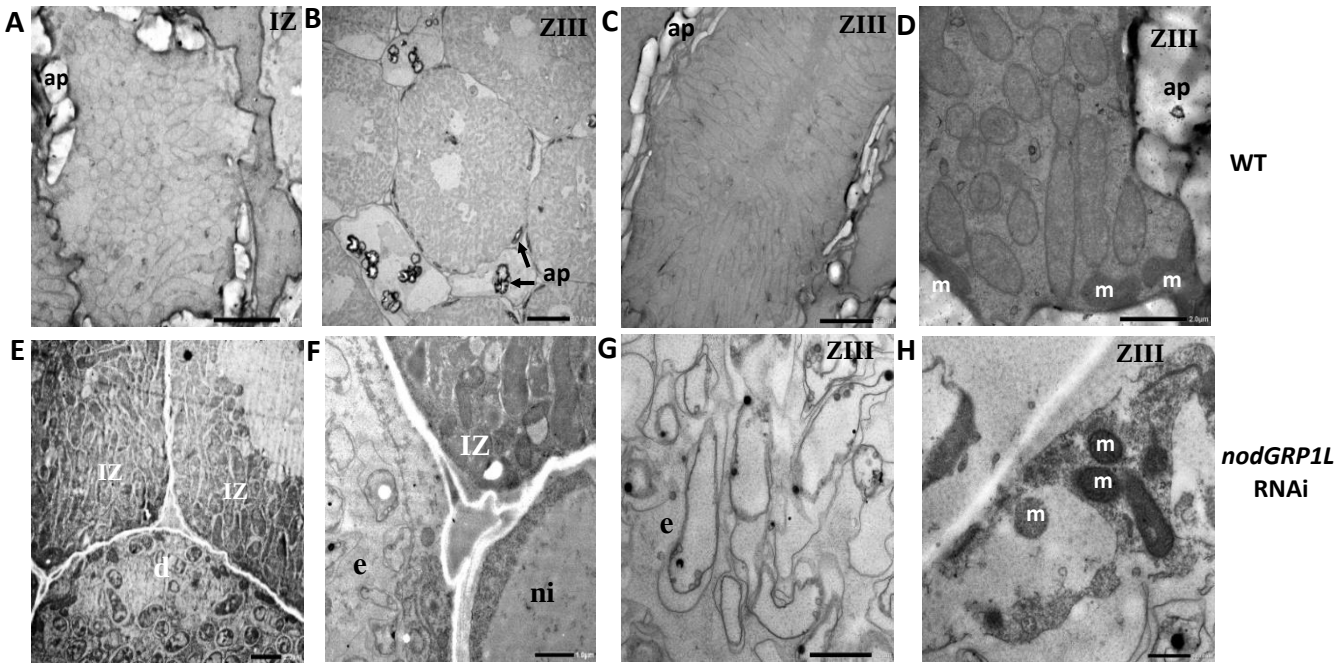

Figure 20. Transmission electron microscopy analysis of IZ and ZIII in 14 dpi WT and *nodGRP1L* RNAi-silenced nodules. WT nodules are shown in (A-D), and *nodGRP1L* RNAi-silenced nodules in (E-H). Healthy bacteroids are observed in the IZ of both WT and *nodGRP1L* RNAi-silenced nodules (A-D, E, F). Degrading bacteroids (d) and empty peribacteroid membranes (e) are detected in *nodGRP1L* RNAi-silenced nodules (E-G). Mitochondria (m) in WT plant cells (D) are larger than those in *nodGRP1L* RNAi-silenced cells (H). In WT nodules, amyloplasts (ap) are large and irregularly shaped in the distal IZ (A) and non-infected plant cells (B) but become smaller and elongated in ZIII (B, C). In contrast, no amyloplasts are observed in any zone of *nodGRP1L* RNAi-silenced nodules (E–H). (ni): non-infected plant cells. Scale bars, 10 µm (B) 5 µm (A, C) 2 µm (E, D) 1 µm (F, G) 900 nm (H).

To validate the absence of amyloplasts in the transgenic nodules, we performed starch staining with Lugol's solution on sections of WT and *nodGRP1L* RNAi-silenced nodules (Fig. 21.). A strong black staining was detected in the interzone IZ (Fig. 21. a, b), consistent with the presence of the starch-containing amyloplasts that are characteristic to normal interzone (IZ) development. In contrast, transgenic nodules completely lacked detectable starch granules, as no staining was observed in any of the developmental zones (Fig. 21. c, d). This striking difference highlights the disruption of normal amyloplast formation and starch storage in the RNAi-silenced nodules, further supporting the impaired establishment of a functional nitrogen fixation zone.

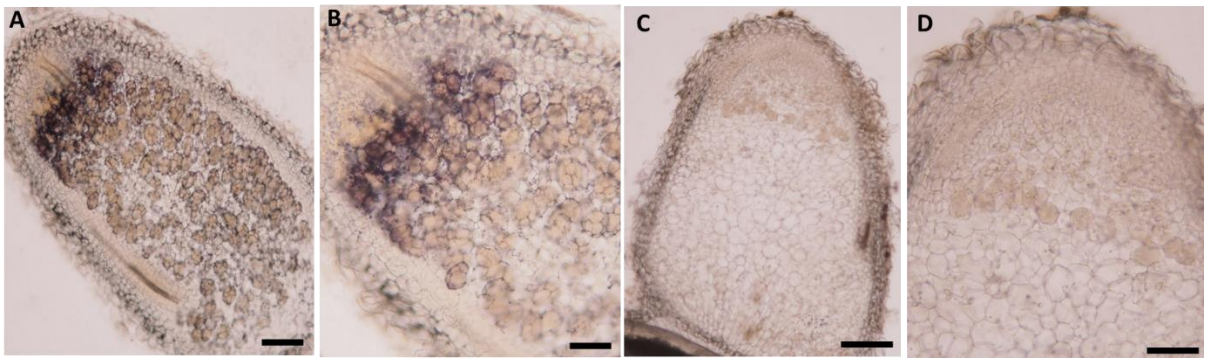

Figure 21. Starch content of the 14 dpi *nodGRP1L* RNAi-silenced nodules visualized by Lugol staining. Sections of WT nodules (A, B) display high content of starch stained in black, while this staining is missing in *nodGRP1L* RNAi-silenced nodules (C, D) indicating the absence of starch in both infected cells and non-infected cells. Scale bars, 250 μm.

4.1.5. Effects of ectopic overexpression of *nodGRP1L* gene on nodule formation and nitrogen fixation

To gain further insight into the function of *nodGRP1L*, we generated a plasmid construct in which the pLjUb promoter drives constitutive expression of this gene. The construct also contained a DsRed fluorescent reporter marking the transgenic tissues. This plasmid was introduced into *M. truncatula* using an *Agrobacterium rhizogenes* strain to induce transgenic hairy roots on the plants which were then inoculated with the microsymbiont bacteria, and plants and nodules were examined at 15 dpi.

Visual inspection revealed that overexpression of *nodGRP1L* led to reduced shoot and root growth (Fig. 22. B) compared with wild-type (WT) control (Fig. 22. A). In contrast, nodule development appeared normal, retaining the characteristic pink coloration and showing no obvious morphological differences from WT nodules. However, nitrogen fixation activity was markedly reduced. Acetylene reduction assays showed that nodules overexpressing *nodGRP1L* exhibited significantly lower nitrogenase activity compared to WT nodules (Fig. 22. C),

indicating that excessive constitutive expression of this gene negatively affects bacteroid nitrogen fixation efficiency.

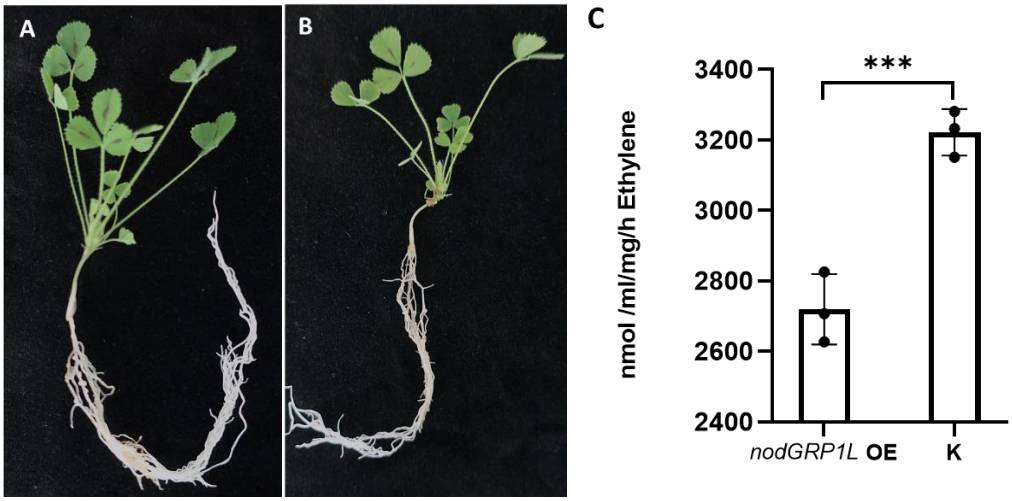

Figure 22. Effects of ectopic overexpression of the *nodGRP1L* gene on nodule development. Plants overexpressing *nodGRP1L* exhibited reduced shoot and root growth (B) compared to the wild type (WT) (A). Ethylene production from three biological replicates was normalized to both nodule weight (mg) and assay duration (hours) for acetylene reduction measurements (C). Statistical significance was determined using an unpaired *t*-test (*** $p \leq 0.001$).

To better understand this phenotype, nodules sections were stained with SYTO9 and PI fluorescent dyes for live\dead staining, and analyzed by confocal laser scanning microscopy. Microscopic observations revealed that early nodule development resulted in normal ZI and ZII, but the interzone (IZ) - where *nodGRP1L* expression is highest - appeared enlarged in the overexpressing nodules (Fig. 23. b) compared to the interzone (IZ) in WT nodules (Fig. 23. a). Although bacteroids elongated within this region, their transformation to bacteroid form is initiated (allowing the production of leghemoglobin that gives the pink colour of the nodules), they rapidly degenerated upon entering the first cell layers of zone III (Fig. 23. e). This indicates that ectopic overexpression of *nodGRP1L* interferes with the transition to fully functional differentiated, nitrogen-fixing bacteroids.

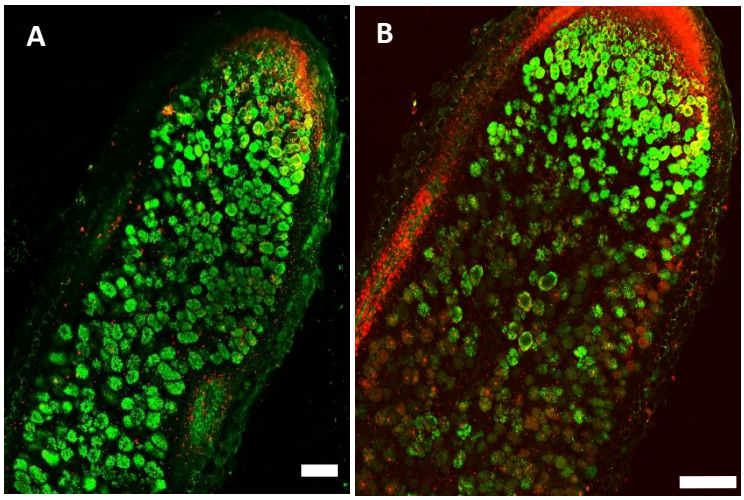

Figure 23. Live\dead staining of 15 dpi nodule where *nodGRP1L* gene is overexpressed using SYTO9 and PI. Nodule sections of WT (A) and transgenic nodules where the *nodGRP1L* gene is overexpressed (B) stained for live (green) or dead (red) bacterial cells. The IZ is large and bacteroids start to die inside the nitrogen fixing zone (ZIII) of the transgenic line (B) compared to the WT nodule (A).

Since a severe starch-amyloplast phenotype was detected in the RNAi-silenced plants, the starch content of the *nodGRP1L* overexpressing nodules was also assessed by Lugol staining (Fig. 24.). This showed that transgenic nodules accumulated noticeably more starch in an extended region comprising multiple cell layers than WT nodules, consistent with an increased number and size of amyloplasts within the infected cells. This phenotype was the exact opposite of that observed in the nodules of the RNAi-silenced plants.

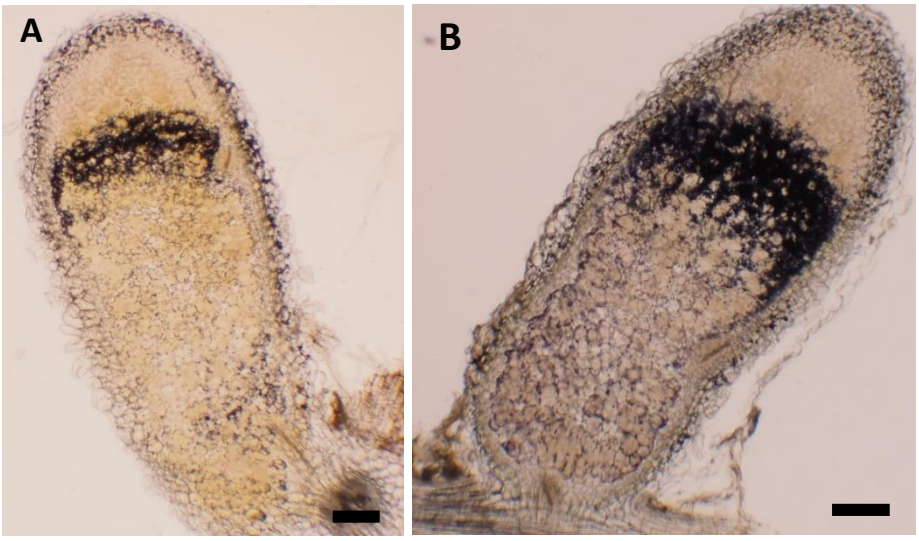

Figure 24. Starch content of the 15 dpi *nodGRP1L* overexpressing nodules visualized by Lugol staining. Nodules sections from (A) WT plant and (B) transgenic hairy roots plant where the *GRP1L* gene is overexpressed under the ubiquitin constitutive promoter. Nodule from the transgenic line (B) have higher content of starch stained with black than nodules from the WT (A), especially in the interzone (IZ). Scale bars, 250 μm.

4.1.6. Identification of the minimal promoter region responsible for the proper expression of *nodGRP1L*

The symbiotic phenotype of the *nodGRP1L* - silenced and overexpressing plants demonstrated that this gene is essential for nodule function in the interzone (IZ), aligning with RNA-seq data indicating strong expression of this gene in that region (Roux et al., 2014). We wanted to determine the minimal promoter region of *nodGRP1L* that drives its specific spatial and temporal expression patterns, aiming to identify the cis-regulatory elements responsible for gene activation in symbiotic nodules. For this purpose, promoter fragments of different lengths (1079 bp, 703 bp, and 419 bp) located upstream of the transcription start site were cloned and fused to the GUS reporter gene. These constructs were introduced into *M. truncatula* plants by hairy root transformation using *A. rhizogenes*, and transgenic roots were inoculated with the adequate *S. meliloti* strain. Since the aim was to determine which promoter fragment is sufficient to drive correct expression of *nodGRP1L,* nodules were collected at two time points: an early stage (6 dpi) and the mature symbiotic stage (14 dpi). GUS staining was done on nodules sections (Fig. 25.). At 6 dpi, all the three promoter fragments showed similar early activity within the nodule tissue (Fig. 25. A-C). In the mature nodules at 14 dpi, though the overall activity the 1079 bp fragment conferred less strong GUS staining, the highest activity is in the Interzone (IZ) for all the different promoter fragments, with weaker staining in the infection zone (ZII) and nitrogen fixation zone (ZIII) (Fig. 25. D-F), consistent with previously reported expression data (Roux et al., 2014). This indicates that the shortest 419 bp promoter fragment contains the regulatory elements necessary for correct spatial and temporal expression of *nodGRP1L*.

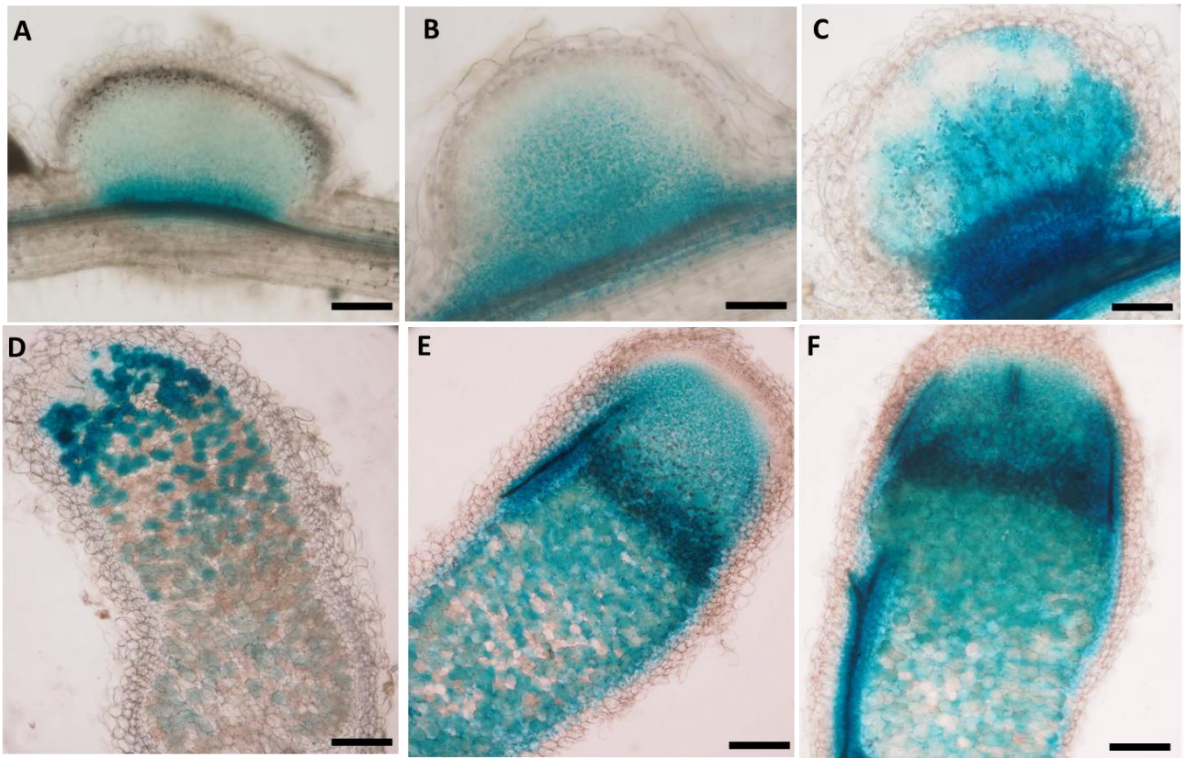

Figure 25. Activity of *nodGRP1L* promoter regions with different length visualized with GUS reporter gene in *M. truncatula* nodules. GUS staining of nodule sections from *M. truncatula* transgenic hairy roots carrying the following lengths of nod*GRP1L* promoter in GUS reporter gene fusion: 1079 bp (a, d), 703 bp (B, E) and 419 bp (C, F). Young nodules were collected at 6 dpi (A-C), while mature nodules were collected at 14 dpi (D-F). All these promoters ensure the expression of the gene in early stages (A-C) and in the IZ with different strengths later on (D-F). Scale bars, 250 μm.

4.1.7. Determining the localization of the nodGRP1L protein in the symbiotic nodule

The impaired symbiotic phenotype of the *nodGRP1L* –silenced and overexpressing plants showed unfinished bacteroid differentiation of rhizobia in *M. truncatula* nodules. Therefore, we sought to determine whether the protein product of this gene can enter bacterial cells and to identify its localization within the nodules.

4.1.7.1 Production of labeled nodGRP1L protein and observing their possible entrance to the symbiotic bacteroids or free-living rhizobia

For a more comprehensive characterization of nodGRP1L, we established a recombinant expression system and successfully expressed the nodGRP1L protein. The recombinant protein migrated at approximately 15 kDa, consistent with its predicted molecular weight, as shown in (Fig. 26.a). For purification, the constructs were designed to include a Strep-tag II attached to the C-terminal of the coding sequence of *nodGRP1L*, an eight–amino acid peptide with high affinity for engineered streptavidin resins. This system enables efficient one-step affinity

purification under physiological conditions, thereby minimizing nonspecific binding and preserving protein functionality (Fig. 26.b) (Schmidt and Skerra, 2007; Waugh, 2011).

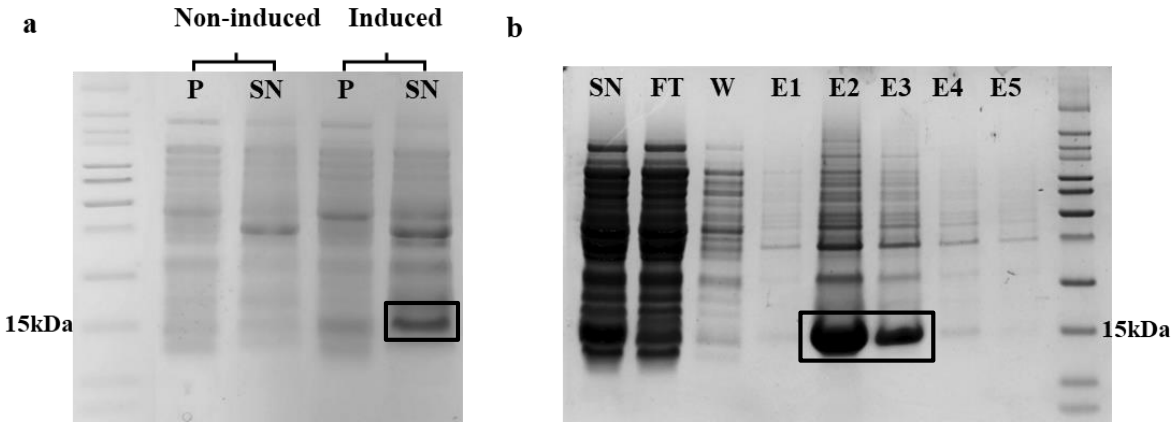

Figure 26. Expression and purification of recombinant nodGRP1L protein. SDS-polyacrylamide gel electrophoresis images showing; (a) the successful induction of *nodGRP1L* in the supernatant fraction (SN) and not in the pellet (P) of the BL321DE3 bacteria lysate, (b) the purification of the nodGRP1L peptide from the BL321DE3 bacteria lysate. The different samples are: FT: flow-through; W: washing; E1-E5: consecutive elutions. Samples were run on a 12% gel and stained with Coomassie Blue. Molecular weight markers are shown next to each experiment and the corresponding molecular weights are indicated. The boxes indicate the expected nodGRP1L-StrepII protein.

By combining the strong expression capacity of the T7-based system with the specificity of Strep-tag II affinity chromatography, we could produce recombinant *nodGRP1L* suitable for downstream labelling with FITC that enabled us to follow if these proteins are able to enter into the bacteroids and/or the free-living rhizobia *in vitro*. Either freshly grown *S. meliloti* cells or bacteroids isolated from 21 dpi nodules of *M. truncatula* were then incubated with the labeled protein in room temperature for 30 minutes followed by detecting FITC signal (green) under confocal microscopy. Bacterial cells were also visualized using the fluorescent FM4-64 dye (red) that stains bacterial membranes (Fig. 27.) Since both samples contained bacterial cells displaying the green fluorescent signals within the cell we concluded that the nodGRP1L protein could enter both the free-living rhizobia and the bacteroids.

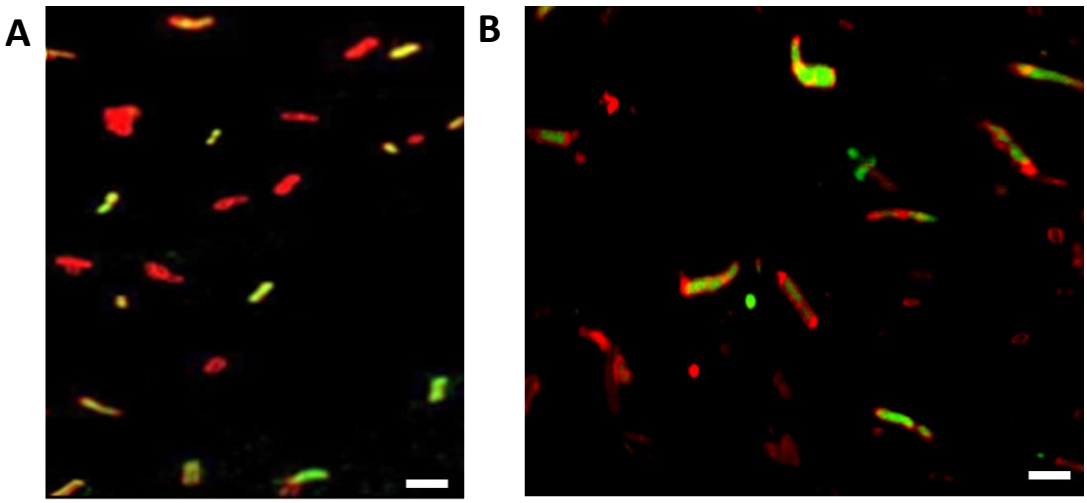

Figure 27. *In vitro* localization of nodGRP1L protein in free-living rhizobia and bacteroids. The green signal of the FITC-labeled nodGRP1L protein was detected together with the red signal of the FM4-64-stained bacterial membranes in free-living *S. meliloti* cells (A) and in isolated bacteroids (B) using confocal laser scanning microscope.

4.1.7.2. *In vivo* localization of nodGRP1L in the symbiotic cells

We generated transgenic hairy roots of *M. truncatula* that are able to express the StrepII-tagged nodGRP1L protein under the control of its native promoter. This approach allowed us to investigate the localization of nodGRP1L within the nodules under conditions that closely resemble its endogenous regulation. To determine whether the protein produced *in planta* is associated with the microsymbiont, we analyzed 21 dpi nodules using western blotting. Total nodule extracts and isolated bacteroid fractions were prepared from the transgenic nodules and probed with anti-StrepII tag antibodies (Fig. 28.). A specific band was detected in the bacteroid fraction (B+) of transgenic nodules, confirming successful expression of the protein and demonstrating that the protein is translocated into bacteroids during symbiosis. A similar signal was also present in the soluble nodule extract (SN+), which is may be explained by the release of bacteroid-derived proteins during the fractionation process. This result is consistent with the outcome of our in vitro experiments with the FITC-labeled protein and provides strong evidence that nodGRP1L is indeed delivered into bacteroids, where it may exert a direct effect on the bacteroid differentiation process.

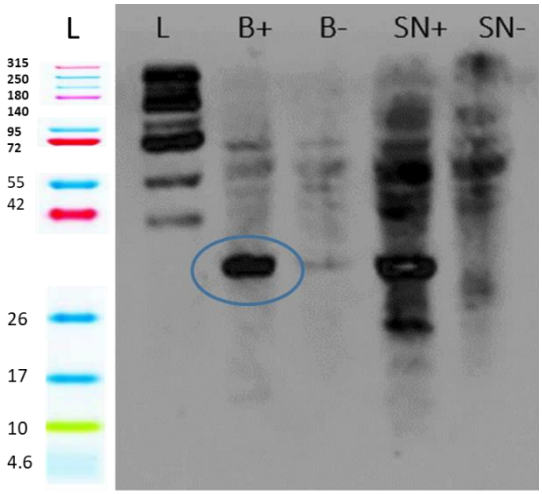

Figure 28. In vivo localization of nodGRP1L protein in *M. truncatula* nodules. Western blot with anti StrepII-tag monoclonal antibodies was used to localize the nodGRP1L-strepII protein under its own promoter. Bacteroids (B) and nodule extracts (SN) fractions were isolated: B+ bacteroid fraction from transgenic nodules; B- bacteroid fraction from WT nodules; SN+ nodule extract fraction from transgenic nodules; SN- nodule extract fraction from WT nodules. The circled band represents nodGRP1L-StrepII protein in the bacteroid fraction of the transgenic roots (B+).

4.1.8. Identification of potential bacterial and plant interaction partners of the nodGRP1L protein

4.1.8.1. Interaction of nodGRP1L protein with membrane lipids

Since nodGRP1L was detected inside bacteroids, it must cross the bacterial membrane, raising the possibility whether nodGRP1L, when secreted toward bacteroids via the plant secretory pathway, can interact with bacterial membrane lipids. To test this, we investigated its lipid-binding capacity, as the membrane of symbiotic bacteroids contains several distinct lipid components. A lipid-binding assay was performed using commercially available lipid strips containing a range of lipid species including components of the bacterial membranes with the recombinant nodGRP1L-StrepII protein and after washing the filters the bound nodGRP1L-StrepII was visualized with anti-StrepII antibody (Fig. 29.). The results showed that nodGRP1L exhibited the strongest affinity for phosphatidylserine (PS) and cardiolipin (CL). In addition, strong binding was observed to 3-sulfogalactosylceramide (3-SGC) and phosphatidylinositol 4-phosphate (PtdIns(4)P), along with weaker interactions with other phospholipids, including phosphatidic acid (PA), phosphatidylglycerol (PG), phosphatidylinositol-4,5-bisphosphate (PtdIns(4,5)P_2), and phosphatidylinositol-3,4,5-trisphosphate (PtdIns(3,4,5)P_3). Notably, several of these lipids (like phosphatidylserine, Cardiolipin, phosphatidic acid and phosphatidylglycerol) are major components of the *S. meliloti* bacteroid membrane

(Sohlenkamp et al., 2004). The results of this assay suggest that nodGRP1L can directly interact with phospholipids found in bacteroid membranes.

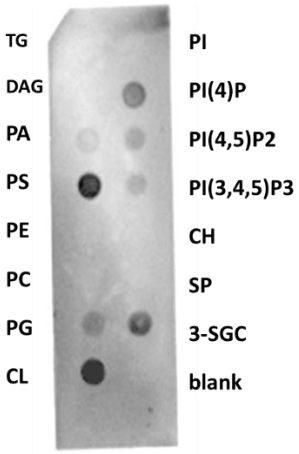

Figure 29. Lipid binding pattern of nodGRP1L protein. The nodGRP1L protein shows strong binding to phosphatidylserine (PS) and Cardiolipin (CL) and also shows weaker binding to other phospholipids (PE, PC, PA, PG, PtdIns(4)P, PtdIns(4,5)P2, PtdIns(3,4,5)P3). Stronger binding sites appear as darker signals. Differences in intensity indicate that the protein shows a preference for certain phospholipids. TG, Triglyceride; DAG, Diacylglycerol; PA, Phosphatidic acid; PS, Phosphatidylserine; PE, Phosphatidylethanolamine; PC, Phosphatidylcholine; PG, Phosphatidylglycerol; CL, Cardiolipin; PI, Phosphatidylinositol; PI4P, Phosphatidylinositol-4-phosphate; PI(4,5)P2, Phosphatidylinositol-4,5-bisphosphate; PI(3,4,5)P3, Phosphatidylinositol-3,4,5-trisphosphate; CH, Cholesterol; SP, Sphingomyelin; 3-SGC, 3-sulfogalactosylceramide.

4.1.8.2. Interaction of nodGRP1L with nodule proteins

To identify potential bacterial and plant protein partners of nodGRP1L, the produced recombinant nodGRP1L-StrepII protein was also used in affinity chromatography (pull-down) experiments. The experiments were performed using nodule extracts from *M. truncatula* (done by Hilda Tiricz), allowing the nodGRP1L-StrepII recombinant protein to bind its interacting partners. The bound proteins were subsequently analyzed by LC–MS/MS-based proteomics (done in BRC Poteomics Lab). Through these pull-down experiments, both bacterial and plant proteins interacting with the recombinant StrepII-tagged nodGRP1L protein were identified.

Analysis of the proteomic data identified several potential bacterial and plant interaction partners: 1694 *M. truncatula* proteins and 364 rhizobia proteins were identified. Among the plant proteins, three nodGRPs and three NCRs were identified - nodGRP2D, nodGRP6B, nodGRP1K, NCR169, NCR007, and NCR582 (Fig. 30.). This finding was further confirmed by additional pull-down experiments performed in our laboratory using other nodGRP proteins.

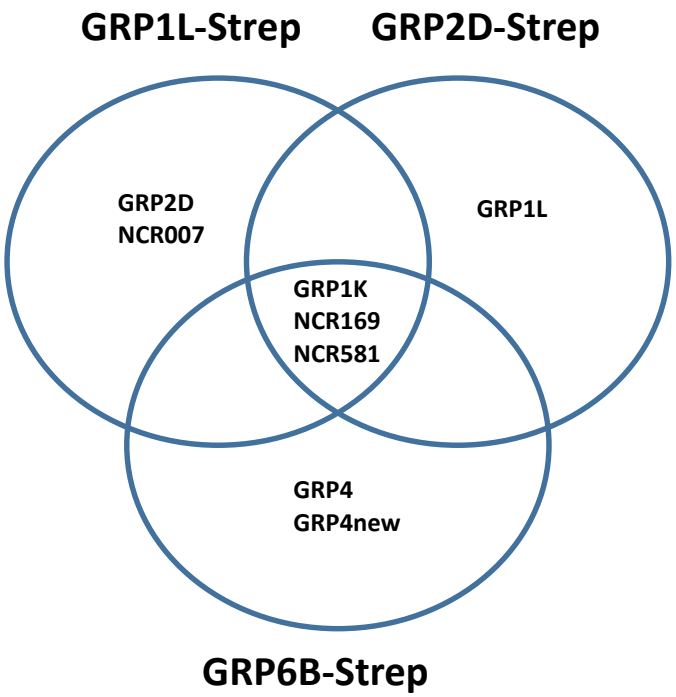

Figure 30. Venn diagram of proteomic data on a pull down experiments (a) showing interacting nodGRP and NCR partners of recombinant GRP1L-StrepII, GRP2D-StrepII and GRP6B-StrepII in *M. truncatula* nodule extract.

4.1.8.3. Quantitative analysis of GRP1L interactions with nodGRP2D and NCR169 by microscale thermophoresis

Microscale thermophoresis (MST) was employed to quantify the interaction between fluorescently labeled protein or peptide detected previously in the pull-down experiments and the unlabeled nodGRP1L. This technique monitors changes in molecular movement along a microscopic temperature gradient, which occur as a consequence of binding-induced alterations in size, charge, hydration shell, or conformation. To quantify binding affinities of nodGRP1L with the identified potential symbiotic plant proteins, we tested one glycine-rich protein (nodGRP2D) and one nodule cysteine-rich peptide (NCR169). For MST measurements, nodGRP2D was conjugated with FITC, whereas NCR169 was labeled with the BODIPY fluorophore, then each was combined with nodGRP1L. The resulted normalized fluorescence values reflect the binding-induced change in molecular movement under a temperature gradient, and were also used to determine binding affinity (Fig. 31.). When tested, 80 nM nodGRP2D-FITC exhibited strong binding to 100 µM nodGRP1L, with a response amplitude of 4.5 (Fig. 31. A). Likewise, 1 µM NCR169-BODIPY bound to 50 µM nodGRP1L, yielding a response amplitude of 30.8 (Fig. 31. B). For the affinity binding determination, a two-fold serial dilution was prepared starting from the concentrations mentioned above. Analysis of the binding curves revealed dissociation constants (Kd) of 458 nM for the nodGRP2D–nodGRP1L interaction

(Fig. 31. C) and 13 µM for the NCR169–nodGRP1L interaction (Fig.31. D). These results confirmed that nodGRP1L can interact with nodGRP2D and NCR169, but with higher affinity towards nodGRP2D.

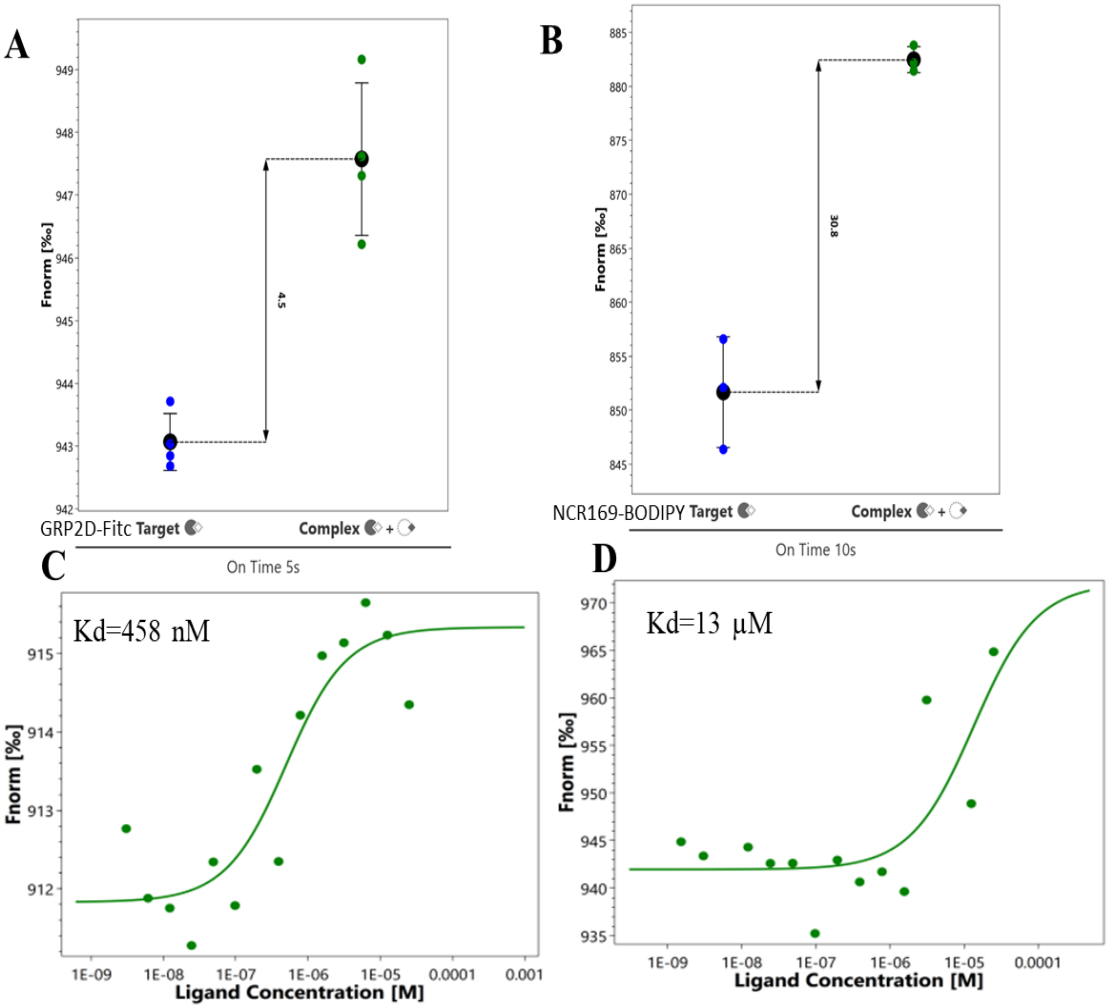

Figure 31. Quantification of the binding affinities of nodGRP1L with nodGRP2D and NCR169 by microscale thermophoresis assay. Binding-induced change in molecular movement under a temperature gradient was shown by the calculated normalized fluorescence values, expressed as a thousandth (Fnorm) between 100 µM nodGRP1L and 80 nM nodGRP2D-FITC (A), and 50 µM nodGRP1L and 1 µM NCR169-BODIPY (B). The affinity of the binding was also measured (C, D) using a gradient of 2-fold dilution starting from the concentration used for the initial test experiments (A, B), respectively.

4.1.8.4. Discovery of nodGRP1L-interacting rhizobial proteins via Yeast Two-Hybrid screening

We further sought potential protein interaction partners of nodGRP1L using a yeast two-hybrid (Y2H) system. An available *S. meliloti* ORFome library was screened to identify interacting proteins with the cloned nodGRP1L bait. Following a strict selection on -His/-Leu/-Trp/-Ade (-HLTA) plates, few colonies were observed, indicating potential positive interaction.

Subsequent sequence analysis identified the *secB* gene in each colony. *SecB* codes for a molecular chaperone that functions within the Sec translocation complex, facilitating the translocation of precursor proteins across the cytoplasmic membrane. To validate this nodGRP1L - SecB interaction, a pairwise Y2H assay was performed by cloning both *nodGRP1L* and *SecB* into the pGADT7 and pDEST-GBKT7 vectors in reciprocal combinations. Growth on -HLTA plates confirmed a specific interaction between the two proteins (Fig. 32.). Moreover, the results suggest a strong interacting ability of SecB to itself and a weaker interaction of the nodGRP1L itself.

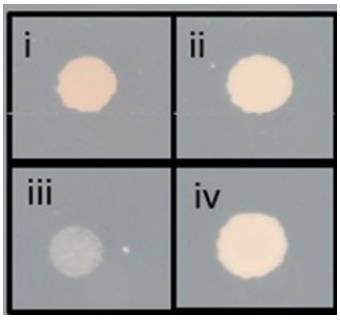

Figure 32. Pairwise yeast two-hybrid assay on SD-HLTA selective medium. AH109 yeast cells co-expressing GRP1L (Gal4 activation, AD) and SecB (Gal4 binding, BD) in all combinations. (i) pGADT7-nodGRP1L + pDEST-GBKT7-SecB. (ii) pGADT7-SecB + pDEST-GBKT7-SecB. (iii) pGADT7-nodGRP1L and pDEST-GBKT7-nodGRP1L (iv) pGADT7-SecB + pDEST-GBKT7-nodGRP1L.

4.1.8.5. *In vivo* validation of the nodGRP1L–SecB interaction using bimolecular fluorescence complementation in *N. benthamiana*

The interaction between nodGRP1L and SecB was further validated *in vivo* using a bimolecular fluorescence complementation (BiFC) assay. In this system, the nodGRP1L protein was fused to the N-terminal fragment of yellow fluorescent protein (YFP), while SecB was fused to the complementary C-terminal fragment of YFP. The two recombinant constructs were cloned into adequate *Agrobacterium tumefaciens* strains, which were used for *N. benthamiana* leaf co-infiltration. Fluorescence signals are only expected if the two proteins interact and the reconstituted YFP gives the signal indicating a physical interaction between the two proteins within plant cells (Fig. 33.). As positive controls, both nodGRP1L and SecB were fused to green fluorescent protein (GFP), and infiltrated into *N. benthamiana* cells respectively to confirm their proper expression in the plant system. Our results confirmed that the two proteins interact with each other *in planta*.

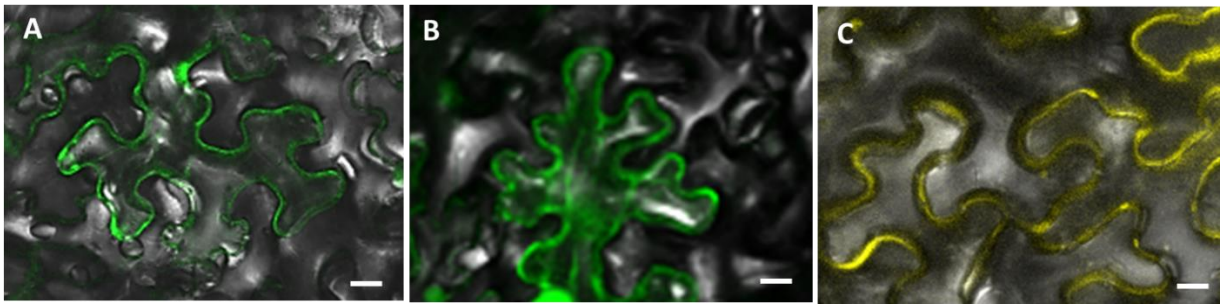

Figure 33. **Bimolecular fluorescence complementation between nodGRP1L and SecB in *N. benthamiana* leaves.** (A) *nodGRP1L* fused to GFP. (B) *SecB* fused to GFP. (C) N-terminal fragment of YFP was fused to the *nodGRP1L*, while C-terminal fragment of YFP was fused to the *SecB* and YFP is expressed when nodGRP1L and SecB proteins interact with each other. The *A. tumefaciens* strains harboring the constructs were infiltrated into young *N. benthamiana* leaves and checked under confocal microscopy 3 days after infiltration. Scale bar 10 μm.

4.2. Multi-approach characterization of the antimicrobial effect of the most potent derivative of the symbiotic NCR169 plant peptide

NCR169 peptide is essential for establishing symbiosis in *Medicago* species (Horváth et al., 2015). Although it does not exhibit antifungal activity, it shows antimicrobial effects. On the other hand, its C-terminal derivative NCR169C$_{17-38}$ demonstrated potent antifungal (Szerencsés et al., 2021, 2025), and antibacterial (Howan et al., 2023) activity. During my PhD, we evaluated the antimicrobial activity of NCR169 and its cysteine variants, as well as shorter fragments - including the potent derivative NCR169C$_{17-38}$ - against a panel of clinically relevant bacterial pathogens, including ESKAPE bacterial pathogens. However, no comparative study has yet investigated how different conditions influence its efficacy. Moreover, its potential in comparison with traditional antibiotics has not been assessed, and its mechanism of action has remained largely unexplored.

4.2.1. pH-dependent solubility and bactericidal activity of NCR169 and its structural variants

NCR169, its oxidized form (NCR169ox), and its variant in which the four cysteines were replaced with serines (NCR169-C$_{9,15,28,33}$/S) (Table 2.A) were chemically synthesized with C-terminal amidation. These peptides were tested for antimicrobial activity against a panel of ESKAPE pathogens - *Enterococcus faecalis*, *Staphylococcus aureus*, *Klebsiella pneumoniae*, *Acinetobacter baumannii*, *Pseudomonas aeruginosa*, *Escherichia coli* - as well as *Listeria monocytogenes* and *Salmonella enterica*. Peptides were applied to 10^6 log-phase bacterial cultures in a two-fold dilution series (25 - 0.1 μM) in potassium phosphate buffer (PPB) at pH

7.4. After three hours of incubation, 5 µl of each treatment was plated on LB agar and incubated overnight at 37 °C to assess bacterial survival. Minimal bactericidal concentrations (MBCs), defined as the lowest concentration eliminating bacterial growth, are presented in Table 2B. NCR169 demonstrated potent bactericidal activity at 3.1 µM against *A. baumannii*, *E. coli* and *S. enterica*; 6.3 µM against *S. aureus* and 12.5 µM against *K. pneumoniae*, *P. aeruginosa* and *L. monocytogenes*, while showing no detectible activity against *E. faecalis* (Table 2.B). These values represent the average of four biological replicates, although significant variability was observed, likely due to the poor solubility of NCR169 at pH 7.4, indicated by a visible white turbidity upon peptide addition. In contrast, both NCR169ox or NCR169-$C_{9,15,28,33}$/S exhibited no visible turbidity and yielded consistent MBC values at this pH. While NCR169ox showed similar or slightly reduced antimicrobial activity compared to NCR169, NCR169-$C_{9,15,28,33}$/S variant demonstrated markedly weaker efficacy, with bactericidal effects restricted to *A. baumannii*, *P. aeruginosa*, and *E. coli*.

Table 2. Minimal bactericidal concentrations (MBC) of NCR169 and its derivatives against *Enterococcus faecalis (Ef); Staphylococcus aureus (Sa); Klebsiella pneumoniae (Kp); Acinetobacter baumannii (Ab); Pseudomonas aeruginosa (Pa); Escherichia coli (Ec); Listeria monocytogenes (Lm); Salmonella enterica (Se). A. Amino acid sequence and isoelectric points (pI values) of the peptides. B. MBC values of the peptides (in µM) in PPB at pH 7.4 and 5.8 (in bold letters) after three hours of treatment.*

A

Peptides	Amino Acid Sequence	pI
NCR169	EDIGHIKYCGIVDDCYKSKKPLFKIWKCVENVCVLWYK	8.6
NCR169ox	EDIGHIKYCGIVDDCYKSKKPLFKIWKCVENVCVLWYK	8.6
NCR169-$C_{9,15,28,33}$/S	EDIGHIKY**S**GIVDD**S**YKSKKPLFKIWK**S**VENV**S**VLWYK	9.7

B

Peptides	pH	*E. f.*	*S. a.*	*K. p.*	*A. b.*	*P. a.*	*E. c.*	*L. m.*	*S. e.*
NCR169	7.4	-	6.3*	12.5*	3.1	12.5*	3.1*	12.5*	3.1*
NCR169ox	7.4	-	25	25	1.6	6.3	6.3	12.5	12.5
NCR169-$C_{9,15,28,33}$/S	7.4	-	-	-	3.1	25	6.3	-	-
NCR169	**5.8**	**-**	**3.1**	**12.5**	**3.1**	**6.3**	**3.1**	**6.3**	**3.1**
NCR169ox	**5.8**	**-**	**3.1**	**3.1**	**3.1**	**6.3**	**1.6**	**3.1**	**3.1**
NCR169-$C_{9,15,28,33}$/S	**5.8**	**-**	**6.3**	**12.5**	**3.1**	**6.3**	**1.6**	**25**	**6.3**

- : lack of bactericidal activity up to 25 µM.

* The best MBC value measured but there were more than two-fold dilution differences in the replicates.

Using PPB at pH 5.8 resolved the solubility problem of NCR169, eliminating visible turbidity and producing reproducible MBC values: 3.1 μM against *S. aureus, A. baumannii, E. coli* and *S. enterica;* and 6.3 μM against *P. aeruginosa* and *L. monocytogenes* (Table 2.B). Both the oxidized form of NCR169 and NCR169-$C_{9,15,28,33}$/S were more active at pH 5.8 showing significantly lower MBC values against most bacteria than at pH 7.4. However, their activities were largely comparable to NCR169 under these acidic conditions. Notably, NCR169ox showed slightly enhanced activity against *K. pneumoniae,* whereas NCR169-$C_{9,15,28,33}$/S was less effective against *L. monocytogenes*. These findings suggest that the cysteine residues in NCR169 are not essential for its antimicrobial activity at pH 5.8, although they may contribute to enhanced efficacy against specific strains such as *L. monocytogenes*.

4.2.2. NCR169$C_{17\text{-}38}$: a C-terminal segment with consistent and potent antibacterial activity

Next, various short derivatives of the NCR169 peptide (Table 3.A) were tested for antimicrobial activity under different conditions. We have shown in previous works that the 22 amino acid long sequence at the C-terminal end, NCR169$C_{17\text{-}38}$, was effective against several fungi, including *Candida* species (Szerencsés et al., 2021) and *Cryptococcus neoformans* (Szerencsés et al., 2025). Moreover, NCR169$C_{17\text{-}38}$ and its substituted derivatives exhibited clear bactericidal effects against eight bacterial strains (Howan et al., 2023), also used in this study. Since adding an eight-residue StrepII-tag (WSHPQFEK) to other NCR peptides either preserved or enhanced their antimicrobial activity (Jenei et al., 2020), we tested a tagged version of NCR169$C_{17\text{-}38}$ (NCR169$C_{17\text{-}38}$-StrepII). A one-residue longer variant, NCR169$_{16\text{-}38}$, which carries Tyr at position 16, was also included in the study. Additionally, four shorter fragments of NCR169$C_{17\text{-}38}$ were tested, including NCR169$_{16\text{-}27}$, previously shown to be active against *E. coli* and *S. meliloti* (Isozumi et al., 2021). As none of the peptides had solubility issues, the antimicrobial tests were performed in PPB pH 7.4.

NCR169$C_{17\text{-}38}$ effectively killed the tested pathogens, as did both NCR169$C_{17\text{-}38}$-StrepII and NCR169$_{16\text{-}38}$ (Table 3.B). Shorter fragments of NCR169$C_{17\text{-}38}$, representing either its C-terminal (NCR169$_{21\text{-}38}$ and NCR169$_{27\text{-}38}$) or N-terminal (NCR169$_{16\text{-}27}$ and NCR169$_{17\text{-}27}$) segments were mostly ineffective at 25 μM, except against *E. coli*, for which MBCs reached up to 25 μM. Given that NCR169$_{16\text{-}27}$, had previously shown strong activity against *E. coli* K12 strain in 5 mM HEPES buffer (pH 7.0) (Isozumi et al., 2021) we tested the activity of NCR169$_{16\text{-}27}$, NCR169$_{17\text{-}27}$, and the longer NCR169$C_{17\text{-}38}$, NCR169$_{16\text{-}38}$ peptides under the same conditions (Table 3.B). MBC values for NCR169$C_{17\text{-}38}$, NCR169$_{16\text{-}38}$ remained similar to those

in PPB. However, NCR169$_{16-27}$ peptide - despite its poor performance in PPB - exhibited significant activity in HEPES, with MBCs comparable to those of NCR169C$_{17-38}$, except for *L. monocytogenes* (12.5 μM) and *E. faecalis* (inactive). The absence of Tyr (NCR169$_{16}$) in NCR169$_{17-27}$, led to a loss of activity against four bacterial species and increased MBCs for *A. baumannii, E. coli* and *S. enterica*.

Table 3. The antimicrobial activity of short derivatives of NCR169. A. Amino acid sequence and pI values of the short peptide fragments. B. MBC values of these peptides (in μM) in PPB (20 mM PPB at pH 7.4) or in HEPES buffer (5 mM HEPES pH 7.0). The minimal bactericidal concentrations (in μM) of peptides are shown against *Enterococcus faecalis (Ef); Staphylococcus aureus (Sa); Klebsiella pneumoniae (Kp); Acinetobacter baumannii (Ab); Pseudomonas aeruginosa (Pa); Escherichia coli (Ec); Listeria monocytogenes (Lm); Salmonella enterica (Se)*

A

Peptides	**Amino Acid Sequence**	**pI**
NCR169C$_{17-38}$	KSKKPLFKIWKCVENVCVLWYK	10.2
NCR169C$_{17-38}$-StrepII	KSKKPLFKIWKCVENVCVLWYKWSHPQFEK	10.1
NCR169$_{16-38}$	YKSKKPLFKIWKCVENVCVLWYK	10.2
NCR169$_{21-38}$	PLFKIWKCVENVCVLWYK	9.1
NCR169$_{27-38}$	KCVENVCVLWYK	8.1
NCR169$_{16-27}$	YKSKKPLFKIWK	11.3
NCR169$_{17-27}$	KSKKPLFKIWK	14

B

Peptides	***Buffer***	***E. f.***	***S. a.***	***K. p.***	***A. b.***	***P. a.***	***E. c.***	***L. m.***	***S. e.***
NCR169C$_{17-38}$	PPB	6.3	3.1	3.1	3.1	3.1	1.6	3.1	3.1
NCR169C$_{17-38}$-StrepII	PPB	3.1	3.1	3.1	3.1	3.1	1.6	3.1	3.1
NCR169$_{16-38}$	PPB	3.1	3.1	3.1	3.1	3.1	1.6	3.1	3.1
NCR169$_{21-38}$	PPB	-	-	-	12.5	-	25	-	-
NCR169$_{27-38}$	PPB	-	-	-	-	-	25	-	-
NCR169$_{16-27}$	PPB	-	-	-	-	-	25	-	-
NCR169$_{17-27}$	PPB	-	-	-	-	-	-	-	-
NCR169C$_{17-38}$	HEPES	3.1	3.1	6.3	1.6	3.1	1.6	3.1	3.1
NCR169$_{16-38}$	HEPES	3.1	1.6	3.1	3.1	3.1	1.6	3.1	1.6
NCR169$_{16-27}$	HEPES	-	3.1	6.3	3.1	3.1	3.1	12.5	3.1
NCR169$_{17-27}$	HEPES	-	-	-	12.5	3.1	6.3	-	25

- : lack of bactericidal activity up to 25 μM.

Further testing in Mueller Hinton Broth (MHB), which contains divalent cations known to reduce cationic AMP activity (Hancock & Stahl, 2006), revealed elevated MBCs (6.3 or 12.5 μM) for NCR169C$_{17-38}$, NCR169C$_{17-38}$-StrepII, and NCR169$_{16-38}$. In this medium NCR169C$_{17-27}$ and NCR169$_{16-27}$ were inactive at 25 μM (Table 4). However, the addition of 0.4 mM EDTA – without affecting bacterial viability - restored the activity of NCR169C$_{17-38}$ and NCR169$_{16-38}$ to PPB-level MBCs. EDTA had only a limited effect on NCR169$_{16-27}$ and NCR169$_{17-27}$, NCR169$_{16-27}$ regained partial activity only against *E. coli* (MBC 6.3 μM). Based on the antimicrobial test results, the most reliable NCR169C$_{17-38}$ was chosen for in-depth analysis and mode-of-action studies. Some key properties were compared with those of other peptide variants (Table 4).

Table 4. Minimal bactericidal concentrations (MBC; in μM) of the selected short peptides on three tested pathogens after 3 h of treatment in MHB in the absence (0) or presence (+) of 0.4 mM EDTA. *Escherichia coli (Ec), Acinetobacter baumannii (Ab), Staphylococcus aureus (Sa).*

Peptides	**EDTA**	***Ec***	***Ab***	***Sa***	**EDTA**	***Ec***	***Ab***	***Sa***
NCR169C$_{17-38}$	**0**	6.3	6.3	12.5	+	1.6	3.1	3.1
NCR169C$_{17-38}$-StrepII	**0**	12.5	6.3	25	+	1.6	3.1	3.1
NCR169$_{16-38}$	**0**	6.3	6.3	25	+	1.6	1.6	3.1
NCR169$_{16-27}$	**0**	-	-	-	+	6.3	-	25
NCR169$_{17-27}$	**0**	-	-	-	+	-	-	-

- : lack of bactericidal activity up to 25 μM

4.2.3. Synergistic effect of NCR169C$_{17-38}$ peptide with conventional antibiotics and other NCRs in the combined treatment of *E. coli*

The use of multiple antimicrobial agents can simultaneously target different physiological pathways in microbial cells, reducing the likelihood of resistance development and increasing treatment efficacy. To explore this strategy, we assessed the combined antibacterial effects of the NCR169C$_{17-38}$ peptide with several antibiotics - specifically polymyxin B, meropenem, and streptomycin - against *E. coli*. In addition, we tested two short peptide derivatives of NCR335 that showed antimicrobial activities earlier (Farkas et al., 2017). These NCR335N$_{1-19}$ and NCR335C$_{13-33}$ short peptides were previously reported to exhibit antifungal activities against *Candida* and *Cryptococcus* species (Szerencsés et al., 2021, Szerencsés et al., 2025). First, the MBC values of the antibiotics and peptides were determined under our experimental conditions (Table 5), allowing us to define appropriate concentration ranges for subsequent combination

studies. Combination treatments were then performed using the standard checkerboard titration method, with each agent co-administered with NCR169C_{17-38}. The efficacy of the combinations was evaluated using the Fractional Bactericidal Concentration (FBC) index (FBC = FBC-A + FBC-B) to determine the nature of the interaction between agents (Table 5). Synergistic interactions were observed when NCR169C_{17-38} was combined with polymyxin B and meropenem, whereas its combination with streptomycin resulted in an additive effect. Moreover, the NCR335-derived fragments NCR335N_{1-19} and NCR335C_{13-33}, which individually displayed bactericidal activity, also exhibited synergistic effects when combined with NCR169C_{17-38}.

Table 5. Combined effect of NCR169$C_{17–38}$ with antibiotics and NCR335 peptide fragments against *E. coli*. MBC value of each Drug A is included, NCR169$C_{17–38}$ was consistently used as Drug B.

Drug A	Drug A MBC (μM)	FBC-A (μM)	FBC-B (μM)	FBC	Action
Polymyxin B	0.8	0.125 (0.1)	0.25 (0.4)	0.38	Synergism
Meropenem	200	0.25 (50)	0.25 (0.4)	0.5	Synergism
Streptomycin	3.125	0.5 (1.6)	0.5 (0.8)	1	Additive
NCR335N_{1-19}	3.125	0.5 (1.6)	0.01 (0.024)	0.5	Synergism
NCR335C_{13-33}	12.5	0.5 (6.25)	0.03 (0.048)	0.5	Synergism

Fractional bactericidal concentration (FBC) index values: < 0.5: synergism; 0.5 < FBC < 1.0: additive; 1.0 < FIC < 2.0: indifferent; >2: antagonism. (μM) corresponds to the concentration of drug A and Drug B for the indicated action.

4.2.4. Biofilm inhibition and eradication by NCR169C_{17-38} in comparison with meropenem and polymyxin B

We examined the capacity of NCR169C_{17-38} to inhibit biofilm formation by *Acinetobacter baumannii*, a pathogen well known for its robust biofilm production and high level of antibiotic resistance. Initially**,** we performed the antimicrobial test in MHB with 24 h treatment of NCR169C_{17-38}, meropenem and polymyxin B against *A. baumannii* and determined their MBC values as usual (Table 6.). Additionally, at the end of the experiment we determined the quantity of the biofilm and thereby evaluated their ability to inhibit biofilm formation during culturing the bacteria in the presence of different concentrations of the agents (Fig. 1.A). We tested NCR169C_{17-38} in a concentration range from 25 μM to 0.4 μM, meropenem from 100 μM to 1.6 μM and polymyxin B from 3.1 μM to 0.05 μM. Biofilm formation by *A. baumannii* was

significantly reduced by all three agents when applied at their respective MBC concentrations, with NCR169C$_{17-38}$ and meropenem remaining effective even at lower doses.

Table 6. MBC values of NCR169C$_{17-38}$, meropenem and polymyxin B against *A. baumanni* after 24 h of treatment in MHB with detecting at the end the biofilm inhibition, and at the end of eradication tests against pre-formed biofilm after 3 h or 24 h treatment.

	NCR169C$_{17-38}$	**Meropenem**	**Polymyxin B**
Inhibition test after 24 hours	6.3 μM	50 μM	0.8 μM
Eradication test after 3 hours	6.3 μM	>100 μM	>3.2 μM
Eradication test after 24 hours	12.5 μM	>100 μM	>3.2 μM

Bacteria that grow and produce biofilm prior to treatment and thereby located within biofilm exhibit higher resistance against antibiotic treatments. To assess whether the NCR169C$_{17-38}$ peptide or the tested antibiotics could eradicate pre-formed biofilms, *A. baumannii* was first cultured in MHB for 24 hours, then treated with NCR169C$_{17-38}$, meropenem or polymyxin B for either 3h or 24 h, using the same concentration range as in the previous experiment. Both bacterial survival within the pre-formed biofilm and the amount of residual biofilm were assessed. The MBC values obtained in these biofilm eradication assays (Table 6.) indicated that the NCR169C$_{17-38}$ peptide was able to kill bacteria with an efficacy comparable to that observed in the planktonic antimicrobial test. In contrast, neither of the two antibiotics eliminated the bacteria completely within the tested concentration range. Quantification of the residual biofilm at the end of the experiments revealed that, after 3 h of treatment, none of the tested antibiotics were able to eradicate the established biofilms. Only NCR169C$_{17-38}$ was capable of degrading the pre-formed biofilm in this short time, and this effect was observed at concentrations exceeding its MBC (at 12.5 and 25 μM; Fig. 34.B). Interestingly, after 24 h of treatment, all agents demonstrated the ability to degrade biofilms, albeit at different effective concentrations. NCR169C$_{17-38}$ and meropenem were successful even at sub-MBC level (Fig. 34.C), whereas polymyxin B required at least their MBC or higher concentrations to achieve significant biofilm eradication.

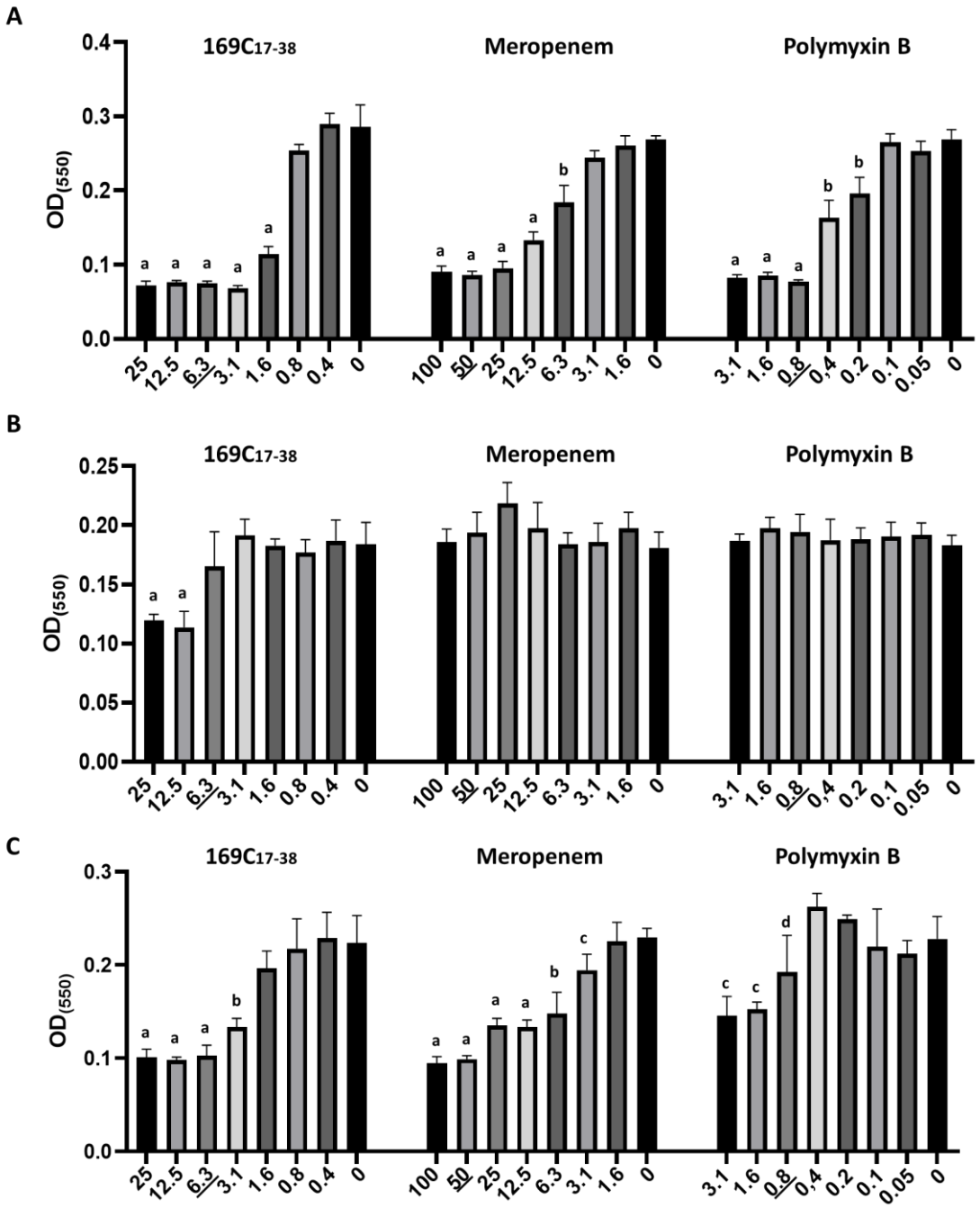

Figure 34. NCR169C$_{17-38}$ effect on biofilm produced by *A. baumannii* compared to antibiotics. After the treatments, the biofilm was visualized by Crystal Violet (CV) staining and quantified by measuring OD_{550}. The peptide and antibiotics were applied in a series of dilutions, with the MBC values underlined. A. Inhibition of biofilm formation by NCR169C$_{17-38}$, meropenem and polymyxin B. B+C Biofilm eradication by NCR169C$_{17-38}$, meropenem and polymyxin B after 3 hours (B) or 24 hours (C) of treatment. The OD (550) values represent the mean ± standard deviation calculated from three independent experiments (a: $p \leq 0.0001$, b: $p \leq 0.001$, c: $p \leq 0.01$, d: $p \leq 0.05$, unpaired t test).

4.2.5. Rapid impact of NCR169C$_{17-38}$ on *E. coli* membrane permeability

Next, we investigated whether the application of NCR169C$_{17-38}$ peptide affects membrane permeability of *E. coli*, and if so, to what extent and how rapidly these changes occur. In the first experiment, *E. coli* cells were exposed to near-MBC concentrations (0.8 and 1.6 μM) of NCR169C$_{17-38}$ for 10 minutes, followed by staining with SYTO 9 (can enter undamaged living cells staining them green) and propidium iodide (PI**,** can enter only cells with damaged membrane and staining them red)**,** and examination by confocal microscopy. While untreated control cells exhibited only the green fluorescence of SYTO 9, bacterial cultures exposed to 0.8 μM peptide showed predominantly red-stained cells, with only a few remaining green, indicating rapid membrane disruption as evidenced by PI uptake (Fig. 35.A). At 1.6 μM peptide, all cells appeared red, demonstrating complete and rapid loss of membrane integrity.

To visualize the morphological changes in *E. coli* induced by NCR169C$_{17-38}$, the same treatment was performed without fluorescent dyes. Instead, the cells were fixed and examined using scanning electron microscopy (SEM)**.** Unlike the smooth, intact morphology of untreated cells, *E. coli* cells treated with 0.8 μM NCR169C$_{17–38}$ displayed evident surface roughening and outer membrane blebbing, indicating peptide-induced structural disintegration (Fig. 35.B). At higher peptide concentration (1.6 μM), more pronounced membrane damage was evident, including visible perforations and extrusion of cellular material from ruptured areas.

To get a more precise assessment of how rapidly NCR169C$_{17-38}$ induces membrane damage, we monitored PI uptake in real time. *E. coli* was treated in a microtiter plate with two-fold dilutions of NCR169C$_{17-38}$ (12.5 - 0.8 μM) and PI fluorescence was measured using a plate reader (Fig. 35.C). For comparison, polymyxin B, a well-known membrane-permeabilizing/damaging antibiotic, was included as a control. A rapid rise in fluorescence within 1–2 minutes was observed upon exposure to NCR169C$_{17-38}$ at MBC or higher concentrations, indicating swift membrane permeabilization. Comparison of PI uptake kinetics of NCR169C$_{17-38}$ and polymyxin B at their respective MBC values showed that NCR169C$_{17-38}$ disrupts bacterial membranes more rapidly and effectively than polymyxin B.

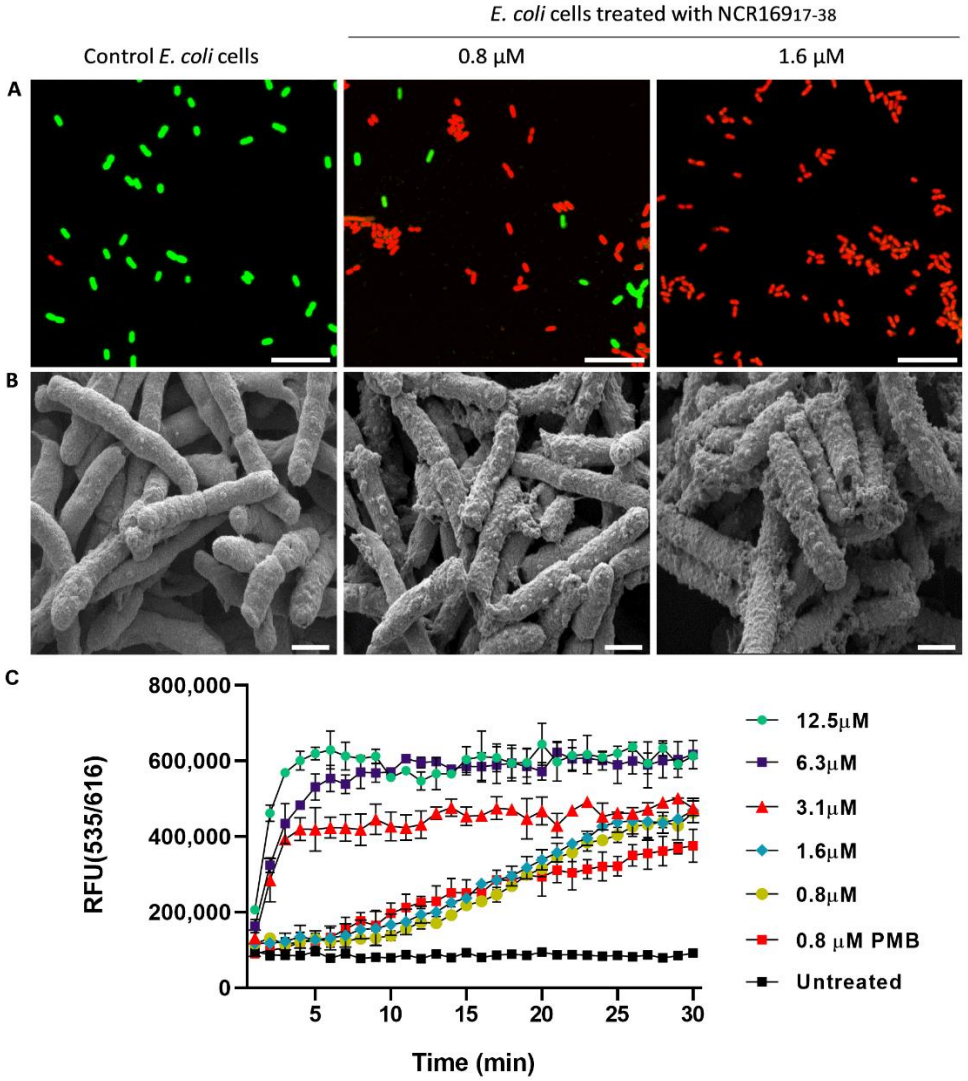

Figure 35. Membrane integrity or damage and morphology of *E. coli* following exposure to various concentrations of the NCR169C$_{17-38}$ peptide. (A) *E. coli* cells were stained with SYTO 9 and PI, and pictures were taken with confocal microscope; scale bar: 10 µM. (B) Cells were treated with the peptide in the absence of fluorescent dyes and imaged using a scanning electron microscope; scale bar: 1 µM. (C) Monitoring of PI uptake in *E. coli* treated with a series of concentrations of NCR169C$_{17-38}$ in Hidex Plate reader. RFU (535/616) = Relative Fluorescence Units (excitation/emission wavelengths). 0.8 µM Polymyxin B (PMB) was used as a control.

4.2.6. Thermal stability and lipid-binding specificity of NCR169C$_{17-38}$

Given that NCR169C$_{17-38}$ and NCR169C$_{17-38}$-StrepII displayed comparable antimicrobial activity, we evaluated the stability of NCR169C$_{17-38}$-StrepII at room temperature and heat stress. Peptide dilutions (25, 12.5, 6.3, and 3.1 µM) in PPB were either incubated overnight at room temperature (RT) or heated at 80 °C for 20 min. Dot blot detection of the peptide with an anti-StrepII antibody confirmed its stability (Fig. 36.A), and antimicrobial assays against *E. coli* revealed unchanged bactericidal activity relative to freshly prepared controls (Fig. 36.B), demonstrating high thermal and storage stability.

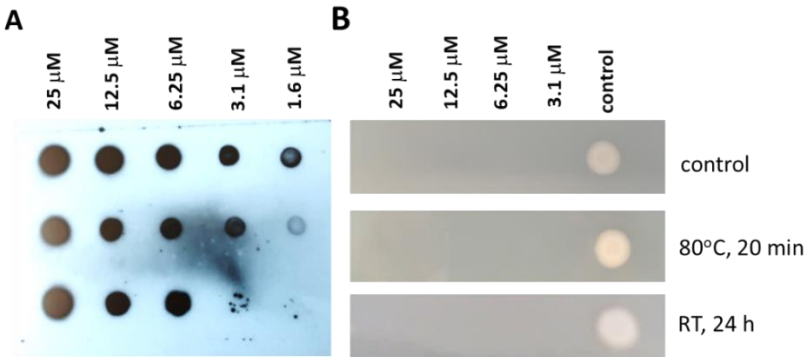

Figure 36. NCR169C$_{17-38}$-StrepII shows high heat stability and preserved antimicrobial activity. (A) Detection of NCR169C$_{17-38}$-StrepII with anti-StrepII antibodies on a dot blot. (B) NCR169C$_{17-38}$-StrepII remains active after 20 minutes of treatment at 80 °C or incubation at room temperature for 24 hrs.

As shown above, NCR169C$_{17-38}$ causes rapid damage to bacterial membranes. Since membrane structure is largely determined by its lipid composition, we next investigated the ability of NCR169C$_{17-38}$-StrepII to bind membrane lipids *in vitro* using a peptide-lipid overlay assay (Fig. 37.A). NCR169C$_{17-38}$-StrepII bound to several anionic lipids, including phosphoinositides, phosphatidic acid, phosphatidylserine, and cardiolipin - a major constituent of bacterial membranes. However, the peptide did not bind to phosphatidylglycerol (PG), a common anionic phospholipid, indicating a degree of specificity in its lipid interactions.

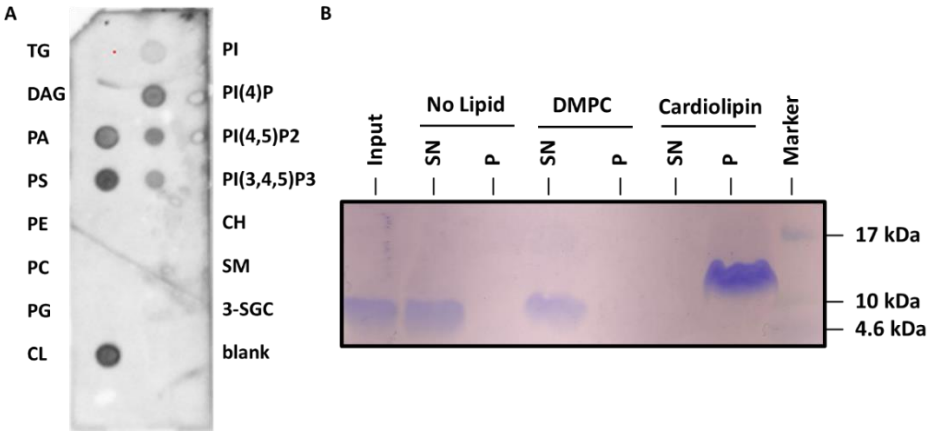

Figure 37. Detecting lipid-binding ability of NCR169C$_{17-38}$. (A) NCR169C$_{17-38}$-StrepII was overlaid onto commercially available lipid strip membrane. The peptide bound to lipids was detected with anti-StrepII-antibody. TG, Triglyceride; DAG, Diacylglycerol; PA, Phosphatidic acid; PS, Phosphatidylserine; PE, Phosphatidylethanolamine; PC, Phosphatidylcholine; PG, Phosphatidylglycerol; CL, Cardiolipin; PI, Phosphatidylinositol; PI4P, Phosphatidylinositol-4-phosphate; PI(4,5)P2, Phosphatidylinositol-4,5-bisphosphate; PI(3,4,5)P3, Phosphatidylinositol-3,4,5-trisphosphate; CH, Cholesterol; SM, Sphingomyelin; 3-SGC, 3-sulfogalactosylceramide. (B) liposome binding assay. 20 µM of NCR169C$_{17-38}$ peptide was incubated with buffer only (No lipid), 2 mM dimyristoyl- phosphatidylcholine (DMPC) liposomes, or 2 mM Cardiolipin liposomes. After incubation and ultra-centrifugation, the supernatant and pellet fractions were analyzed by Glycine-SDS-PAGE. Input is also no lipid sample but before ultra-centrifugation.

To further confirm the cardiolipin-binding, we performed a liposome binding assay using two phospholipids: cardiolipin (positive in the overlay assay) and DMPC; (dimyristoyl-phosphatidylcholine) that is a derivative of phosphatidylcholine that showed no binding on the lipid strip. Prepared liposomes were incubated with NCR169C$_{17-38}$, then separated by ultracentrifugation. Peptide remaining in the supernatant (sn) fraction indicated no binding, whereas peptide detected in the pellet (p) fraction indicated liposome association. In this setup, NCR169C$_{17-38}$ bound strongly to cardiolipin liposomes but showed no binding to DMPC liposomes (Fig. 37.B).

4.2.7. Peptide - nucleic acid interactions and binding dynamics

To explore whether the NCR169C$_{17-38}$ peptide has secondary intracellular targets of the bacterial cells beyond the primary membrane disruption, we tested its possible interaction with nucleic acids in gel retardation assays. A pilot experiment indicated strong DNA-binding capacity, prompting us to include the parental NCR169 peptide and the shorter derivatives NCR169$_{16-27}$ and NCR169$_{17-27}$ for comparison (Fig. 38.). When 100 ng *E. coli* genomic DNA was incubated without peptide, it migrated as a clear single band, whereas treatments with 10 or 100 μM peptides resulted in altered patterns (Fig. 38. A). NCR169C$_{17-38}$ showed the strongest effect, completely preventing DNA migration from the well at the lower concentration; at higher concentration, no staining was visible even in the well, suggesting DNA-peptide aggregates made the DNA inaccessible to ethidium bromide. NCR169 also displayed solid binding by fully blocking migration at 100 μM. By contrast, NCR169$_{16-27}$ and NCR169$_{17-27}$ exhibited only weak binding, indicated by faint band shifts and well staining. Similar results were obtained with total *E. coli* RNA (Fig. 38.B). NCR169C$_{17-38}$ and NCR169 completely blocked RNA migration at high concentrations, and at low concentration faint migration signals of RNA could be detected, though the 23S and 16S ribosomal RNA bands disappeared. The shorter derivatives again displayed weaker binding, detectable only at high concentrations. To further probe DNA binding, the interaction of NCR169C$_{17-38}$ with circular plasmid DNA was characterized by using a dilution series of the peptide (Fig. 38.C). Increasing peptide concentrations progressively reduced the quantity of migrating DNA, with complete retention of DNA in the well at higher concentrations, confirming a concentration-dependent interaction. The DNA-binding kinetics were quantified using SYBR Gold fluorescence (Fig. 38.D). Half of the DNA samples were not treated with peptides at the start, and these displayed the highest fluorescence signals. Samples treated with peptides at time zero showed an immediate decrease in fluorescence, consistent with rapid DNA binding. The extent of signal reduction followed

the same hierarchy observed in gel assays: NCR169C$_{17-38}$ > NCR169 > NCR169$_{16-27}$ > NCR169$_{17-27}$. Peptide addition at 14 min similarly caused an abrupt drop in fluorescence to peptide-specific levels. To test if peptide removal would recover the DNA–SYBR Gold fluorescence to control values, Proteinase K was added at 27 min to all reactions. A prompt effect was observed with the shortest NCR169$_{16-27}$ peptide which showed a marked fluorescence increase that stabilized but did not fully reach the original control level. In contrast, fluorescence values in the NCR169 samples remained unchanged, while those of NCR169C$_{17-38}$ or NCR169$_{17-27}$ increased slightly and gradually to the same limited extent. Thus, NCR169$_{16-27}$ proved to be the most sensitive to Proteinase K treatment, NCR169 was resistant, and NCR169C$_{17-38}$ together with NCR169$_{17-27}$ displayed only partial sensitivity. These results demonstrate that NCR169C$_{17-38}$ binds strongly and rapidly to both DNA and RNA in a concentration-dependent manner, forming stable nucleic acid complexes that are only partially reversible by protease treatment.

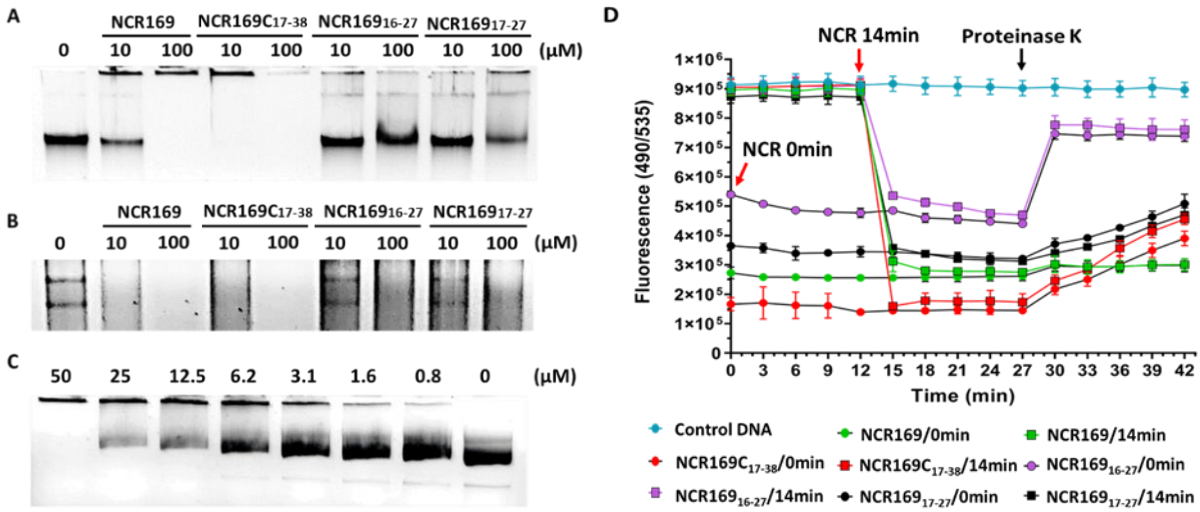

Figure 38. *In vitro* interaction of NCR169C$_{17-38}$, NCR169, NCR169$_{16-27}$ and NCR169$_{17-27}$ with nucleic acids. (A) Gel retardation assay of 100 ng *E. coli* genomic DNA incubated with 0, 10, or 100 μM peptide. (B) Same setup as in (A), but using 100 ng *E. coli* total RNA. (C) Interaction of NCR169C$_{17-38}$ with 250 ng circular plasmid DNA at varying concentrations. (D) Real-time monitoring of DNA binding by fluorescence of SYBR Gold–DNA complexes (excitation 490 nm, emission 535 nm). Peptides (10 μM) were added to 100 ng DNA at 0 or 14 min (red arrows); Proteinase K (1 mg/mL) was added at 27 min (black arrow).

4.2.8. Differential gene expression in *E. coli* exposed to NCR169C$_{17-38}$.

Genome-wide transcriptome profiling was performed to examine early global gene expression changes in *E. coli* exposed to a sub-MBC dose of the NCR169C$_{17-38}$ peptide for 20 minutes in culture medium. Differentially expressed genes (DEGs) were identified by comparing treated

and untreated cultures. This analysis revealed significant changes in 503 genes. 450 genes were downregulated, while 53 genes were up-regulated (Fig. 39.). 458 DEGs were mapped to 439 annotated *E. coli* genes of the ATCC_8739 genome database, while 45 genes codes for hypothetical proteins.

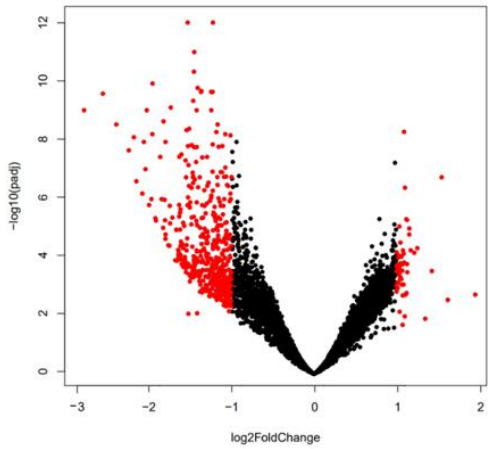

Figure 39. Volcano plot showing differentially expressed genes in *E coli* treated with NCR169C$_{17-38}$.

Kyoto Encyclopedia of Genes and Genomes (KEGG) pathway enrichment analysis was initially performed on the DEGs to identify key pathways that were affected by the NCR169C$_{17-38}$ treatment of *E. coli* (Fig. 40.). The highly enriched pathways show an active response from the *E. coli* bacteria in attempt to control the ongoing stress. The affected KEGG pathways can be classified into five major categories as shown in (Supplementary Table 1.): membrane and lipid metabolism, stress response and resistance mechanisms, metabolism and energy production, amino acid and secondary metabolite biosynthesis, and translational and genetic responses. These pathways highlight broad bacterial adaptations, including membrane remodeling (Category 1), altered motility and communication (Category 2), metabolic reprogramming (Category 3), enhanced amino acid and metabolite biosynthesis (Category 4), and increased demands for protein synthesis, transcript processing, and DNA/RNA repair (Category 5). The categorization indicate that peptide treatment triggers coordinated structural, metabolic, and genetic adaptations that promote bacterial survival under stress.

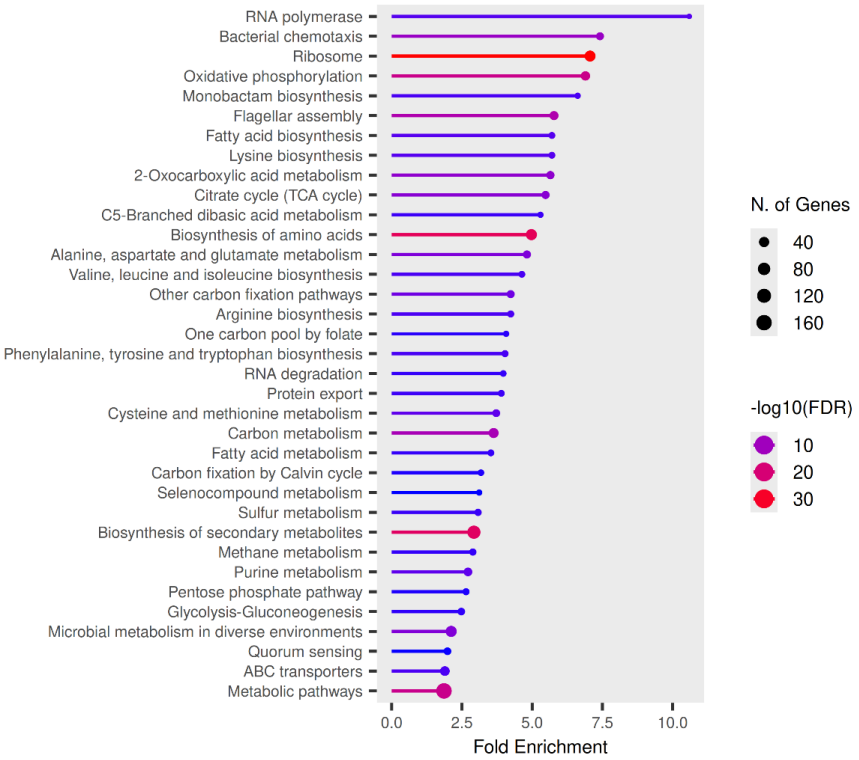

Figure 40. KEGG pathway terms associated with the (DEGs) in *E coli* treated with NCR169C$_{17\text{-}38}$ on the y-axis and Fold enrichment on the x-axis: Circle size indicates the number of genes involved in the pathway, the bigger the circle, the more the genes. The color indicates significance; light color shows high significance, while dark color shows low significance.

To explore potential biological mechanisms linked to the identified DEGs, GO functional annotation and enrichment analyses were conducted on the upregulated and downregulated genes revealing substantial differences in the biological process (BP), cellular component (CC), and molecular function (MF) terms (Fig. 41. A-C). Across all three GO categories, downregulated DEGs were markedly more abundant than upregulated ones. In the BP category, enrichment analysis identified 155 downregulated terms associated with 521 genes, compared to only 16 upregulated terms involving 17 genes. For MF, 155 downregulated terms linked to 415 genes were found, whereas just 9 upregulated terms representing 9 genes were detected. Similarly, in the CC category, 30 downregulated terms encompassing 134 genes were observed, while only a single upregulated term involving 4 genes was enriched. The apparent excess of genes in the GO analysis relative to the transcriptome dataset arises because individual genes are frequently annotated to multiple GO terms. Consequently, the same gene can contribute to several terms, inflating per-term counts even though the overall number of unique genes matches the DEG list.

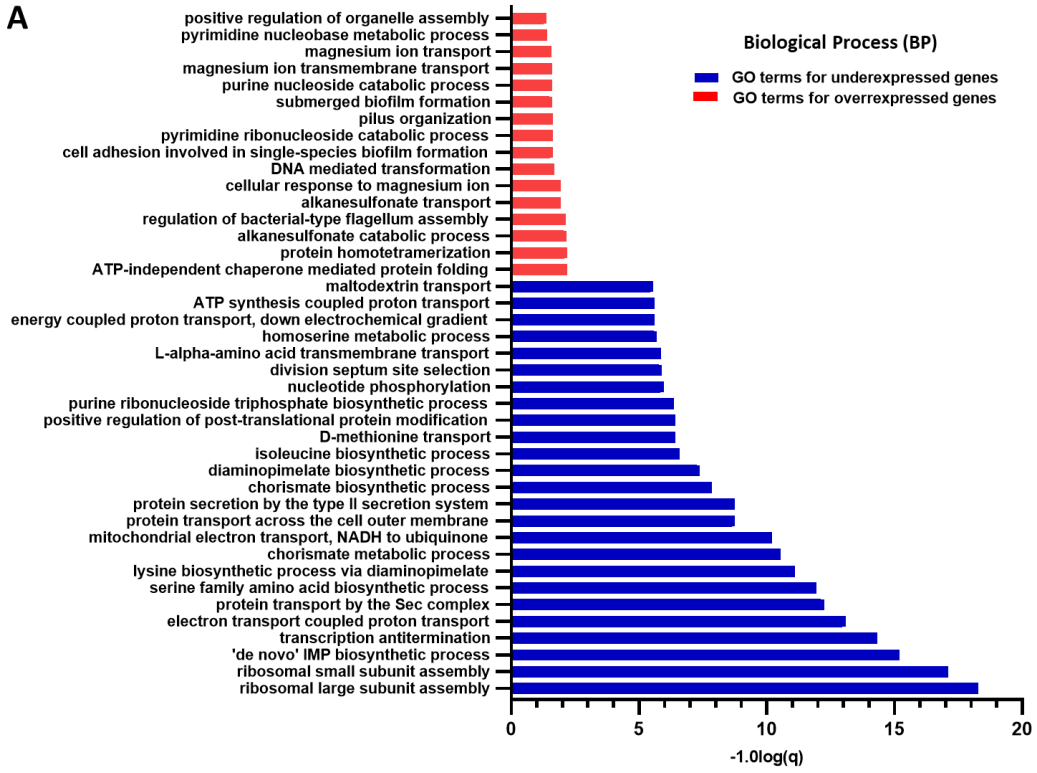
A
positive regulation of organelle assembly
pyrimidine nucleobase metabolic process
magnesium ion transport
magnesium ion transmembrane transport
purine nucleoside catabolic process
submerged biofilm formation
pilus organization
pyrimidine ribonucleoside catabolic process
cell adhesion involved in single-species biofilm formation
DNA mediated transformation
cellular response to magnesium ion
alkanesulfonate transport
regulation of bacterial-type flagellum assembly
alkanesulfonate catabolic process
protein homotetramerization
ATP-independent chaperone mediated protein folding
maltodextrin transport
ATP synthesis coupled proton transport
energy coupled proton transport, down electrochemical gradient
homoserine metabolic process
L-alpha-amino acid transmembrane transport
division septum site selection
nucleotide phosphorylation
purine ribonucleoside triphosphate biosynthetic process
positive regulation of post-translational protein modification
D-methionine transport
isoleucine biosynthetic process
diaminopimelate biosynthetic process
chorismate biosynthetic process
protein secretion by the type II secretion system
protein transport across the cell outer membrane
mitochondrial electron transport, NADH to ubiquinone
chorismate metabolic process
lysine biosynthetic process via diaminopimelate
serine family amino acid biosynthetic process
protein transport by the Sec complex
electron transport coupled proton transport
transcription antitermination
'de novo' IMP biosynthetic process
ribosomal small subunit assembly
ribosomal large subunit assembly
0
5
10
15
20
-1.0log(q)
Biological Process (BP)
GO terms for underexpressed genes
GO terms for overrexpressed genes

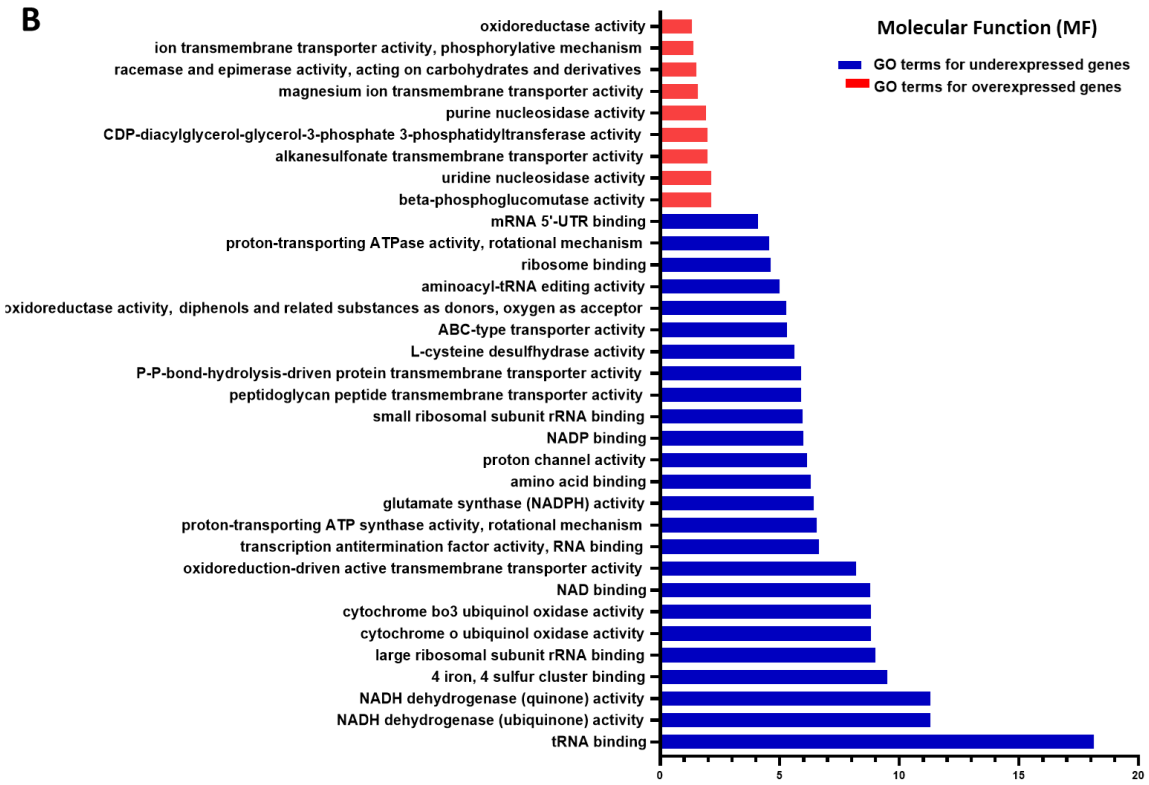
B
oxidoreductase activity
ion transmembrane transporter activity, phosphorylative mechanism
racemase and epimerase activity, acting on carbohydrates and derivatives
magnesium ion transmembrane transporter activity
purine nucleosidase activity
CDP-diacylglycerol-glycerol-3-phosphate 3-phosphatidyltransferase activity
alkanesulfonate transmembrane transporter activity
uridine nucleosidase activity
beta-phosphoglucomutase activity
mRNA 5'-UTR binding
proton-transporting ATPase activity, rotational mechanism
ribosome binding
aminoacyl-tRNA editing activity
oxidoreductase activity, diphenols and related substances as donors, oxygen as acceptor
ABC-type transporter activity
L-cysteine desulfhydrase activity
P-P-bond-hydrolysis-driven protein transmembrane transporter activity
peptidoglycan peptide transmembrane transporter activity
small ribosomal subunit rRNA binding
NADP binding
proton channel activity
amino acid binding
glutamate synthase (NADPH) activity
proton-transporting ATP synthase activity, rotational mechanism
transcription antitermination factor activity, RNA binding
oxidoreduction-driven active transmembrane transporter activity
NAD binding
cytochrome bo3 ubiquinol oxidase activity
cytochrome o ubiquinol oxidase activity
large ribosomal subunit rRNA binding
4 iron, 4 sulfur cluster binding
NADH dehydrogenase (quinone) activity
NADH dehydrogenase (ubiquinone) activity
tRNA binding
0
5
10
15
20
Molecular Function (MF)
GO terms for underexpressed genes
GO terms for overexpressed genes

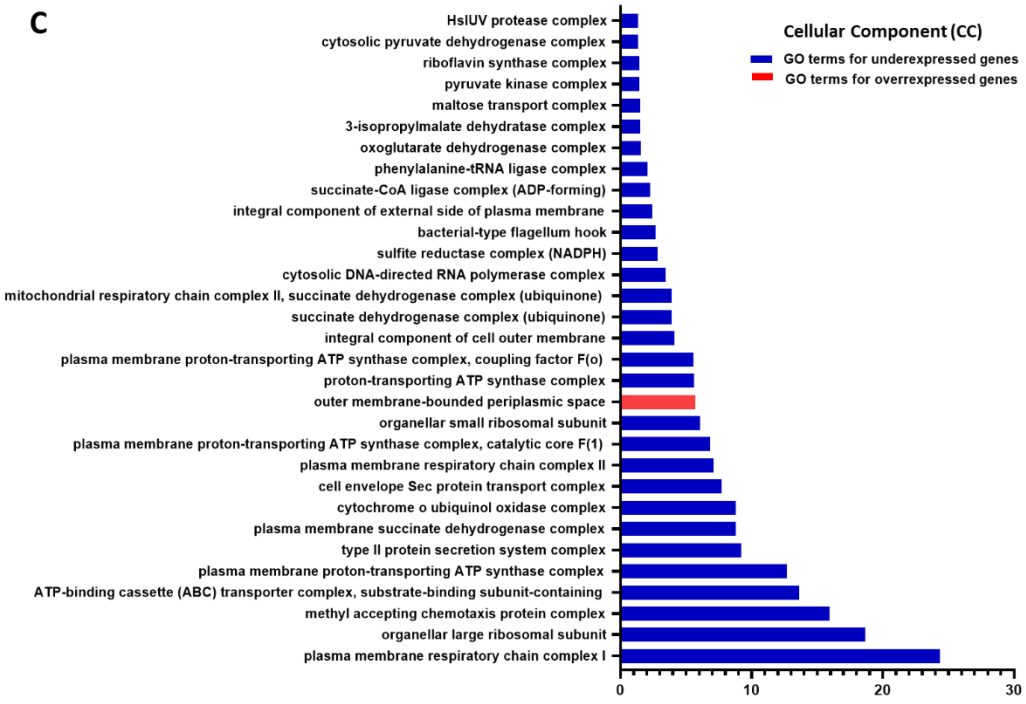

Figure 41. GO enrichment analysis of DEGs in E coli treated with NCR169C17-38 annotated in three main categories: (A) biological process, (B) molecular function, and (C) cellular component.

The peptide appears to induce a broad suppression of bacterial functions, with only a limited subset of genes upregulated, presumably to support cellular rescue and survival. Upregulation of several stress-related genes was observed, including those involved in membrane stress response (*osmB, cpxP, arnC, arnC2, ynbA*), magnesium transport (*mgtA, mgtS*), sulfur metabolism (*ssuA, ssuD*), and oxidative stress (*ycjU, fixX*). *E. coli* also activated genes associated with modulation of host immune responses (*prgK, hcpA*) and biofilm formation (*yehB, yehD, bdM, csgE, ycfS*). Furthermore, upregulation of genes enhancing the translation of stress-related transcripts (*rihB*) or mitigating cellular damage (*yodB, hcpA*) reflects additional adaptive strategies employed by the bacteria to cope with the imposed stress.

The KEGG and GO analyses revealed that NCR169C$_{17\text{-}38}$ treatment caused a broad suppression of core bacterial functions. A substantial fraction of downregulated genes was involved in protein synthesis, particularly ribosomal components, translation factors, and aminoacyl-tRNA ligases, indicating a strong inhibition of the translational machinery. Energy production pathways were also markedly affected, with reduced expression of genes associated with ATP synthesis, glycolysis, the tricarboxylic acid cycle, and the electron transport chain. In parallel, key regulators of cell division and transcription were suppressed. Genes involved in cell envelope integrity, including outer membrane transporters, peptidoglycan and fatty acid

biosynthesis, and lipid metabolism, showed significantly lower expression, consistent with impaired membrane maintenance. Metabolic pathways supporting amino acid and nucleotide biosynthesis were also downregulated, further reflecting a global shutdown of anabolic processes. Finally, genes governing motility, flagellar assembly, and chemotaxis were strongly repressed, suggesting that adaptive movement and environmental sensing were deprioritized under peptide-induced stress. Validation of the transcriptome analysis was performed on ten selected DEGs using RT-qPCR, which confirmed the reliability of the sequencing results (Fig. 42.).

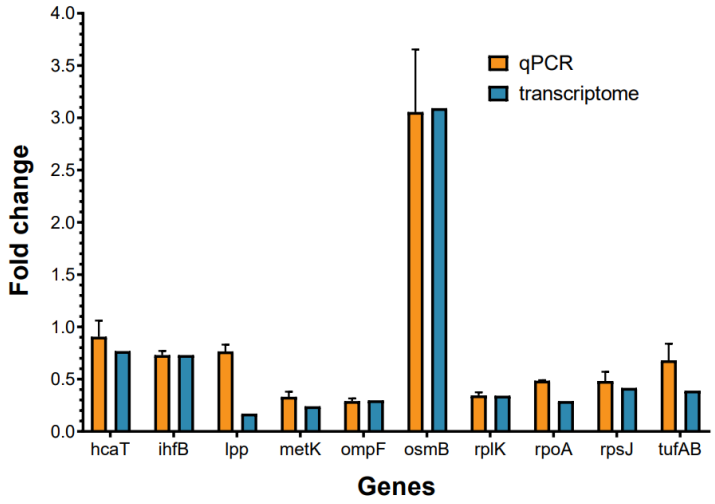

Figure 42. Validation of transcriptomic results by RT-qPCR reactions. The RT-qPCR values are the result of three technical replicates and the diagram indicates the standard deviation of the values.

5. Discussion

5.1. Significance of nodGRP1L in symbiotic nitrogen fixation

Our study reveals that nodGRP1L plays a crucial role in the development of nitrogen-fixing nodules in *Medicago truncatula* and in maintaining an effective symbiotic relationship between the plant and its bacterial partner. Using a combination of molecular, cellular, and protein-interaction approaches, we investigated the function, regulation, localization, and interacting partners of nodGRP1L during symbiosis.

Silencing of *nodGRP1L* by RNA interference in *M. truncatula* plants caused marked morphological abnormalities that led to impaired nodule formation and the development of non-functional nodules. The RNAi-silenced plants displayed the characteristic symptoms of nitrogen starvation, i.e. reduced growth and a less developed root system. This was due to the presence of only underdeveloped small and white Fix^- nodules that lacked leghemoglobin and were not able to fix nitrogen. qRT-PCR confirmed that silencing of the *nodGRP1L* gene was resulted in significant reduction of its mRNA in these nodules, but no downregulation was detected in other *nodGRP* family members tested. In RNAi-silenced nodules, the zonation pattern was disrupted. Rhizobia were present in the infection zone (ZII) and the interzone (IZ), but the region that should form the nitrogen fixation zone (ZIII) remained rhizobia-free. These observations indicate that nodGRP1L is required for successful rhizobial differentiation into nitrogen-fixing bacteroids. This potential function is consistent with the strong IZ-specific expression of *nodGRP1L* gene based on RNA-seq data collected on laser-dissected nodules sections (Roux et al., 2014) and further confirmed in our promoter-GUS reporter gene experiments exhibiting the strongest GUS staining in the nodules interzone (IZ) for all the three different promoter fragments tested. The results of this latter experiment allowed us to narrow down the promoter region required for proper *nodGRP1L* expression to a 419 bp segment, within which we now aim to identify the relevant cis-regulatory elements.

Ultrastructural analysis revealed that *nodGRP1L* RNAi-silenced nodules were completely devoid of the starch-containing amyloplasts in all developmental zones. There are other impaired *M. truncatula* nodules described in the literature with similar phenotype, but there is either no report concerning their amyloplast content or rather an increased number of amyloplasts are stated - as it was recently described also for the NCR169 mutant by (Horváth et al., 2015). This major structural difference suggests that *nodGRP1L* is essential for maintaining the metabolic integrity of nodule cells. Its silencing might have a direct effect on

the availability of starch and thereby disrupts bacteroid differentiation and viability, and increases vesicle trafficking, collectively leading to bacteroid degeneration within the infected cells and the loss of symbiotic function.

In the *M. truncatula* transgenic hairy roots, the constitutive ectopic overexpression of *nodGRP1L* driven by an ubiquitin promoter only smaller nodules were visible too, however these had a light pinkish colour. Microscopic studies revealed that the bacteroids could differentiate, but then soon had a premature degeneration and thus performed very limited nitrogenase activity and nitrogen fixation. This phenotype together with the RNAi-silenced nodules highlighted the necessity of precise temporal and spatial regulation of the *nodGRP1L* expression. In contrast to the amyloplast phenotype of the RNAi-silenced nodules, the nodules overexpressing the gene has accumulated large quantities of starch similarly to other nodules impaired in their nitrogen fixation. Continuous delivery of photosynthates to the nodules, combined with reduced nitrogen fixation and bacteroid activity, likely causes carbohydrate accumulation within amyloplasts. Such altered starch deposition is a common hallmark of defective symbiotic interactions and further underscores the functional disruption caused by *nodGRP1L* overexpression.

Similarly, to NCRs, nodGRPs also have a signal peptide that drives the mature proteins via the secretory pathway through the plant membrane from the cytosol. Since it was shown for NCR247 to be transferred into the bacteroids (Farkas et al., 2014) we tested whether the larger nodGRP1L protein was also able to enter into rhizobia. Our results proved that nodGRP1L was able to penetrate bacterial membranes and localize inside both free-living *S. meliloti* cells and bacteroids isolated from wild-type nodules. This localization was confirmed through two complementary approaches: *in vitro*, by incubating *S. meliloti* with FITC-labeled peptide and detecting intracellular fluorescence; and *in vivo*, by expressing StrepII-tagged *nodGRP1L* in transgenic hairy roots and detecting the tagged protein within nodule cells. These findings suggest that nodGRP1L can also cross the bacterial membrane and potentially act inside the bacterial cytoplasm.

Our protein–protein interaction studies identified the rhizobial SecB, a molecular chaperone that operates within the Sec translocation pathway, assisting the transport of precursor proteins across the cytoplasmic membrane (Bechtluft et al., 2010) as a direct interacting partner of *nodGRP1L*. This interaction was initially detected through yeast two-hybrid screening using a *S. meliloti* cDNA library and subsequently validated by pairwise assays, pull-down experiments, and bimolecular fluorescence complementation (BiFC) in planta. Since SecB functions in bacterial protein folding and translocation, its interaction with *nodGRP1L* suggests

that this host-derived protein might participate in a broader molecular network that influences bacterial protein stability or activity within infected cells. Given that some nodule-specific cysteine-rich (NCR) peptides also rely on bacterial chaperones and secretion systems for proper processing and targeting (Farkas et al., 2014), the *nodGRP1L–SecB* interaction may represent a functional convergence between host nodGRPs and bacterial symbiotic adaptation pathways. The potential interaction between *nodGRP1L* and other nodGRPs or NCR peptides is particularly intriguing. Both peptide families are abundant in nodules and share structural characteristics such as small size, intrinsic disorder, and the ability to interact with microbial targets. It is plausible that nodGRP1L, through its flexible glycine-rich domain, contributes to the stabilization or modulation of NCR-bacteroid interactions. This could explain the phenotypic similarities between *nodGRP1L*-silenced nodules and NCR-deficient mutants, both of which exhibit impaired bacteroid differentiation and reduced nitrogen fixation efficiency.

Collectively, our findings identify *nodGRP1L* as a novel nodule-specific regulator essential for proper bacteroid differentiation and functional symbiosis. Its precise promoter activity, essential role in maintaining bacteroid viability, and confirmed interaction with SecB point to a model in which nodGRP1L helps coordinate the plant–bacterium relationship to sustain effective nitrogen fixation. Future studies should investigate whether nodGRP1L directly interacts with NCR peptides or other nodGRPs, and how these molecular networks contribute to maintaining the delicate equilibrium between host control and bacterial differentiation that underpins successful legume–rhizobium symbiosis.

5.2. NCR169C$_{17\text{-}38}$ is a potent antimicrobial peptide with multiple modes of action

Our results recognized NCR169C$_{17\text{-}38}$ as the most potent AMP derivative of the symbiotic plant peptide NCR169, with consistent bactericidal activity against a wide range of clinically relevant pathogens, including members of the ESKAPE group, as well as *Listeria monocytogenes* and *Salmonella enterica*. Importantly, this activity was maintained under physiological conditions (pH 7.4) and across multiple assay environments.

The original NCR169 peptide, produced during *Medicago truncatula–Sinorhizobium meliloti* symbiosis, displayed poor solubility at neutral pH, resulting in variable *in vitro* antimicrobial performance against both Gram-negative and Gram-positive pathogens. The oxidized form (NCR169ox), and the cysteine-free variant NCR169-C$_{9,15,28,33}$/S showed reduced activity at neutral pH. Acidic conditions not only improved peptide solubility but also leveled the efficacy of all of these peptides, highlighting the importance of local physicochemical environments in determining NCR peptide activity. The activity of the cysteine-free variant suggests that, although the presence of cysteines is undoubtedly important for symbiotic function (Horvath et

al., 2015), it is not necessary for the antimicrobial effect. Among the various shorter derivatives, the C-terminal fragment of NCR169C$_{17-38}$ showed the strongest and most consistent bactericidal effect. This 22-amino-acid peptide retains most of the positively charged lysines (six out of seven), both tryptophans, and two short motifs (KIWK and LWYK) resembling the conserved AMP motif XWZX, known to enhance amphiphilicity and membrane interaction (Lee et al., 2018). All shorter peptide fragments resulted in a significant or complete loss of activity in the initially tested PPB buffer. In an earlier study (Isozumi et al., 2021) solving the NMR structure of the NCR169 peptide, the shorter fragment NCR169$_{16-27}$ was previously shown to be active against *E. coli* and *S. meliloti* in HEPES buffer. Comparing the activity of the peptides against the tested bacterial pathogens in different buffers, the MBC values of NCR169$_{16-27}$ were comparable to those of NCR169C$_{17-38}$, only in HEPES buffer. However, even under this condition, NCR169$_{16-27}$ peptide exhibited lower activity against *L. monocytogenes* (12.5 μM) and was inactive against *E. faecalis*. In contrast, NCR169C$_{17-38}$ peptide maintained strong antibacterial efficacy across all tested media, including HEPES and PPB buffers, as well as Mueller–Hinton broth, a clinically standardized medium according to the National Committee for Clinical Laboratory Standards (1979), containing divalent cations. This medium might influence the antimicrobial activity of the peptides - consistent with the observation that the antimicrobial activity of NCR plant peptides depends on the test conditions (Farkas et al., 2018). As expected, the presence of these ions slightly increased the MBC values of NCR169C$_{17-38}$ against *E. coli, A. baumannii* and *S. aureaus* (6.3, 6.3, and 12.5 μM, respectively), but this reduction in potency was fully restored by the addition of low concentrations of EDTA, which chelates inhibitory cations. These findings reinforce NCR169C$_{17-38}$ as the minimal unit required for reliable broad-spectrum antimicrobial activity.

Combination assays revealed that NCR169C$_{17-38}$ exhibits synergistic effects with polymyxin B and meropenem, but not with streptomycin, against *E. coli*. Synergism likely arises from complementary mechanisms and suggests that combination strategies could enhance therapeutic efficacy and delay resistance. Similarly, combining NCR169C$_{17-38}$ with NCR335-derived fragments enhanced bactericidal activity, supporting the idea that cocktails of NCR peptides may represent an effective therapeutic strategy.

One of the most striking findings was the ability of NCR169C$_{17-38}$ to prevent and eradicate *A. baumannii* biofilms. *A. baumannii* is a major multidrug-resistant pathogen whose persistence is largely attributed to its ability to form biofilms on medical devices and host tissues. Within biofilms, bacterial cells are highly protected from antibiotics, immune responses, and environmental stress, often leading to chronic and recurrent infections (Choudhary et al., 2022;

Mendes et al., 2023). Besides the NCR169C$_{17-38}$ peptide, both antibiotics - meropenem and polymyxin B - were able to inhibit biofilm formation by *A. baumannii* when added to fresh planktonic cultures. However, when these agents were applied against bacteria within a pre-formed biofilm, only NCR169C$_{17-38}$ was able to significantly eradicate the biofilm after a 3-hour treatment and kill the sessile bacteria as effectively as it did in planktonic conditions. After 24 hours of treatment, all three antimicrobial agents caused a significant reduction in biofilm when applied at higher concentrations, nonetheless, NCR169C$_{17-38}$ retained significant activity even at sub-MBC concentrations. The MBC values obtained in these biofilm eradication assays indicated that only the NCR169C$_{17-38}$ peptide could kill biofilm-embedded bacteria with an efficacy comparable to that observed in the planktonic cultures. The ability to act against biofilm-associated cells highlights a significant advantage of NCR169C$_{17-38}$ over standard treatments.

The potent antimicrobial activity of the NCR169C$_{17-38}$ peptide can be attributed to its rapid and extensive disruption of bacterial membranes. Fluorescence microscopy, scanning electron microscopy, and real-time propidium iodide (PI) uptake assays consistently demonstrated that the bacterial membrane is the primary target of the peptide's action. Remarkably, the rate of permeabilization induced by NCR169C$_{17-38}$ exceeded that of polymyxin B, a last-resort antibiotic, highlighting the peptide's potency. Lipid-binding assays revealed its preferential binding to cardiolipin over phosphatidylglycerol, suggesting a degree of specificity for distinct bacterial membrane components. Since cardiolipin is enriched in bacterial but not mammalian cell membranes, this selectivity likely contributes to both the antimicrobial efficacy and low cytotoxicity of the peptide - a feature of considerable therapeutic value. Consistent with this, NCR169C$_{17-38}$ peptide has been previously shown to be non-cytotoxic to human keratinocyte HaCaT cells (Szerencsés et al., 2021), mouse macrophage J774.2 cells (Szerencsés et al., 2025), and to lack hemolytic activity (Howan et al., 2023).

Across all *in vitro* assays, NCR169C$_{17-38}$ demonstrated antimicrobial potency, membrane permeabilization, and biofilm removal capacities equal to or greater than those of polymyxin B, underscoring its strong therapeutic potential.

Mechanistically, transcriptome profiling revealed that exposure to sublethal concentrations of NCR169C$_{17-38}$ induces profound global transcriptional reprogramming in *E. coli*. More than 500 genes were differentially expressed within 20 minutes, with an overwhelming dominance of downregulated genes. This global suppression encompassed key cellular functions, including ribosome biogenesis, translation, energy production, lipid and cell wall biosynthesis, and motility. The inhibition of these essential pathways reflects a rapid and comprehensive

shutdown of bacterial metabolism and growth - a hallmark of effective antimicrobial action (Tomasinsig et al., 2004; Jenssen et al., 2006; Kintses et al., 2019). The small subset of upregulated genes was primarily associated with stress response, membrane remodeling, and detoxification pathways, consistent with bacterial attempts to mitigate membrane damage and oxidative stress (Peschel & Sahl, 2006; Andersson et al., 2016; Bechinger & Gorr, 2017). These findings suggest that NCR169C$_{17\text{-}38}$ exerts a dual mechanism of action: immediate physical disruption of membrane integrity, followed by secondary intracellular effects that disturb nucleic acid stability and transcriptional control. The capacity of NCR169C$_{17\text{-}38}$ to bind nucleic acids further expands its antimicrobial profile beyond mere membrane disruption. DNA and RNA binding assays demonstrated strong, concentration-dependent interactions, forming stable peptide–nucleic acid complexes that only partially dissociate upon protease treatment. Such interactions likely contribute to the observed transcriptional silencing and metabolic arrest, providing an additional layer of antibacterial activity. Together with its preferential binding to cardiolipin - a major anionic lipid of bacterial membranes but absent from mammalian membranes - this selectivity underpins both its potency and safety.

From a pharmacological perspective, NCR169C$_{17–38}$ combines several highly desirable attributes: broad-spectrum antimicrobial and antifungal (Szerencsés et al., 2021, 2025) activity, rapid bactericidal kinetics, antibiofilm capacity, synergism with antibiotics, high physicochemical stability, and lack of cytotoxicity to mammalian cells. These properties position it as a strong candidate for therapeutic development, either as a standalone antimicrobial or as an adjuvant to enhance antibiotic efficacy. Its stability at elevated temperatures and in storage further supports practical applicability in clinical or agricultural contexts.

6. Acknowledgement

I would like to express my deepest gratitude to my supervisor, Prof. Eva Kondorosi, and Dr. Gabriella Endre, for their unwavering support, guidance, and understanding throughout my doctoral research. Their invaluable mentorship and advice, from the very beginning of my project to its completion, have been essential in helping me reach this milestone.

I am also grateful to my colleagues in the Institute of Plant Biology at the Biological Research Centre for their collaboration and assistance during my work

I also thank Dr. Aladár Pettkó-Szandtner for his help in the proteomics experiments, Dr. Ildikó Domonkos for teaching me how to use the scanning electron microscope (SEM), Tamás Polgár for taking the transmission electron microscope (TEM) images, and Dr. Krisztián Laczi for helping me perform the gas chromatography measurements. I would also like to thank the Cellular Imaging Laboratory (CILab) for their assistance with the microscopy work.

Finally, I am profoundly thankful to my family. Words cannot fully capture the depth of my gratitude to my parents for their unwavering belief in me, their constant encouragement, and the sacrifices they have made to support me. I carry in my heart the memory of my father, who passed away during this journey, yet whose wisdom, encouragement, and presence remained with me every step of the way. I am equally grateful to my siblings, whose companionship and motivation have been a source of strength throughout this journey. I also wish to thank my friends, whose understanding, encouragement, and shared moments of joy and challenge have provided balance and inspiration. Their collective support, care, and love have been invaluable in helping me overcome obstacles and achieve this milestone.

7. Summary

This study integrates plant molecular genetics, symbiotic physiology, and antimicrobial peptide biology to elucidate two major aspects of *Medicago truncatula*–rhizobium symbiosis and peptide functionality: the biological role of the nodule-specific glycine-rich protein nodGRP1L in nitrogen fixation, and the antimicrobial potential of the plant-derived peptide NCR169C$_{17–38}$ as a therapeutic candidate. Together, these findings contribute to a deeper understanding of the molecular mechanisms governing both symbiotic nitrogen fixation and plant-derived antimicrobial defense strategies.

The role of nodGRP1L in symbiotic nitrogen fixation

Our data demonstrate that nodGRP1L is indispensable for the proper formation and functioning of nitrogen-fixing nodules in *M. truncatula*. Through a combination of molecular, genetic, and cellular approaches, we investigated its expression, localization, and protein interactions to clarify its functional role during the symbiotic process.

Promoter activity assays revealed that *nodGRP1L* expression is strictly confined to the interzone (IZ) region of nodules, where rhizobia undergo differentiation into bacteroids. This spatial restriction supports its classification as a *nodule-specific glycine-rich protein* (GRP) and underscores its regulatory connection to bacteroid maturation rather than to general plant stress responses.

Functional analysis using RNA interference (RNAi) provided direct evidence for the essential role of *nodGRP1L* in nodule organogenesis. Silenced plants exhibited reduced growth, poorly developed roots, and smaller, white nodules devoid of leghemoglobin, leading to a Fix$^-$ phenotype indicative of complete nitrogen fixation failure. Transmission electron microscopy revealed a total absence of amyloplasts in all developmental zones of these nodules, implying that *nodGRP1L* is required for maintaining cellular energy metabolism and structural integrity within infected cells. The observed loss of bacteroid viability and increased vesicle dynamics in silenced lines likely reflect cellular responses to disrupted symbiotic homeostasis.

Conversely, overexpression of *nodGRP1L* resulted in premature bacteroid degeneration and reduced nitrogen fixation efficiency. The overexpressing nodules accumulated starch excessively, suggesting impaired carbon–nitrogen balance due to the continued influx of photosynthates despite decreased symbiotic activity. This dual phenotype—loss of function causing underdeveloped nodules and overexpression leading to premature degeneration—

highlights the necessity for precise temporal and spatial regulation of *nodGRP1L* expression for stable symbiotic performance.

Localization studies revealed that nodGRP1L can penetrate bacterial membranes and localize within *Sinorhizobium meliloti* cells. This was demonstrated both *in vitro* using FITC-labeled peptides added to bacterial cultures and *in vivo* in transgenic hairy roots expressing StrepII-tagged *nodGRP1L*, where the tagged protein was detected inside bacteroids. These results imply that nodGRP1L may act within the bacterial cytoplasm, potentially influencing symbiont physiology directly.

Protein–protein interaction studies identified the bacterial chaperone SecB as a direct interactor of nodGRP1L. The interaction was first discovered through yeast two-hybrid (Y2H) screening and later validated by pairwise assays, pull-down experiments, and bimolecular fluorescence complementation (BiFC) in planta. SecB functions as a key component of the Sec translocation pathway, facilitating proper folding and export of bacterial proteins. The nodGRP1L–SecB interaction suggests that this host-derived protein may interface with bacterial chaperone systems to modulate protein processing or stability during symbiosis. This discovery resonates with the known behavior of nodule-specific cysteine-rich (NCR) peptides, many of which rely on bacterial membrane transport and chaperone systems for delivery and function. Thus, the interaction between nodGRP1L and SecB may reflect a functional convergence between GRPs and NCR peptides in orchestrating the fine balance of bacterial differentiation and host control within the symbiotic nodule.

Furthermore, the potential of nodGRP1L to interact with other GRPs or NCRs provides a new conceptual framework for understanding symbiotic coordination. Both families share structural flexibility and the ability to interact with microbial targets, and they are co-expressed in the nodule infection zone. nodGRP1L might thus act as a molecular mediator or stabilizer in NCR–bacteroid interactions. This could explain why *nodGRP1L*-silenced nodules resemble NCR-deficient mutants, both displaying impaired bacteroid differentiation and ineffective nitrogen fixation.

In summary, *nodGRP1L* emerges as a novel regulator of nodule function required for maintaining bacteroid integrity and metabolic activity. Its specific promoter activity, cytoplasmic localization within bacteria, and confirmed interaction with SecB together suggest that nodGRP1L is an integral component of the molecular dialogue that enables a stable and functional plant–microbe symbiosis.

The antimicrobial potential of NCR169C$_{17–38}$

In the second part of this work, we characterized NCR169C$_{17–38}$**,** a truncated derivative of the *M. truncatula* symbiotic peptide NCR169, as a powerful broad-spectrum antimicrobial peptide (AMP) with multiple modes of action. NCR169C$_{17–38}$ consistently exhibited strong bactericidal activity against Gram-negative and Gram-positive pathogens, including multidrug-resistant ESKAPE pathogens (*Enterococcus faecium, Staphylococcus aureus, Klebsiella pneumoniae, Acinetobacter baumannii, Pseudomonas aeruginosa*, and *Enterobacter* spp.), as well as *Listeria monocytogenes* and *Salmonella enterica*. Unlike the parent peptide NCR169, whose activity was pH-dependent due to poor solubility, the truncated variant retained potency under physiological conditions and across various media. Sequence analysis revealed that NCR169C$_{17–38}$ preserves key features of the native peptide—most positively charged lysine residues, two tryptophans, and the amphiphilic motifs KIWK and LWYK—conferring strong membrane affinity. These characteristics explain its high antimicrobial efficacy and stability compared to shorter or cysteine-free variants. Synergy assays indicated that NCR169C$_{17–38}$ acts cooperatively with antibiotics such as polymyxin B and meropenem, suggesting the potential for combination therapies that enhance efficacy while minimizing resistance development. Notably, the peptide displayed remarkable antibiofilm activity against *A. baumannii*. It not only prevented biofilm formation but also eradicated established biofilms, a significant advancement over traditional antibiotics, which typically fail against biofilm-embedded bacteria. Mechanistic studies using fluorescence microscopy, scanning electron microscopy, and propidium iodide uptake assays showed that NCR169C$_{17–38}$ disrupts bacterial membranes more rapidly and extensively than polymyxin B. Lipid-binding assays further revealed preferential binding to cardiolipin, a lipid enriched in bacterial membranes but absent from mammalian cells, accounting for its high selectivity and low cytotoxicity. Consistent with this, NCR169C$_{17–38}$ was non-hemolytic and non-toxic to mammalian cells across all tested concentrations. Transcriptomic analysis of *E. coli* exposed to sublethal doses of NCR169C$_{17–38}$ revealed global transcriptional repression affecting over 500 genes. The peptide downregulated essential pathways related to translation, energy metabolism, lipid synthesis, and motility, effectively shutting down bacterial growth and metabolism. A smaller group of upregulated genes corresponded to stress response and membrane repair functions. Furthermore, direct binding of NCR169C$_{17–38}$ to nucleic acids suggests that its action extends beyond membrane disruption to intracellular interference, contributing to its bactericidal potency.

8. References

Abdi, M., Mirkalantari, S., & Amirmozafari, N. (2019). Bacterial resistance to antimicrobial peptides. *Journal of peptide science : an official publication of the European Peptide Society*, *25*(11), e3210. https://doi.org/10.1002/psc.3210

Ageitos, J. M., Sánchez-Pérez, A., Calo-Mata, P., & Villa, T. G. (2017). Antimicrobial peptides (AMPs): Ancient compounds that represent novel weapons in the fight against bacteria. *Biochemical pharmacology*, *133*, 117–138. https://doi.org/10.1016/j.bcp.2016.09.018

Alunni, B., Kevei, Z., Redondo-Nieto, M., Kondorosi, A., Mergaert, P., & Kondorosi, E. (2007). Genomic organization and evolutionary insights on GRP and NCR genes, two large nodule-specific gene families in Medicago truncatula. *Molecular plant-microbe interactions : MPMI*, *20*(9), 1138–1148. https://doi.org/10.1094/MPMI-20-9-1138

Andersson, D. I., Hughes, D., & Kubicek-Sutherland, J. Z. (2016). Mechanisms and consequences of bacterial resistance to antimicrobial peptides. *Drug resistance updates: reviews and commentaries in antimicrobial and anticancer chemotherapy*, 26, 43–57. https://doi.org/10.1016/j.drup.2016.04.002

Arouri, A., Dathe, M., & Blume, A. (2009). Peptide induced demixing in PG/PE lipid mixtures: A mechanism for the specificity of antimicrobial peptides towards bacterial membranes? Biochimica Et Biophysica Acta, 1788(3), 650–659. https://doi.org/10.1016/j.bbamem.2008.11.022

Bechinger, B., & Gorr, S.-U. (2017). Antimicrobial peptides: Mechanisms of action and resistance. Journal of Dental Research, 96(3), 254–260. https://doi.org/10.1177/0022034516679973

Bechtluft, P., Nouwen, N., Tans, S. J., & Driessen, A. J. (2010). SecB-a chaperone dedicated to protein translocation. *Molecular bioSystems*, *6*(4), 620–627. https://doi.org/10.1039/b915435c

Bergersen, F. J. (1997). *Physiology of nitrogen fixation in free-living and symbiotic microorganisms.* Cambridge University Press.

Brewin, N. J. (2004). Plant Cell Wall Remodelling in the Rhizobium–Legume Symbiosis. *Critical Reviews in Plant Sciences*, *23*(4), 293–316. https://doi.org/10.1080/07352680490480734

Brogden K. A. (2005). Antimicrobial peptides: pore formers or metabolic inhibitors in bacteria?. *Nature reviews. Microbiology*, *3*(3), 238–250. https://doi.org/10.1038/nrmicro1098

Browne, K., Chakraborty, S., Chen, R., Willcox, M. D., Black, D. S., Walsh, W. R., & Kumar, N. (2020). A New Era of Antibiotics: The Clinical Potential of Antimicrobial Peptides. *International journal of molecular sciences*, *21*(19), 7047. https://doi.org/10.3390/ijms21197047

Bulen, W. A., & LeComte, J. R. (1966). The nitrogenase system from *Azotobacter*: two-enzyme requirement for N_2 reduction, ATP-dependent hydrogen evolution, and ATP hydrolysis. *Proceedings of the National Academy of Sciences of the United States of America*, *56*(3), 979–986. https://doi.org/10.1073/pnas.56.3.979

Burris, R. H., & Roberts, G. P. (1993). Biological nitrogen fixation. *Annual Review of Nutrition*, *13*, 317–335. https://doi.org/10.1146/annurev.nu.13.070193.001533

Canfield, D. E., Glazer, A. N., & Falkowski, P. G. (2010). *The evolution and future of Earth's nitrogen cycle.* Science, 330(6001), 192–196. https://doi.org/10.1126/science.1186120

Cao, J., de la Fuente-Nunez, C., Ou, R. W., Torres, M. T., Pande, S. G., Sinskey, A. J., & Lu, T. K. (2018). Yeast-Based Synthetic Biology Platform for Antimicrobial Peptide Production. *ACS synthetic biology*, *7*(3), 896–902. https://doi.org/10.1021/acssynbio.7b00396

Carpenter, C. D., Kreps, J. A., & Simon, A. E. (1994). Genes encoding glycine-rich *Arabidopsis thaliana* proteins with RNA-binding motifs are influenced by cold treatment and an endogenous circadian rhythm. *Plant Physiology*, *104*(3), 1015–1025. https://doi.org/10.1104/pp.104.3.1015

Carvalho, de Oliveira A., & Gomes, V. M. (2007). Role of plant lipid transfer proteins in plant cell physiology-a concise review. *Peptides*, *28*(5), 1144–1153. https://doi.org/10.1016/j.peptides.2007.03.004

Catoira, R., Galera, C., de Billy, F., Penmetsa, R. V., Journet, E. P., Maillet, F., Rosenberg, C., Cook, D., Gough, C., & Dénarié, J. (2000). Four genes of *Medicago truncatula* controlling components of a nod factor transduction pathway. *The Plant cell*, *12*(9), 1647–1666. https://doi.org/10.1105/tpc.12.9.1647

Cebolla, A., Vinardell, J. M., Kiss, E., Oláh, B., Roudier, F., Kondorosi, A., & Kondorosi, E. (1999). The mitotic inhibitor ccs52 is required for endoreduplication and ploidy-dependent cell enlargement in plants. *The EMBO journal*, *18*(16), 4476–4484. https://doi.org/10.1093/emboj/18.16.4476

Chan, W. and P. White, Fmoc Solid Phase Peptide Synthesis: A Practical Approach. 1999, Oxford University Press.

Chen, A. P., Zhong, N. Q., Qu, Z. L., Wang, F., Liu, N., & Xia, G. X. (2007). Root and vascular tissue-specific expression of glycine-rich protein AtGRP9 and its interaction with AtCAD5, a cinnamyl alcohol dehydrogenase, in Arabidopsis thaliana. *Journal of plant research*, *120*(2), 337–343. https://doi.org/10.1007/s10265-006-0058-8

Choudhary, M., Shrivastava, R., & Vashistt, J. (2022). *Acinetobacter baumannii* Biofilm Formation: Association with Antimicrobial Resistance and Prolonged Survival under Desiccation. Current microbiology, 79(12), 361. https://doi.org/10.1007/s00284-022-03071-5

Ciumac, D., Gong, H., Hu, X., & Lu, J. R. (2019). Membrane targeting cationic antimicrobial peptides. *Journal of colloid and interface science*, *537*, 163–185. https://doi.org/10.1016/j.jcis.2018.10.103

Czolpinska, M., & Rurek, M. (2018). Plant Glycine-Rich Proteins in Stress Response: An Emerging, Still Prospective Story. *Frontiers in plant science*, *9*, 302. https://doi.org/10.3389/fpls.2018.00302

de Bertoldi, M., Vallini, G., & Pera, A. (1983). The biology of composting: A review. Waste Management & Research, 1(2), 157–176. https://doi.org/10.1016/0734-242X(83)90055-1

Dini, I., De Biasi, M. G., & Mancusi, A. (2022). An Overview of the Potentialities of Antimicrobial Peptides Derived from Natural Sources. *Antibiotics (Basel, Switzerland)*, *11*(11), 1483. https://doi.org/10.3390/antibiotics11111483

Dixon, R., & Kahn, D. (2004). Genetic regulation of biological nitrogen fixation. *Nature Reviews Microbiology*, *2*(8), 621–631. https://doi.org/10.1038/nrmicro954

Downie J. A. (2014). Legume nodulation. *Current biology: CB*, *24*(5), R184–R190. https://doi.org/10.1016/j.cub.2014.01.028

Downie JA and Kondorosi E (2021) Why Should Nodule Cysteine-Rich (NCR) Peptides Be Absent From Nodules of Some Groups of Legumes but Essential for Symbiotic N-Fixation in Others? *Front. Agron.* 3:654576. https://doi.org/10.3389/fagro.2021.654576

Education Ltd. (n.d.). *The nitrogen cycle* [Diagram]. In *GCSE Biology revision: The Nitrogen Cycle*. from https://www.shalom-education.com/courses/gcse-biology/lessons/ecosystems/topic/the-nitrogen-cycle/

Ehrhardt, D. W., Wais, R., & Long, S. R. (1996). Calcium spiking in plant root hairs responding to Rhizobium nodulation signals. *Cell*, *85*(5), 673–681. https://doi.org/10.1016/s0092-8674(00)81234-9

Elnagdy, S., & AlKhazindar, M. (2020). The Potential of Antimicrobial Peptides as an Antiviral Therapy against COVID-19. *ACS pharmacology & translational science*, *3*(4), 780–782. https://doi.org/10.1021/acsptsci.0c00059

Erdem Büyükkiraz, M., & Kesmen, Z. (2022). Antimicrobial peptides (AMPs): A promising class of antimicrobial compounds. *Journal of applied microbiology*, *132*(3), 1573–1596. https://doi.org/10.1111/jam.15314

Erisman, J. W., Sutton, M. A., Galloway, J., Klimont, Z., & Winiwarter, W. (2008). How a century of ammonia synthesis changed the world. *Nature Geoscience*, *1*(10), 636-639. https://doi.org/10.1038/ngeo325

Farkas, A., Maróti, G., Durgő, H., Györgypál, Z., Lima, R. M., Medzihradszky, K. F., Kereszt, A., Mergaert, P., & Kondorosi, É. (2014). *Medicago truncatula* symbiotic peptide NCR247 contributes to bacteroid differentiation through multiple mechanisms. *Proceedings of the National Academy of Sciences of the United States of America*, *111*(14), 5183–5188. https://doi.org/10.1073/pnas.1404169111

Farkas, A., Maróti, G., Kereszt, A., & Kondorosi, É. (2017). Comparative Analysis of the Bacterial Membrane Disruption Effect of Two Natural Plant Antimicrobial Peptides. Frontiers in microbiology, 8, 51. https://doi.org/10.3389/fmicb.2017.00051

Farkas, A., Pap, B., Kondorosi, É., & Maróti, G. (2018). Antimicrobial Activity of NCR Plant Peptides Strongly Depends on the Test Assays. *Frontiers in microbiology*, *9*, 2600. https://doi.org/10.3389/fmicb.2018.02600

Fay P. (1992). Oxygen relations of nitrogen fixation in cyanobacteria. *Microbiological reviews*, *56*(2), 340–373. https://doi.org/10.1128/mr.56.2.340-373.1992

Fournier, J., Timmers, A. C., Sieberer, B. J., Jauneau, A., Chabaud, M., & Barker, D. G. (2008). Mechanism of infection thread elongation in root hairs of Medicago truncatula and dynamic interplay with associated rhizobial colonization. *Plant physiology*, *148*(4), 1985–1995. https://doi.org/10.1104/pp.108.125674

Franssen, H. J., Vijn, I., Yang, W. C., & Bisseling, T. (1992). Developmental aspects of the Rhizobium-legume symbiosis. *Plant molecular biology*, *19*(1), 89–107. https://doi.org/10.1007/BF00015608

Fu, Z. Q., Guo, M., Jeong, B. R., Tian, F., Elthon, T. E., Cerny, R. L., Staiger, D., & Alfano, J. R. (2007). A type III effector ADP-ribosylates RNA-binding proteins and quells plant immunity. *Nature*, *447*(7142), 284–288. https://doi.org/10.1038/nature05737

Gage D. J. (2004). Infection and invasion of roots by symbiotic, nitrogen-fixing rhizobia during nodulation of temperate legumes. *Microbiology and molecular biology reviews: MMBR*, *68*(2), 280–300. https://doi.org/10.1128/MMBR.68.2.280-300.2004

Galloway, J. N., Dentener, F. J., Capone, D. G., Boyer, E. W., Howarth, R. W., Seitzinger, S. P., Asner, G. P., Cleveland, C. C., Green, P. A., Holland, E. A., Karl, D. M., Michaels, A. F., Porter, J. H., Townsend, A. R., & Vöosmarty, C. J. (2004). Nitrogen Cycles: Past, Present, and Future. *Biogeochemistry*, *70*(2), 153–226. https://doi.org/10.1007/s10533-004-0370-0

Gordon, Y. J., Romanowski, E. G., & McDermott, A. M. (2005). A review of antimicrobial peptides and their therapeutic potential as anti-infective drugs. *Current eye research*, *30*(7), 505–515. https://doi.org/10.1080/02713680590968637

Gruber, N., & Galloway, J. N. (2008). *An Earth-system perspective of the global nitrogen cycle.* Nature, 451(7176), 293–296. https://doi.org/10.1038/nature06592

Guefrachi, I., Nagymihaly, M., Pislariu, C. I., Van de Velde, W., Ratet, P., Mars, M., Udvardi, M. K., Kondorosi, E., Mergaert, P., & Alunni, B. (2014). Extreme specificity of NCR gene

expression in *Medicago truncatula*. *BMC genomics*, *15*(1), 712. https://doi.org/10.1186/1471-2164-15-712

Güngör, B., Biró, J. B., Domonkos, Á., Horváth, B., & Kaló, P. (2023). Targeted mutagenesis of *Medicago truncatula* Nodule-specific Cysteine-Rich (NCR) genes using the *Agrobacterium rhizogenes*-mediated CRISPR/Cas9 system. *Scientific reports*, *13*(1), 20676. https://doi.org/10.1038/s41598-023-47608-5

Guo, C., Cong, P., He, Z., Mo, D., Zhang, W., Chen, Y., & Liu, X. (2015). Inhibitory activity and molecular mechanism of protegrin-1 against porcine reproductive and respiratory syndrome virus in vitro. *Antiviral therapy*, *20*(6), 573–582. https://doi.org/10.3851/IMP2918

Györgyey, J., Vaubert, D., Jiménez-Zurdo, J. I., Charon, C., Troussard, L., Kondorosi, A., & Kondorosi, E. (2000). Analysis of *Medicago truncatula* nodule expressed sequence tags. *Molecular plant-microbe interactions: MPMI*, *13*(1), 62–71. https://doi.org/10.1094/MPMI.2000.13.1.62

Haag, A. F., Baloban, M., Sani, M., Kerscher, B., Pierre, O., Farkas, A., Longhi, R., Boncompagni, E., Hérouart, D., Dall'angelo, S., Kondorosi, E., Zanda, M., Mergaert, P., & Ferguson, G. P. (2011). Protection of *Sinorhizobium* against host cysteine-rich antimicrobial peptides is critical for symbiosis. *PLoS biology*, *9*(10), e1001169. https://doi.org/10.1371/journal.pbio.1001169

Hancock, R. E., & Sahl, H. G. (2006). Antimicrobial and host-defense peptides as new anti-infective therapeutic strategies. *Nature biotechnology*, *24*(12), 1551–1557. https://doi.org/10.1038/nbt1267

Hardy, R. W. F., Holsten, R. D., Jackson, E. K., & Burns, R. C. (1968). The acetylene–ethylene assay for N_2 fixation: Laboratory and field evaluation. *Plant Physiology, 43*(8), 1185–1207. https://doi.org/10.1104/pp.43.8.1185

Horváth, B., Domonkos, Á., Kereszt, A., Szűcs, A., Ábrahám, E., Ayaydin, F., Bóka, K., Chen, Y., Chen, R., Murray, J. D., Udvardi, M. K., Kondorosi, É., & Kaló, P. (2015). Loss of the nodule-specific cysteine rich peptide, NCR169, abolishes symbiotic nitrogen fixation in the Medicago truncatula dnf7 mutant. *Proceedings of the National Academy of Sciences of the United States of America*, *112*(49), 15232–15237. https://doi.org/10.1073/pnas.1500777112

Horváth, B., Güngör, B., Tóth, M., Domonkos, Á., Ayaydin, F., Saifi, F., Chen, Y., Biró, J. B., Bourge, M., Szabó, Z., Tóth, Z., Chen, R., & Kaló, P. (2023). The Medicago truncatula nodule-specific cysteine-rich peptides, NCR343 and NCR-new35 are required for the maintenance of rhizobia in nitrogen-fixing nodules. The New phytologist, 239(5), 1974–1988. https://doi.org/10.1111/nph.19097

Howan, D. H. O., Jenei, S., Szolomajer, J., Endre, G., Kondorosi, É., & Tóth, G. K. (2023). Enhanced Antibacterial Activity of Substituted Derivatives of NCR169C Peptide. International journal of molecular sciences, 24(3), 2694. https://doi.org/10.3390/ijms24032694

Hsieh, I. N., & Hartshorn, K. L. (2016). The Role of Antimicrobial Peptides in Influenza Virus Infection and Their Potential as Antiviral and Immunomodulatory Therapy. *Pharmaceuticals (Basel, Switzerland), 9*(3), 53. https://doi.org/10.3390/ph9030053

Huan, Y., Kong, Q., Mou, H., & Yi, H. (2020). Antimicrobial Peptides: Classification, Design, Application and Research Progress in Multiple Fields. *Frontiers in microbiology*, *11*, 582779. https://doi.org/10.3389/fmicb.2020.582779

Isozumi, N., Masubuchi, Y., Imamura, T., Mori, M., Koga, H., & Ohki, S. (2021). Structure and antimicrobial activity of NCR169, a nodule-specific cysteine-rich peptide of *Medicago truncatula*. Scientific reports, 11(1), 9923. https://doi.org/10.1038/s41598-021-89485-w

Jenei, S., Tiricz, H., Szolomájer, J., Tímár, E., Klement, É., Al Bouni, M. A., Lima, R. M., Kata, D., Harmati, M., Buzás, K., Földesi, I., Tóth, G. K., Endre, G., & Kondorosi, É. (2020). Potent Chimeric Antimicrobial Derivatives of the *Medicago truncatula* NCR247 Symbiotic Peptide. Frontiers in microbiology, 11, 270. https://doi.org/10.3389/fmicb.2020.00270

Jenssen, H., Hamill, P., & Hancock, R. E. (2006). Peptide antimicrobial agents. Clinical microbiology reviews, 19(3), 491–511. https://doi.org/10.1128/CMR.00056-05

Jiménez-Zurdo, J. I., Frugier, F., Crespi, M. D., & Kondorosi, A. (2000). Expression profiles of 22 novel molecular markers for organogenetic pathways acting in alfalfa nodule development. *Molecular plant-microbe interactions: MPMI*, *13*(1), 96–106. https://doi.org/10.1094/MPMI.2000.13.1.96

Joo, H. S., Fu, C. I., & Otto, M. (2016). Bacterial strategies of resistance to antimicrobial peptides. *Philosophical transactions of the Royal Society of London. Series B, Biological sciences*, *371*(1695), 20150292. https://doi.org/10.1098/rstb.2015.0292

Karunakaran, R., Haag, A. F., East, A. K., Ramachandran, V. K., Prell, J., James, E. K., Scocchi, M., Ferguson, G. P., & Poole, P. S. (2010). BacA is essential for bacteroid development in nodules of galegoid, but not phaseoloid, legumes. *Journal of bacteriology*, *192*(11), 2920–2928. https://doi.org/10.1128/JB.00020-10

Keller, B., Templeton, M. D., & Lamb, C. J. (1989). Specific localization of a plant cell wall glycine-rich protein in protoxylem cells of the vascular system. *Proceedings of the National Academy of Sciences of the United States of America*, *86*(5), 1529–1533. https://doi.org/10.1073/pnas.86.5.1529

Kereszt A, Mergaert P, Montiel J, Endre G and Kondorosi É (2018) Impact of Plant Peptides on Symbiotic Nodule Development and Functioning. *Front. Plant Sci.* 9:1026. https://doi.org/10.3389/fpls.2018.01026

Kereszt, A., Mergaert, P., & Kondorosi, E. (2011). Bacteroid development in legume nodules: evolution of mutual benefit or of sacrificial victims?. *Molecular plant-microbe interactions: MPMI*, *24*(11), 1300–1309. https://doi.org/10.1094/MPMI-06-11-0152

Kevei, Z., Vinardell, J. M., Kiss, G. B., Kondorosi, A., & Kondorosi, E. (2002). Glycine-rich proteins encoded by a nodule-specific gene family are implicated in different stages of symbiotic nodule development in Medicago spp. *Molecular plant-microbe interactions: MPMI*, *15*(9), 922–931. https://doi.org/10.1094/MPMI.2002.15.9.922

Kim, M., Chen, Y., Xi, J., Waters, C., Chen, R., & Wang, D. (2015). An antimicrobial peptide essential for bacterial survival in the nitrogen-fixing symbiosis. *Proceedings of the National Academy of Sciences of the United States of America*, *112*(49), 15238–15243. https://doi.org/10.1073/pnas.1500123112

Kintses, B., Jangir, P. K., Fekete, G., Számel, M., Méhi, O., Spohn, R., Daruka, L., Martins, A., Hosseinnia, A., Gagarinova, A., Kim, S., Phanse, S., Csörgő, B., Györkei, Á., Ari, E., Lázár, V., Nagy, I., Babu, M., Pál, C., & Papp, B. (2019). Chemical-genetic profiling reveals limited cross-resistance between antimicrobial peptides with different modes of action. Nature communications, 10(1), 5731. https://doi.org/10.1038/s41467-019-13618-z

Kondorosi, E., Banfalvi, Z. & Kondorosi, A. (1984). Physical and genetic analysis of a symbiotic region of *Rhizobium meliloti*: Identification of nodulation genes. *Molec. Gen. Genet.* 193, 445–452. https://doi.org/10.1007/BF00382082

Kondorosi, E., Mergaert, P., & Kereszt, A. (2013). A paradigm for endosymbiotic life: cell differentiation of Rhizobium bacteria provoked by host plant factors. *Annual review of microbiology*, *67*, 611–628. https://doi.org/10.1146/annurev-micro-092412-155630

Kondorosi, A., Vinardell, J. M., Uchiumi, T., Mergaert, P., & Kondorosi, E. (2005). Cell Cycle and Symbiosis. In Y.-P. Wang, M. Lin, Z.-X. Tian, C. Elmerich, & W. E. Newton (Eds.),

Biological Nitrogen Fixation, Sustainable Agriculture and the Environment (pp. 147–151). Springer Netherlands. https://doi.org/10.1007/1-4020-3570-5_35

Küster, H., Schröder, G., Frühling, M., Pich, U., Rieping, M., Schubert, I., Perlick, A. M., & Pühler, A. (1995). The nodule-specific VfENOD-GRP3 gene encoding a glycine-rich early nodulin is located on chromosome I of *Vicia faba* L. and is predominantly expressed in the interzone II-III of root nodules. *Plant molecular biology*, *28*(3), 405–421. https://doi.org/10.1007/BF00020390

Kuypers, M. M. M., Marchant, H. K., & Kartal, B. (2018). *The microbial nitrogen-cycling network.* Nature Reviews Microbiology, 16(5), 263–276. https://doi.org/10.1038/nrmicro.2018.9

Lee, M. Y., Park, S. C., Jung, M., Shin, M. K., Kang, H. L., Baik, S. C., Cheong, G. W., Jang, M. K., & Lee, W. K. (2018). Cell-selectivity of tryptophan and tyrosine in amphiphilic α-helical antimicrobial peptides against drug-resistant bacteria. Biochemical and biophysical research communications, 505(2), 478–484. https://doi.org/10.1016/j.bbrc.2018.09.095

Leitgeb, B., Szekeres, A., Manczinger, L., Vágvölgyi, C., & Kredics, L. (2007). The history of alamethicin: a review of the most extensively studied peptaibol. *Chemistry & biodiversity*, *4*(6), 1027–1051. https://doi.org/10.1002/cbdv.200790095

Lerouge, P., Roche, P., Faucher, C., Maillet, F., Truchet, G., Promé, J. C., & Dénarié, J. (1990). Symbiotic host-specificity of Rhizobium meliloti is determined by a sulphated and acylated glucosamine oligosaccharide signal. *Nature*, *344*(6268), 781–784. https://doi.org/10.1038/344781a0

Liang, X., Zhang, X., Lian, K., Tian, X., Zhang, M., Wang, S., Chen, C., Nie, C., Pan, Y., Han, F., Wei, Z., & Zhang, W. (2020). Antiviral effects of Bovine antimicrobial peptide against TGEV *in vivo* and *in vitro*. *Journal of veterinary science*, *21*(5), e80. https://doi.org/10.4142/jvs.2020.21.e80

Lima, R. M., Kylarová, S., Mergaert, P., & Kondorosi, É. (2020). Unexplored Arsenals of Legume Peptides With Potential for Their Applications in Medicine and Agriculture. Frontiers in microbiology, 11, 1307. https://doi.org/10.3389/fmicb.2020.01307

Lima, A. M., Azevedo, M. I. G., Sousa, L. M., Oliveira, N. S., Andrade, C. R., Freitas, C. D. T., & Souza, P. F. N. (2022). Plant antimicrobial peptides: An overview about classification, toxicity and clinical applications. *International journal of biological macromolecules*, *214*, 10–21. https://doi.org/10.1016/j.ijbiomac.2022.06.043

Lima, R. M., Rathod, B. B., Tiricz, H., Howan, D. H. O., Al Bouni, M. A., Jenei, S., Tímár, E., Endre, G., Tóth, G. K., & Kondorosi, É. (2022). Legume Plant Peptides as Sources of Novel Antimicrobial Molecules Against Human Pathogens. Frontiers in molecular biosciences, 9, 870460. https://doi.org/10.3389/fmolb.2022.870460

Limpens, E., & Bisseling, T. (2003). Signaling in symbiosis. *Current opinion in plant biology*, *6*(4), 343–350. https://doi.org/10.1016/s1369-5266(03)00068-2

Lin, L., Chi, J., Yan, Y., Luo, R., Feng, X., Zheng, Y., Xian, D., Li, X., Quan, G., Liu, D., Wu, C., Lu, C., & Pan, X. (2021). Membrane-disruptive peptides/peptidomimetics-based therapeutics: Promising systems to combat bacteria and cancer in the drug-resistant era. *Acta pharmaceutica Sinica. B*, *11*(9), 2609–2644. https://doi.org/10.1016/j.apsb.2021.07.014

Łotocka, B., Kopcińska, J., & Skalniak, M. (2012). Review article: The meristem in indeterminate root nodules of Faboideae. *Symbiosis (Philadelphia, Pa.)*, *58*(1-3), 63–72. https://doi.org/10.1007/s13199-013-0225-3

Mangeon, A., Junqueira, R. M., & Sachetto-Martins, G. (2010). Functional diversity of the plant glycine-rich proteins superfamily. *Plant signaling & behavior*, *5*(2), 99–104. https://doi.org/10.4161/psb.5.2.10336

Maróti, G., & Kondorosi, E. (2014). Nitrogen-fixing Rhizobium-legume symbiosis: are polyploidy and host peptide-governed symbiont differentiation general principles of endosymbiosis?. *Frontiers in microbiology*, *5*, 326. https://doi.org/10.3389/fmicb.2014.00326

Maróti, G., Downie, J. A., & Kondorosi, É. (2015). Plant cysteine-rich peptides that inhibit pathogen growth and control rhizobial differentiation in legume nodules. *Current opinion in plant biology*, *26*, 57–63. https://doi.org/10.1016/j.pbi.2015.05.031

Maróti, G., Kereszt, A., Kondorosi, E., & Mergaert, P. (2011). Natural roles of antimicrobial peptides in microbes, plants and animals. *Research in microbiology*, *162*(4), 363–374. https://doi.org/10.1016/j.resmic.2011.02.005

Mazu, T. K., Bricker, B. A., Flores-Rozas, H., & Ablordeppey, S. Y. (2016). The Mechanistic Targets of Antifungal Agents: An Overview. *Mini reviews in medicinal chemistry*, *16*(7), 555–578. https://doi.org/10.2174/1389557516666160118112103

Mendes, S. G., Combo, S. I., Allain, T., Domingues, S., Buret, A. G., & Da Silva, G. J. (2023). Co-regulation of biofilm formation and antimicrobial resistance in Acinetobacter baumannii: from mechanisms to therapeutic strategies. European journal of clinical microbiology & infectious diseases: official publication of the European Society of Clinical Microbiology, 42(12), 1405–1423. https://doi.org/10.1007/s10096-023-04677-8

Mergaert, P., Nikovics, K., Kelemen, Z., Maunoury, N., Vaubert, D., Kondorosi, A., & Kondorosi, E. (2003). A novel family in *Medicago truncatula* consisting of more than 300 nodule-specific genes coding for small, secreted polypeptides with conserved cysteine motifs. *Plant physiology*, *132*(1), 161–173. https://doi.org/10.1104/pp.102.018192

Mergaert, P., Uchiumi, T., Alunni, B., Evanno, G., Cheron, A., Catrice, O., Mausset, A. E., Barloy-Hubler, F., Galibert, F., Kondorosi, A., & Kondorosi, E. (2006). Eukaryotic control on bacterial cell cycle and differentiation in the Rhizobium-legume symbiosis. Proceedings of the National Academy of Sciences of the United States of America, 103(13), 5230–5235. https://doi.org/10.1073/pnas.0600912103

Mikuláss, K. R., Nagy, K., Bogos, B., Szegletes, Z., Kovács, E., Farkas, A., Váró, G., Kondorosi, É., & Kereszt, A. (2016). Antimicrobial nodule-specific cysteine-rich peptides disturb the integrity of bacterial outer and inner membranes and cause loss of membrane potential. Annals of clinical microbiology and antimicrobials, 15(1), 43. https://doi.org/10.1186/s12941-016-0159-8

Montiel, J., Downie, J. A., Farkas, A., Bihari, P., Herczeg, R., Bálint, B., Mergaert, P., Kereszt, A., & Kondorosi, É. (2017). Morphotype of bacteroids in different legumes correlates with the number and type of symbiotic NCR peptides. *Proceedings of the National Academy of Sciences of the United States of America*, *114*(19), 5041–5046. https://doi.org/10.1073/pnas.1704217114

Murray J. D. (2011). Invasion by invitation: rhizobial infection in legumes. *Molecular plant-microbe interactions : MPMI*, *24*(6), 631–639. https://doi.org/10.1094/MPMI-08-10-0181

Mus, F., Crook, M. B., Garcia, K., Costas, A. G., Geddes, B. A., Kouri, E. D., Paramasivan, P., Ryu, M.-H., Oldroyd, G. E. D., Poole, P. S., Udvardi, M. K., Voigt, C. A., Ané, J.-M., & Peters, J. W. (2016). Symbiotic nitrogen fixation and the challenges to its extension to nonlegumes. *Applied and Environmental Microbiology*, *82*(13), 3698–3710. https://doi.org/10.1128/AEM.01055-16

Mylona, P., Pawlowski, K., & Bisseling, T. (1995). Symbiotic Nitrogen Fixation. *The Plant cell*, *7*(7), 869–885. https://doi.org/10.1105/tpc.7.7.869

Nallu, S., Silverstein, K. A., Samac, D. A., Bucciarelli, B., Vance, C. P., & VandenBosch, K. A. (2013). Regulatory patterns of a large family of defensin-like genes expressed in nodules of Medicago truncatula. *PloS one*, *8*(4), e60355. https://doi.org/10.1371/journal.pone.0060355

National Committee for Clinical Laboratory Standards. (1979). Performance standards for antimicrobic disc susceptibility tests (2nd ed.; NCCLS Approved Standard ASM-2). NCCLS.

Oke, V., & Long, S. R. (1999). Bacteroid formation in the Rhizobium-legume symbiosis. *Current opinion in microbiology*, *2*(6), 641–646. https://doi.org/10.1016/s1369-5274(99)00035-1

Oldroyd, G. E. D., Murray, J. D., Poole, P. S., & Downie, J. A. (2011). The rules of engagement in the legume–rhizobial symbiosis. *Annual Review of Genetics*, *45*, 119–144. https://doi.org/10.1146/annurev-genet-110410-132549

Oldroyd, G. E., & Downie, J. A. (2008). Coordinating nodule morphogenesis with rhizobial infection in legumes. *Annual review of plant biology*, *59*, 519–546. https://doi.org/10.1146/annurev.arplant.59.032607.092839

Ördögh, L., Vörös, A., Nagy, I., Kondorosi, E., & Kereszt, A. (2014). Symbiotic plant peptides eliminate *Candida albicans* both in vitro and in an epithelial infection model and inhibit the proliferation of immortalized human cells. BioMed research international, 2014, 320796. https://doi.org/10.1155/2014/320796

Ott, T., van Dongen, J. T., Günther, C., Krusell, L., Desbrosses, G., Vigeolas, H., Bock, V., Czechowski, T., Geigenberger, P., & Udvardi, M. K. (2005). Symbiotic leghemoglobins are crucial for nitrogen fixation in legume root nodules but not for general plant growth and development. *Current biology: CB*, *15*(6), 531–535. https://doi.org/10.1016/j.cub.2005.01.042

Pallaghy, P. K., Nielsen, K. J., Craik, D. J., & Norton, R. S. (1994). A common structural motif incorporating a cystine knot and a triple-stranded beta-sheet in toxic and inhibitory polypeptides. *Protein science: a publication of the Protein Society*, *3*(10), 1833–1839. https://doi.org/10.1002/pro.5560031022

Park, A. R., Cho, S. K., Yun, U. J., Jin, M. Y., Lee, S. H., Sachetto-Martins, G., & Park, O. K. (2001). Interaction of the Arabidopsis receptor protein kinase Wak1 with a glycine-rich protein, AtGRP-3. *The Journal of biological chemistry*, *276*(28), 26688–26693. https://doi.org/10.1074/jbc.M101283200

Pearson, J., & Stewart, G. R. (1993). The deposition of atmospheric ammonia and its effects on plants. *The New phytologist*, *125*(2), 283–305. https://doi.org/10.1111/j.1469-8137.1993.tb03882.x

Pecrix, Y., Staton, S. E., Sallet, E., Lelandais-Brière, C., Moreau, S., Carrère, S., Blein, T., Jardinaud, M. F., Latrasse, D., Zouine, M., Zahm, M., Kreplak, J., Mayjonade, B., Satgé, C., Perez, M., Cauet, S., Marande, W., Chantry-Darmon, C., Lopez-Roques, C., Bouchez, O Bérard A., Debellé, F., Muños, S., Bendahmane, A., Bergès, H., Niebel, A., Buitink, J., Frugier, F., Benhamed, M., Crespi, M., Gouzy, J., Gamas, P. (2018). Whole-genome landscape of *Medicago truncatula* symbiotic genes. *Nature plants*, *4*(12), 1017–1025. https://doi.org/10.1038/s41477-018-0286-7

Peng, S., Lai, K., Tian, Y., & Wang, X. (2014). Evaluation of three reference genes of *Escherichia coli* for mRNA expression level normalization in view of salt and organic acid stress exposure in food. FEMS Microbiology Letters, 355(1), 78–84. https://doi.org/10.1111/1574-6968.12494

Penterman, J., Abo, R. P., De Nisco, N. J., Arnold, M. F., Longhi, R., Zanda, M., & Walker, G. C. (2014). Host plant peptides elicit a transcriptional response to control the *Sinorhizobium meliloti* cell cycle during symbiosis. *Proceedings of the National Academy of Sciences of the United States of America*, *111*(9), 3561–3566. https://doi.org/10.1073/pnas.1400450111

Perlick, A. M., Albus, U., Stavridis, T., Frühling, M., Küster, H., & Pühler, A. (1996). The *Vicia faba* lipoxygenase gene VfLOX1 is expressed in the root nodule parenchyma. *Molecular plant-microbe interactions : MPMI*, *9*(9), 860–863. https://doi.org/10.1094/mpmi-9-0860

Peschel, A., & Sahl, H.-G. (2006). The co-evolution of host cationic antimicrobial peptides and microbial resistance. Nature Reviews Microbiology, 4(7), 529–536. https://doi.org/10.1038/nrmicro1441

Pfalzgraff, A., Brandenburg, K., & Weindl, G. (2018). Antimicrobial Peptides and Their Therapeutic Potential for Bacterial Skin Infections and Wounds. *Frontiers in pharmacology*, *9*, 281. https://doi.org/10.3389/fphar.2018.00281

Puppo, A., Groten, K., Bastian, F., Carzaniga, R., Soussi, M., Lucas, M. M., de Felipe, M. R., Harrison, J., Vanacker, H., & Foyer, C. H. (2005). Legume nodule senescence: roles for redox and hormone signalling in the orchestration of the natural aging process. *The New phytologist*, *165*(3), 683–701. https://doi.org/10.1111/j.1469-8137.2004.01285.x

Qi, S., Gao, B., & Zhu, S. (2022). A Fungal Defensin Inhibiting Bacterial Cell-Wall Biosynthesis with Non-Hemolysis and Serum Stability. *Journal of fungi (Basel, Switzerland)*, *8*(2), 174. https://doi.org/10.3390/jof8020174

Reinhold-Hurek, B., & Hurek, T. (2011). Living inside plants: Bacterial endophytes. *Current Opinion in Plant Biology*, *14*(4), 435–443. https://doi.org/10.1016/j.pbi.2011.04.004

Rekha, S.N. Naik, and R. Prasad, Pesticide residue in organic and conventional food-risk analysis. Journal of Chemical Health and Safety, 2006. 13(6): p. 12-19.

Ringli, C., Keller, B., & Ryser, U. (2001). Glycine-rich proteins as structural components of plant cell walls. *Cellular and molecular life sciences: CMLS*, *58*(10), 1430–1441. https://doi.org/10.1007/PL00000786

Roth, L. E., & Stacey, G. (1989). Bacterium release into host cells of nitrogen-fixing soybean nodules: the symbiosome membrane comes from three sources. *European journal of cell biology*, *49*(1), 13–23.

Roux, B., Rodde, N., Jardinaud, M. F., Timmers, T., Sauviac, L., Cottret, L., Carrère, S., Sallet, E., Courcelle, E., Moreau, S., Debellé, F., Capela, D., de Carvalho-Niebel, F., Gouzy, J., Bruand, C., & Gamas, P. (2014). An integrated analysis of plant and bacterial gene expression in symbiotic root nodules using laser-capture microdissection coupled to RNA sequencing. *The Plant journal : for cell and molecular biology*, *77*(6), 817–837. https://doi.org/10.1111/tpj.12442

Roy, S., Liu, W., Nandety, R. S., Crook, A., Mysore, K. S., Pislariu, C. I., Frugoli, J., Dickstein, R., & Udvardi, M. K. (2020). *Celebrating 20 years of genetic discoveries in legume nodulation and symbiotic nitrogen fixation. The Plant Cell*, *32*(1), 15–41. https://doi.org/10.1105/tpc.19.00279

Sachetto-Martins, G., Franco, L. O., & de Oliveira, D. E. (2000). Plant glycine-rich proteins: a family or just proteins with a common motif?. *Biochimica et biophysica acta*, *1492*(1), 1–14. https://doi.org/10.1016/s0167-4781(00)00064-6

Sankari, S., Babu, V. M. P., Bian, K., Alhhazmi, A., Andorfer, M. C., Avalos, D. M., Smith, T. A., Yoon, K., Drennan, C. L., Yaffe, M. B., Lourido, S., & Walker, G. C. (2022). A haem-sequestering plant peptide promotes iron uptake in symbiotic bacteria. *Nature microbiology*, *7*(9), 1453–1465. https://doi.org/10.1038/s41564-022-01192-y

Schlesinger, W. H., & Bernhardt, E. S. (2013). *Biogeochemistry: An Analysis of Global Change* (3rd ed.). Academic Press.

Schröder, G., Fruhling, M., Puhler, A., & Perlick, A. M. (1997). The temporal and spatial transcription pattern in root nodules of *Vicia faba* nodulin genes encoding glycine-rich proteins. *Plant molecular biology*, *33*(1), 113–123. https://doi.org/10.1023/a:1005779116272

Silva, T., & Gomes, M. S. (2017). Immuno-Stimulatory Peptides as a Potential Adjunct Therapy against Intra-Macrophagic Pathogens. *Molecules (Basel, Switzerland)*, *22*(8), 1297. https://doi.org/10.3390/molecules22081297

Singh, A., Duche, R. T., Wandhare, A. G., Sian, J. K., Singh, B. P., Sihag, M. K., Singh, K. S., Sangwan, V., Talan, S., & Panwar, H. (2023). Milk-Derived Antimicrobial Peptides: Overview, Applications, and Future Perspectives. Probiotics and antimicrobial proteins, 15(1), 44–62. https://doi.org/10.1007/s12602-022-10004-y

Singh, B., Dahiya, M., Kumar, V., Ayyagari, A., Chaudhari, D. N., & Ahire, J. J. (2025). Biofilm and Antimicrobial Resistance: Mechanisms, Implications, and Emerging Solutions. Microbiology Research, 16(8), 183. https://doi.org/10.3390/microbiolres16080183

Slavokhotova, A. A., Shelenkov, A. A., Andreev, Y. A., & Odintsova, T. I. (2017). Hevein-Like Antimicrobial Peptides of Plants. *Biochemistry. Biokhimiia*, *82*(13), 1659–1674. https://doi.org/10.1134/S0006297917130065

Smil, V. (2001). Enriching the Earth: Fritz Haber, Carl Bosch, and the Transformation of World Food Production. MIT Press.

Sohlenkamp, C., de Rudder, K. E., & Geiger, O. (2004). Phosphatidylethanolamine is not essential for growth of Sinorhizobium meliloti on complex culture media. *Journal of bacteriology*, *186*(6), 1667–1677. https://doi.org/10.1128/JB.186.6.1667-1677.2004

Spohn, R., Daruka, L., Lázár, V., Martins, A., Vidovics, F., Grézal, G., Méhi, O., Kintses, B., Számel, M., Jangir, P. K., Csörgő, B., Györkei, Á., Bódi, Z., Faragó, A., Bodai, L., Földesi, I., Kata, D., Maróti, G., Pap, B., Wirth, R., … Pál, C. (2019). Integrated evolutionary analysis reveals antimicrobial peptides with limited resistance. *Nature communications*, *10*(1), 4538. https://doi.org/10.1038/s41467-019-12364-6

Sprent, J. I. (2009). *Legume nodulation: A global perspective.* Wiley-Blackwell.

Stec B. (2006). Plant thionins--the structural perspective. *Cellular and molecular life sciences: CMLS*, *63*(12), 1370–1385. https://doi.org/10.1007/s00018-005-5574-5

Su, T., Han, M., Cao, D., & Xu, M. (2020). Molecular and Biological Properties of Snakins: The Foremost Cysteine-Rich Plant Host Defense Peptides. *Journal of fungi (Basel, Switzerland)*, *6*(4), 220. https://doi.org/10.3390/jof6040220

Sun, Q., Wang, K., She, R., Ma, W., Peng, F., & Jin, H. (2010). Swine intestine antimicrobial peptides inhibit infectious bronchitis virus infectivity in chick embryos. *Poultry science*, *89*(3), 464–469. https://doi.org/10.3382/ps.2009-00461

Sylvia, D. M., Fuhrmann, J. J., Hartel, P. G., & Zuberer, D. A. (2005). *Principles and applications of soil microbiology* (2nd ed.). Pearson Prentice Hall.

Szerencsés, B., Gácser, A., Endre, G., Domonkos, I., Tiricz, H., Vágvölgyi, C., Szolomajer, J., Howan, D. H. O., Tóth, G. K., Pfeiffer, I., & Kondorosi, É. (2021). Symbiotic NCR Peptide Fragments Affect the Viability, Morphology and Biofilm Formation of Candida Species. International journal of molecular sciences, 22(7), 3666. https://doi.org/10.3390/ijms22073666

Szerencsés, B., Papp, C., Pál, A., Jenei, S., Németh, N., Vágvölgyi, C., Ayaydin, F., Endre, G., Kondorosi, É., & Pfeiffer, I. (2025). Plant-derived nodule-specific cysteine-rich peptides as potent antifungal agents against *Cryptococcus neoformans*: mechanisms of action, chimeric peptide enhancement, and immunomodulatory effects. Current research in microbial sciences, 9, 100407. https://doi.org/10.1016/j.crmicr.2025.100407

Taiz, L., Zeiger, E., Moller, I. M., & Murphy, A. (2015). Plant Physiology and Development (6th ed.). Sinauer Associates.

Tajbakhsh, M., Karimi, A., Fallah, F., & Akhavan, M. M. (2017). Overview of ribosomal and non-ribosomal antimicrobial peptides produced by Gram positive bacteria. *Cellular and Molecular Biology*, *63*(10), 20–32. https://doi.org/10.14715/cmb/2017.63.10.4

Tang, S. S., Prodhan, Z. H., Biswas, S. K., Le, C. F., & Sekaran, S. D. (2018). Antimicrobial peptides from different plant sources: Isolation, characterisation, and purification. *Phytochemistry*, *154*, 94–105. https://doi.org/10.1016/j.phytochem.2018.07.002

Tiricz, H., Szucs, A., Farkas, A., Pap, B., Lima, R. M., Maróti, G., Kondorosi, É., & Kereszt, A. (2013). Antimicrobial nodule-specific cysteine-rich peptides induce membrane depolarization-associated changes in the transcriptome of Sinorhizobium meliloti. *Applied and environmental microbiology*, *79*(21), 6737–6746. https://doi.org/10.1128/AEM.01791-13

Tomasinsig, L., Scocchi, M., Mettulio, R., & Zanetti, M. (2004). Genome-wide transcriptional profiling of the Escherichia coli response to a proline-rich antimicrobial peptide. Antimicrobial agents and chemotherapy, 48(9), 3260–3267. https://doi.org/10.1128/AAC.48.9.3260-3267.2004

Tscherner, M., Schwarzmüller, T., & Kuchler, K. (2011). Pathogenesis and Antifungal Drug Resistance of the Human Fungal Pathogen *Candida glabrata*. *Pharmaceuticals*, *4*(1), 169–186. https://doi.org/10.3390/ph4010169

Udvardi, M. K., & Day, D. A. (1997). METABOLITE TRANSPORT ACROSS SYMBIOTIC MEMBRANES OF LEGUME NODULES. *Annual review of plant physiology and plant molecular biology*, *48*, 493–523. https://doi.org/10.1146/annurev.arplant.48.1.493

Ueki, S., & Citovsky, V. (2002). The systemic movement of a tobamovirus is inhibited by a cadmium-ion-induced glycine-rich protein. *Nature cell biology*, *4*(7), 478–486. https://doi.org/10.1038/ncb806

Van de Velde, W., Zehirov, G., Szatmari, A., Debreczeny, M., Ishihara, H., Kevei, Z., Farkas, A., Mikulass, K., Nagy, A., Tiricz, H., Satiat-Jeunemaître, B., Alunni, B., Bourge, M., Kucho, K., Abe, M., Kereszt, A., Maroti, G., Uchiumi, T., Kondorosi, E., & Mergaert, P. (2010). Plant peptides govern terminal differentiation of bacteria in symbiosis. Science (New York, N.Y.), 327(5969), 1122–1126. https://doi.org/10.1126/science.1184057

Vasse, J., de Billy, F., Camut, S., & Truchet, G. (1990). Correlation between ultrastructural differentiation of bacteroids and nitrogen fixation in alfalfa nodules. *Journal of bacteriology*, *172*(8), 4295–4306. https://doi.org/10.1128/jb.172.8.4295-4306.1990

Velivelli, S. L. S., Czymmek, K. J., Li, H., Shaw, J. B., Buchko, G. W., & Shah, D. M. (2020). Antifungal symbiotic peptide NCR044 exhibits unique structure and multifaceted mechanisms of action that confer plant protection. *Proceedings of the National Academy of Sciences of the United States of America*, *117*(27), 16043–16054. https://doi.org/10.1073/pnas.2003526117

Villalobos-Delgado, L., et al., Natural antimicrobial agents to improve foods shelf life. 2019. p. 125-157.

Vitousek, P. M., Aber, J. D., Howarth, R. W., Likens, G. E., Matson, P. A., Schindler, D. W., Schlesinger, W. H., & Tilman, D. G. (1997). Human alteration of the global nitrogen cycle: Sources and consequences. *Ecological Applications*, *7*(3), 737–750. https://doi.org/10.1890/1051-0761(1997)007[0737:HAOTGN]2.0.CO;2

Wang G. (2022). Unifying the classification of antimicrobial peptides in the antimicrobial peptide database. *Methods in enzymology*, *663*, 1–18. https://doi.org/10.1016/bs.mie.2021.09.006

Wang, D., Griffitts, J., Starker, C., Fedorova, E., Limpens, E., Ivanov, S., Bisseling, T., & Long, S. (2010). A nodule-specific protein secretory pathway required for nitrogen-fixing symbiosis. *Science (New York, N.Y.)*, *327*(5969), 1126–1129. https://doi.org/10.1126/science.1184096

Wang, Q., Liu, J., & Zhu, H. (2018). Genetic and Molecular Mechanisms Underlying Symbiotic Specificity in Legume-Rhizobium Interactions. *Frontiers in plant science*, *9*, 313. https://doi.org/10.3389/fpls.2018.00313

Whitehead, L. F., & Day, D. A. (1997). The peribacteroid membrane. *Physiologia Plantarum*, *100*(1), 30–44. https://doi.org/10.1111/j.1399-3054.1997.tb03452.x

Xiao, T. T., Schilderink, S., Moling, S., Deinum, E. E., Kondorosi, E., Franssen, H., Kulikova, O., Niebel, A., & Bisseling, T. (2014). Fate map of *Medicago truncatula* root nodules. *Development (Cambridge, England)*, *141*(18), 3517–3528. https://doi.org/10.1242/dev.110775

Xiao, W., Jiang, W., Chen, Z., Huang, Y., Mao, J., Zheng, W., Hu, Y., & Shi, J. (2025). Advance in peptide-based drug development: Delivery platforms, therapeutics and vaccines. *Signal Transduction and Targeted Therapy*, *10*(1), 74. https://doi.org/10.1038/s41392-024-02107-5

Yokoyama, R., & Nishitani, K. (2006). Identification and characterization of *Arabidopsis thaliana* genes involved in xylem secondary cell walls. *Journal of plant research*, *119*(3), 189–194. https://doi.org/10.1007/s10265-006-0261-7

Young, N. D., Debellé, F., Oldroyd, G. E., Geurts, R., Cannon, S. B., Udvardi, M. K., Benedito, V. A., Mayer, K. F., Gouzy, J., Schoof, H., Van de Peer, Y., Proost, S., Cook, D. R., Meyers, B. C., Spannagl, M., Cheung, F., De Mita, S., Krishnakumar, V., Gundlach, H., Zhou, S., … Roe, B. A. (2011). The Medicago genome provides insight into the evolution of rhizobial symbioses. *Nature*, *480*(7378), 520–524. https://doi.org/10.1038/nature10625

Zhang, H., Lv, J., Ma, Z., Ma, J., & Chen, J. (2025). Advances in Antimicrobial Peptides: Mechanisms, Design Innovations, and Biomedical Potential. *Molecules (Basel, Switzerland)*, *30*(7), 1529. https://doi.org/10.3390/molecules30071529

Zhang, S., Wang, T., Lima, R. M., Pettkó-Szandtner, A., Kereszt, A., Downie, J. A., & Kondorosi, E. (2023). Widely conserved AHL transcription factors are essential for NCR gene expression and nodule development in *Medicago*. *Nature plants*, *9*(2), 280–288. https://doi.org/10.1038/s41477-022-01326-4

Zhou, K., Zhou, L., Lim, Q., Zou, R., Stephanopoulos, G., & Too, H. P. (2011). Novel reference genes for quantifying transcriptional responses of *Escherichia coli* to protein overexpression by quantitative PCR. BMC molecular biology, 12, 18. https://doi.org/10.1186/1471-2199-12-18

9. List of publications

Peer-reviewed publications

Al Bouni, M. A., Lima, R. M., Jenei, S., Tiricz, H., Tímár, E., Domonkos, I., Kondorosi, É., & Endre, G. (2025). A plant-derived antimicrobial peptide with multiple mechanisms of action exhibiting antibacterial and antibiofilm activities comparable to or superior to polymyxin B. *Current Research in Microbial Sciences*, 100535. https://doi.org/10.1016/j.crmicr.2025.100535

IF: 5.8

Jenei, S., Tiricz, H., Szolomájer, J., Tímár, E., Klement, É., **Al Bouni**, **M. A.**, Lima, R. M., Kata, D., Harmati, M., Buzás, K., Földesi, I., Tóth, G. K., Endre, G., & Kondorosi, É. (2020). Potent Chimeric Antimicrobial Derivatives of the Medicago truncatula NCR247 Symbiotic Peptide. Frontiers in microbiology, 11, 270. https://doi.org/10.3389/fmicb.2020.00270

IF: 4.5

Lima, R. M., Rathod, B. B., Tiricz, H., Howan, D. H. O., **Al Bouni, M. A.**, Jenei, S., Tímár, E., Endre, G., Tóth, G. K., & Kondorosi, É. (2022). Legume Plant Peptides as Sources of Novel Antimicrobial Molecules Against Human Pathogens. *Frontiers in molecular biosciences*, *9*, 870460. https://doi.org/10.3389/fmolb.2022.870460

IF: 4.0

MTMT: 10074884

10. Appendix

Supplementary Table 1. The (KEGG) pathway terms identified in our data grouped into five main categories, and the number of genes enriched in each pathway.

Category	KEGG Pathway ID	Nu. of Genes
1. Membrane and Lipid Metabolism	**Fatty acid biosynthesis (eco00061) and C5-Branched dibasic acid metabolism (eco00660)** – Compensatory membrane remodeling.	7-5
	Fatty acid metabolism (eco01212) – Adaptations in lipid processing.	7
	ABC transporters (eco02010) – Changes in nutrient and ion transport.	32
	Bacterial secretion system (eco03070) – Impact on protein transport.	7
2. Stress Response and Resistance Mechanisms	**Oxidative phosphorylation (eco00190)** – Suggests oxidative stress.	28
	Sulfur metabolism (eco00920) – Potential response to reactive oxygen species.	9
	Quorum sensing (eco02024) – Bacterial communication for survival.	12
	Bacterial chemotaxis (eco02030) – Limiting movement in response to stress.	14
	Flagellar assembly (eco02040) – Motility changes due to membrane stress.	24
3. Metabolism and Energy Production	**Carbon metabolism (eco01200)** – Central energy metabolism shift.	37
	Citrate cycle (TCA cycle) (eco00020) – Changes in energy production.	15
	Glycolysis/Gluconeogenesis (eco00010) – Energy source adjustments.	11
	Pentose phosphate pathway (eco00030) – NADPH production for stress defense.	8
	Butanoate metabolism (eco00650) – Energy balance shifts.	7
	Metabolic pathways (eco01100) and Microbial metabolism in diverse environments (eco01120) – Necessary metabolic changes during the stress.	163-54
4. Amino Acid and Secondary Metabolite Biosynthesis	**Biosynthesis of amino acids (eco01230)** – Central pathway integrating multiple amino acid biosynthesis particularly under stress conditions.	54
	Biosynthesis of secondary metabolites (eco01110) – Potential antibiotic resistance mechanisms.	97
	Aminoacyl-tRNA biosynthesis (eco00970) – Adjustments in translation.	17
	Valine, leucine, and isoleucine biosynthesis (eco00290) – Branched-chain amino acid biosynthesis critical for stress adaptation.	7

	Cysteine and methionine metabolism (eco00270) and Glycine, serine, and threonine metabolism (eco00260) – Protein synthesis shifts vital for stress adaptation.	13-8
	Lysine biosynthesis (eco00300), **Arginine biosynthesis (eco00220)** – Essential amino acids for survival.	7-8
	2-Oxocarboxylic acid metabolism (eco01210) – Central metabolic hub linking amino acid biosynthesis and energy production.	16
	Phenylalanine, tyrosine, and tryptophan biosynthesis (eco00400) – Aromatic amino acids signaling molecules important in stress adaptation	8
5. Translational and Genetic Responses	**Ribosome (eco03010)** – Increased protein synthesis demand.	52
	RNA degradation (eco03018) – Processing of stress-induced transcripts.	6
	Protein export (eco03060) – Adaptations in stress protein secretion.	7
	Monobactam biosynthesis (eco00261), **Novobiocin biosynthesis (eco00401)** – Antibiotic resistance responses.	5-2
	Biosynthesis of cofactors (eco01240) – Enzyme cofactor adjustments.	21
	One carbon pool by folate (eco00670) – Nucleotide biosynthesis adaptation.	5
	Purine metabolism (eco00230) – Nucleotide repair responses.	20
	Methane metabolism (eco00680) – Potential alternative metabolic shifts.	9
	Selenocompound metabolism (eco00450) – Possible stress response.	5

Supplementary Table 2. qPCR primers for validation of the mRNA sequencing data.

Gene	**Primer name**	**Primer sequence**
lpp	lppcoli_qPCR_F	TGGTACTGGGCGCGGTAATC
	lppcoli_qPCR_R	AGCAGCCTGAACGTCGGAAC
metK	metKcoli_qPCR_F	GCCAGCACCTATCACCTATG
	metKcoli_qPCR_R	AGCGATTTCTGGTCGATCTC
hcaT	hcaTcoli_qPCR_F	GCTGCTCGGCTTTCTCATCC
	hcaTcoli_qPCR_R	CCAACCACGCTGACCAACC
cysG	cysGcoli_qPCR_F	TTGTCGGCGGTGGTGATGTC
	cysGcoli_qPCR_R	ATGCGGTGAACTGTGGAATAAACG
ihfB	ihfBcoli_qPCR_F	GCGGTTTCGGCAGTTTCT
	ihfBcoli_qPCR_R	CGCAGTTCTTTACCAGGTTT
tufA/B	tufA/Bcoli_qPCR_F	TCGTTCGTGGTTCTGCTCTG
	tufA/Bcoli_qPCR_R	TCAATCGCACGCTCTGGTTC
ompF	ompFcoli_qPCR_F	TGGCGGCGTTGCTACCTATC
	ompFcoli_qPCR_R	TTAGAGCGGCGTGCAGTGTC
rplK	rplKcoli_qPCR_F	ACCGTTTACGCTGACCGTTC
	rplKcoli_qPCR_R	TTGGTCTGCGCGATTTCCTG
osmB	osmBcoli_qPCR_F	AAATGACCGCGGCTGTTCTG
	osmBcoli_qPCR_R	GCTGCACCACCTAATGTACC

rpsJ	rpsJcoli_qPCR_F	ATCAAGCAACCGCGGAAATC
	rpsJcoli_qPCR_R	ATGTCAACCAGACGCAAGTG
rpoA	rpoAcoli_qPCR_F	GCCACCTGACCGATGAGAAC
	rpoAcoli_qPCR_R	TACGCTCCACAGGGCTGTAG
Mt40S	Mt40S_F	CCGCAAGGACTGTTCAAGAT
	Mt40S_R	TATCGGTCCATTCTGGAAGC
nodGRP1L	nodGRP1L_rtPCR_F	AGGGGGAAAGTGATGGAAAC
	nodGRP1L_rtPCR_R	CCACCACCTCCCATCTTTC
nodGRP3A	nodGRP3A_rtPCR_F	AGACTGGGGAGGCTCATTTT
	nodGRP3A_rtPCR_R	TTTGCACCTTTTTCATGTGC
nodGRP3C	nodGRP3C_rtPCR_F	TGTTCTTTATTTGTGCCCTAATTCT
	nodGRP3C_rtPCR_R	TGGATGACTCGATTACCACAAT
nodGRP4	nodGRP4_rtPCR_F	GGGAACGTCCAAGAGAAAGA
	nodGRP4_rtPCR_R	CCTCCTATCAAAAACCCTTCG